國立交通大學

電機學院微電子奈米科技產業研發碩士班

碩士論文

利用陽極電極的調變來改善氧化鉿薄膜之電阻
式轉換記憶體其單極操作特性研究

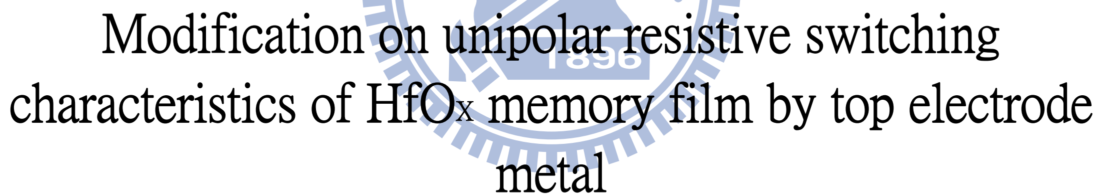

Modification on unipolar resistive switching characteristics of HfO_x memory film by top electrode metal

研 究 生：賴威仁

指導教授：張國明　教授

中 華 民 國 九 十 八 年 九 月

利用陽極電極的調變來改善氧化鉿薄膜之電阻式轉換記憶體其單極操作特性研究

Modification on unipolar resistive switching characteristics of HfO_x memory film by top electrode metal

研 究 生：賴威仁 Student：Wei-Ren Lai

指導教授：張國明 博士 Advisor：Dr. Kow-Ming Chang

國 立 交 通 大 學

電機學院微電子奈米科技產業研發碩士班

碩 士 論 文

A Thesis
Submitted to College of Electrical and Computer Engineering
National Chiao Tung University
in partial Fulfillment of the Requirements
for the Degree of Master
in
Industrial Technology R & D Master Program on
Microelectronics and Nano Sciences
September 2009
Hsinchu, Taiwan, Republic of China

中 華 民 國 九 十 八 年 九 月

利用陽極電極的調變來改善氧化鉿薄膜之電阻式轉換記憶體其單極操作特性研究

學生：賴威仁　　　　　　　　　　　　　　　指導教授：張國明 博士

國立交通大學電機學院產業研發碩士班

摘　要

這篇論文中，首先我們探討不同限流對電阻式記憶體的影響，然後利用不同的金屬當上電極於氧化鉿/氮化鈦的結構，接著討論電極與各種金屬的功函數和各種金屬的氧化自由能之間的關係。在同樣限流下，可觀察到氧化自由能較低的金屬，沒有電阻式操作的特性，而且氧化自由能較高的金屬，耐操度較差。因為自由能較低的金屬容易在接面處形成金屬氧化物，會導致細絲無法燒斷且不能電阻式操作，而自由能較高的金屬容易在電阻式操作中失去氧離子。因此我們研究用惰性金屬/易反應金屬來當上電極，例如鈀/鋁、鈀/鈦、鉑/鈦等。此種結構具有非常好的電阻式操作的特性，可在高溫下操作，耐久性測

試中可轉態超過 4000 次，資料保存能力可達十年。我們的研究顯示惰性金屬/易反應金屬/氧化鉿/氮化鈦的電阻式記憶體是很有希望被應用在下個世代的非揮發性記憶體。

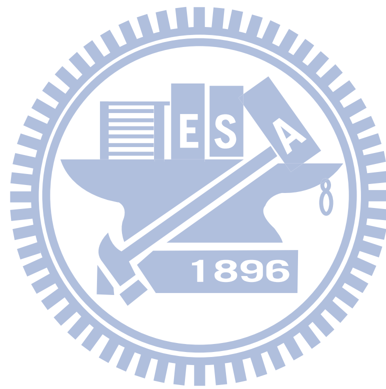

Modification on unipolar resistive switching characteristics of HfO_x memory film by top electrode metal

Student：Wei-Ren Lai　　Advisors：Dr. Kow-Ming Chang

Industrial Technology R & D Master Program of
Electrical and Computer Engineering College
National Chiao Tung University

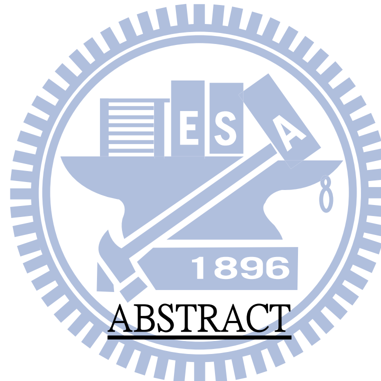

ABSTRACT

In this thesis, first, we discuss to influence resistive memory for different compliance current, then the different metals were used as the electrode based on the HfO_x/TiN structure. Afterward, we discuss the electrode dependence with various metals work function and free energy of oxidation of various metals. For the same compliance current, lower free energy of oxidation of metals were observed no resistive switching characteristics, and higher free energy of oxidation of metals is bad for endurance test. Because lower free energy of oxidation of metals were easier formed metal oxide at interface, which resulted the filaments were not ruptured and no resistive switching, and higher free energy of oxidation of metals on resistive switching is easier losing oxygen

ions. Therefore, we studied with inert metal/reactive metal as top electrode, such as Pd/Al, Pd/Ti, Pt/Ti, and etc. This structure has very good resistive switching characteristics, which could be operated at high temperature, endurance was more than 4000 cycles, and data retention was over ten years. Our study shows that the inert metal/reactive metal/HfO_x/TiN resistive memory is a promising candidate for next-generation nonvolatile memory device application.

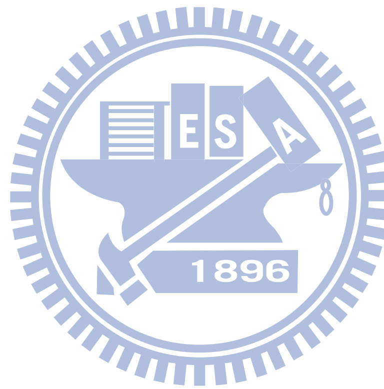
ESA 1896

誌謝

首先，我要感謝指導教授張國明老師，在碩士班的兩年研究生涯裡給予我熱心的教導，且老師也時常與我們分享人生的經驗與待人處事的道理，對我在生活上或學術知識上都有莫大的幫助。

其次，要感謝實驗室的各位學長，對於我實驗上的建議與協助，尤其是曾文賢學長，在我的研究中提出了許多建言，更在我有問題的時候為我解惑；以及黃菘宏學長，不但訓練了我許多的機台，還時常教導我許多實驗上的問題，使我獲益良多；還有，感謝實驗室同學呂成家、陳信宇、廖彥凱、吳天佑、黃俊傑學弟、林煒力學弟，和其他曾經幫助過我的實驗室同學與其他實驗室的朋友，由於你們，讓我的研究和論文可以很順利的完成。

此外，還要感謝長庚大學的劉國辰教授，提供我們試片與材料分析的經費，以及王水進教授、賴瓊惠教授和劉國辰教授在口試中對我論文內容，提出的建議與看法，讓我對研究題目有更進一步的想法，另外也感謝交通大學奈米中心的何惟梅小姐、林聖欽先生、陳悅婷小姐、黃國華先生，交通大學貴儀中心的鄭淑娟小姐，國家奈米元件實驗室的簡秀芳小姐、許瓊姿小姐等人的熱心協助，並且提供良好的研究環境與資源。

最後，要特別感謝我的奶奶吳愛珠女士與父母賴孟津先生和許玉美女士，以及我的家人，能在我實驗失意時給予我心靈上的慰藉與鼓勵，是我能順利碩士畢業的最大力量。

賴威仁于新竹交通大學 2009 年 9 月

Contents

Chinese Abstract ... i
English Abstract ... iii
Acknowledgements ... v
Contents ... vi
Table Captions ... viii
Figure Captions ... ix

Chapter 1 Introduction ... 1

1.1 Introduction to nonvolatile memory ... 1
1.2 Introduction to next-generation nonvolatile memories ... 2
1.2.1 Ferroelectric Random Access Memory ... 2
1.2.2 Magnetroresistive Random Access Memory ... 3
1.2.3 Phase Change Random Access Memory ... 3
1.2.4 Resistive Random Access Memory ... 4
1.3 Introduction to Resistive Random Access Memory ... 5
1.3.1 Forming process and resistive switching polarities ... 5
1.3.2 Top electrodes ... 6
1.3.3 Resistive switching films ... 6
1.4 Conduction mechanisms ... 7
1.4.1 Schottky emission ... 7
1.4.2 Frenkel-Poole emission ... 7
1.4.3 Tunnel or Field emission ... 8
1.4.4 Space-charge-limited current ... 8
1.4.5 Ohmic conduction ... 8
1.4.6 Ionic conduction ... 8
1.5 Filament model ... 9

Chapter 2 Experiment Details ... 18

2.1 Experimental procedure ... 18
2.2 Material analyses ... 19
2.2.1 Atomic force microscopy ... 19
2.2.2 X-ray photoelectron spectroscopy ... 19
2.2.3 Focus ion beam ... 20

2.2.4 Transmission electron microscopy and Energy dispersive spectroscopy... 21
2.3 Electrical measurements 21
2.3.1 Current-voltage measurement 22
2.3.2 Endurance measurement 22
2.3.3 Data retention time measurement 22

Chapter 3 Results and Discussion 27
3.1 Defined some resistive switching parameters 27
3.1.1 Resistive switching parameters 27
3.1.2 Compliance current 27
3.2 Various metal of top electrodes 28
3.2.1 Electrical properties of various top electrodes 29
3.2.2 Work function of various metals 31
3.2.3 Free energy of various metals 32
3.3 Resistive switching characteristics of Pd/Al/HfO_x/TiN structure 34
3.3.1 Electrical properties 35
3.3.2 Retention property 37
3.3.3 Thermal stability 37
3.3.4 Curve fitting of current-voltage plots 38
3.3.5 Material analyses 38
3.3.6 Electrical properties of Pd/Ti/HfO_x/TiN structure 39
3.4 Resistive switching characteristics of Pt/Ti/HfO_x/TiN structure 40
3.4.1 Electrical properties 40
3.4.2 Retention property 40
3.4.3 Curve fitting of current-voltage plots 40
3.4.4 Material analyses 41

Chapter 4 Conclusion 88

Chapter 5 Future Work 89

References 90

Table Captions

Chapter 1 Introduction

Table 1-1 Comparison with the Flash memory and next-generation NVMs....................11
Table 1-2 Basic conduction mechanisms in insulator...11

Chapter 3 Results and Discussion

Table 3-1 Comparison with the work function and resistive switching parameters of various metals...42
Table 3-2 Comparison with the free energy of oxide formation of electrode metals and resistive switching parameters of various metals..42
Table 3-3 Comparison with the Pd/HfO_x/TiN with N_2 versus without N_2 and the Ti/HfO_x/TiN versus TiN/HfO_x/TiN..43
Table 3-4 Comparison with the different thickness of Al of Pd/Al/HfO_x/TiN structure and resistive switching parameters of the deivces. 43

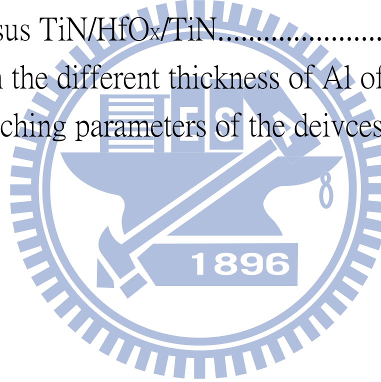

Figure Captions

Chapter 1 Introduction 1

Fig. 1-1 Typical floating-gate flash memory 12
Fig. 1-2 ABO_3 structure (perovskite structures). 12
Fig. 1-3 Polarization hysteresis curve of the FeRAM material 12
Fig. 1-4 MFSFET structure of the FeRAM 13
Fig. 1-5 Parallel state (low resistance state) and antiparallel state (high resistance state) of the MRAM 13
Fig. 1-6 Basic memory cell of the PCRAM 14
Fig. 1-7 Time-temperature relationship of the PCRAM 14
Fig. 1-8 (a) Typical I-V curves of the unipolar resistive switching. (b) Typical I-V curves of the bipolar resistive switching 15
Fig. 1-9 Typical I-V curve of the nonpolar resistive switching 15
Fig. 1-10 Schematic of the filament in an oxide 16
Fig. 1-11 CAFM results for RRAM in (a) LRS and (b) HRS 16
Fig. 1-12 Schematic diagram for switching from LRS to HRS. (a) LRS formed by positive bias on TE. [(b)-(e)] Nucleation and propagation of a filament when negative bias is applied on TE. (f) HRS is attained 17

Chapter 2 Experiment Details 18

Fig. 2-1 The device structure of our sample 24
Fig. 2-2 AFM image of $HfO_x/TiN/Ti/SiO_2/Si$ structure 24
Fig. 2-3 The rms surface roughness of $HfO_x/TiN/Ti/SiO_2/Si$ structure 25
Fig. 2-4 XPS intensity of $HfO_x/TiN/Ti/SiO_2/Si$ structure 25
Fig. 2-5 XPS atomic concentration of $HfO_x/TiN/Ti/SiO_2/Si$ structure 26
Fig. 2-6 XPS binding energy of HfO_x films 26

Chapter 3 Results and Discussion 27

Fig. 3-1 Typical I-V characteristics of unipolar resistive switching 44
Fig. 3-2 Various compliance current of RRAM. (a) 5 **μA** (b) 5 mA 45
Fig. 3-3 The typical I-V curve of $Pt/HfO_x/TiN$ structure (5 mA) 46
Fig. 3-4 Distribution of V_{SET} and V_{RESET} of $Pt/HfO_x/TiN$ structure (5 mA). 46
Fig. 3-5 Resistance of HRS and LRS of $Pt/HfO_x/TiN$ structure by 0.08 V read bias

(5 mA)......47
Fig. 3-6 The typical I-V curve of Pt/HfO_x/TiN structure (50 **μA**)......47
Fig. 3-7 Distribution of V_{SET} and V_{RESET} of Pt/HfO_x/TiN structure (50 **μA**)......48
Fig. 3-8 Resistance of HRS and LRS of Pt/HfO_x/TiN structure by 0.08 V read bias (50**μA**)......48
Fig. 3-9 The typical I-V curve of Pd/HfO_x/TiN structure (5 mA).......49
Fig. 3-10 Distribution of V_{SET} and V_{RESET} of Pd/HfO_x/TiN structure (5 mA)......49
Fig. 3-11 Resistance of HRS and LRS of Pd/HfO_x/TiN structure by 0.08 V read bias (5 mA)......50
Fig. 3-12 The typical I-V curve of Pd/HfO_x/TiN structure (50 **μA**)......50
Fig. 3-13 Distribution of V_{SET} and V_{RESET} of Pd/HfO_x/TiN structure (50 **μA**)......51
Fig. 3-14 Resistance of HRS and LRS of Pd/HfO_x/TiN structure by 0.08 V read bias (50 **μA**)......51
Fig. 3-15 The typical I-V curve of Cu/HfO_x/TiN structure......52
Fig. 3-16 Distribution of V_{SET} and V_{RESET} of Cu/HfO_x/TiN structure......52
Fig. 3-17 Resistance of HRS and LRS of Cu/HfO_x/TiN structure by 0.08 V read bias...53
Fig. 3-18 The typical I-V curve of Ni/HfO_x/TiN structure......53
Fig. 3-19 Distribution of V_{SET} and V_{RESET} of Ni/HfO_x/TiN structure......54
Fig. 3-20 Resistance of HRS and LRS of Ni/HfO_x/TiN structure by 0.08 V read bias ...54
Fig. 3-21 The typical I-V curve of Ti/HfO_x/TiN structure......55
Fig. 3-22 Distribution of V_{SET} and V_{RESET} of Ti/HfO_x/TiN structure......55
Fig. 3-23 Resistance of HRS and LRS of Ti/HfO_x/TiN structure by 0.08 V read bias....56
Fig. 3-24 Forming process of Al/HfO_x/TiN structure......56
Fig. 3-25 RESET process of Al/HfO_x/TiN structure......57
Fig. 3-26 Ellingham diagram of representative high-κ dielectrics showing the free energy of formation as a function of temperature......57
Fig. 3-27 Ellingham diagram plotting the standard free energies of the formation of oxides of the metals......58
Fig. 3-28 The typical I-V curve of Pd/HfO_x/TiN structure with N_2 6 sccm 30 second....59
Fig. 3-29 Distribution of V_{SET} and V_{RESET} of Pd/HfO_x/TiN structure with N_2 6 sccm 30 second......59
Fig. 3-30 Resistance of HRS and LRS of Pd/HfO_x/TiN structure with N_2 6 sccm 30 second by 0.08 V read bias......60
Fig. 3-31 The typical I-V curve of TiN/HfO_x/TiN structure......60
Fig. 3-32 Distribution of V_{SET} and V_{RESET} of TiN/HfO_x/TiN structure......61
Fig. 3-33 Resistance of HRS and LRS of TiN/HfO_x/TiN structure by 0.08 V read bias.61
Fig. 3-34 The typical I-V curve of Pd/Al(20 Å)/HfO_x/TiN structure......62
Fig. 3-35 Distribution of V_{SET} and V_{RESET} of Pd/Al(20 Å)/HfO_x/TiN structure......62

Fig. 3-36 Resistance of HRS and LRS of Pd/Al(20 Å)/HfO_x/TiN structure by 0.08 V read bias 63
Fig. 3-37 The typical I-V curve of Pd/Al(50 Å)/HfO_x/TiN structure 63
Fig. 3-38 Distribution of V_{SET} and V_{RESET} of Pd/Al(50 Å)/HfO_x/TiN structure 64
Fig. 3-39 Resistance of HRS and LRS of Pd/Al(50 Å)/HfO_x/TiN structure by 0.08 V read bias 64
Fig. 3-40 The typical I-V curve of Pd/Al(75 Å)/HfO_x/TiN structure 65
Fig. 3-41 Distribution of V_{SET} and V_{RESET} of Pd/Al(75 Å)/HfO_x/TiN structure 65
Fig. 3-42 Resistance of HRS and LRS of Pd/Al(75 Å)/HfO_x/TiN structure by 0.08 V read bias 66
Fig. 3-43 The typical I-V curve of Pd/Al(100 Å)/HfO_x/TiN structure 66
Fig. 3-44 Distribution of V_{SET} and V_{RESET} of Pd/Al(100 Å)/HfO_x/TiN structure. 67
Fig. 3-45 Resistance of HRS and LRS of Pd/Al(100 Å)/HfO_x/TiN structure by 0.08 V read bias 67
Fig. 3-46 The typical I-V curve of Pd/Al(150 Å)/HfO_x/TiN structure for SET process..68
Fig. 3-47 The typical I-V curve of Pd/Al(150 Å)/HfO_x/TiN structure for RESET process 68
Fig. 3-48 The typical I-V curve of Al/HfO_x/TiN structure for etching Al to 30 Å....69
Fig. 3-49 Distribution of V_{SET} and V_{RESET} of Al/HfO_x/TiN structure for etching Al to 30 Å 69
Fig. 3-50 Resistance of HRS and LRS of Al/HfO_x/TiN structure for etching Al to 30 Å by 0.08 V read bias. 70
Fig. 3-51 The typical I-V curve of Al(30 Å)/HfO_x/TiN structure. 70
Fig. 3-52 Distribution of V_{SET} and V_{RESET} of Al(30 Å)/HfO_x/TiN structure. 71
Fig. 3-53 Resistance of HRS and LRS of Al(30 Å)/HfO_x/TiN structure by 0.08 V read bias 71
Fig. 3-54 The typical I-V curve of Pd/Al(35 Å)/HfO_x/TiN structure (1~2650 cycles)....72
Fig. 3-55 The typical I-V curve of Pd/Al(35 Å)/HfO_x/TiN structure (2651~4000 cycles) 72
Fig. 3-56 Distribution of V_{SET} and V_{RESET} of Pd/Al(35 Å)/HfO_x/TiN structure (1~2650 cycles) 73
Fig. 3-57 Distribution of V_{SET} and V_{RESET} of Pd/Al(35 Å)/HfO_x/TiN structure (2651~4000 cycles) 73
Fig. 3-58 Resistance of HRS and LRS of Pd/Al(35 Å)/HfO_x/TiN structure by 0.08 V read bias 74
Fig. 3-59 Retention time of Pd/HfO_x/TiN structure at 85 ℃ by 0.08 V read bias....74
Fig. 3-60 Retention time of Pd/Al(35 Å)/HfO_x/TiN structure at 175 ℃ by 0.08 V read bias 75

Fig. 3-61 Temperature dependence of LRS at low to median bias 75
Fig. 3-62 Temperature dependence of HRS at low to median bias 76
Fig. 3-63 I-V curve fitting of LRS 76
Fig. 3-64 I-V curve fitting of HRS at small bias region 77
Fig. 3-65 I-V curve fitting of HRS at large bias region 77
Fig. 3-66 XPS intensity of Pd/Al/HfO_x/TiN structure 78
Fig. 3-67 XPS atomic concentration of Pd/Al/HfO_x/TiN structure 78
Fig. 3-68 XPS binding energy of Al/HfO_x interface 79
Fig. 3-69 TEM micrograth of Pd/Al/HfO_x/TiN/Ti/SiO2/Si structure 79
Fig. 3-70 High resolution TEM image of Al/HfOX interface 80
Fig. 3-71 EDS analysis of the Al layer 80
Fig. 3-72 The typical I-V curve of Pd/Ti(30 Å)/HfO_x/TiN structure 81
Fig. 3-73 Distribution of V_{SET} and V_{RESET} of Pd/Ti(30 Å)/HfO_x/TiN structure 81
Fig. 3-74 Resistance of HRS and LRS of Pd/Ti(30 Å)/HfO_x/TiN structure by 0.08 V read bias 82
Fig. 3-75 The typical I-V curve of Pt/Ti(30 Å)/HfO_x/TiN structure 82
Fig. 3-76 Distribution of V_{SET} and V_{RESET} of Pt/Ti(30 Å)/HfO_x/TiN structure 83
Fig. 3-77 Resistance of HRS and LRS of Pt/Ti(30 Å)/HfO_x/TiN structure by 0.08 V read bias 83
Fig. 3-78 Retention time of Pt/Ti(30 Å)/HfO_x/TiN structure at 85 ℃ by 0.08 V read bias 84
Fig. 3-79 I-V curve fitting of LRS of Pt/Ti(30 Å)/HfO_x/TiN structure. 84
Fig. 3-80 I-V curve fitting of HRS of Pt/Ti(30 Å)/HfO_x/TiN structure at small bias region. 85
Fig. 3-81 I-V curve fitting of HRS of Pt/Ti(30 Å)/HfO_x/TiN structure at large bias region 85
Fig. 3-82 XPS intensity of Pt/Ti/HfO_x/TiN structure 86
Fig. 3-83 XPS atomic concentration of Pt/Ti/HfO_x/TiN structure 86
Fig. 3-84 XPS binding energy of Ti/HfO_x interface 87

Chapter 1 Introduction

1.1 Introduction to nonvolatile memory

The nonvolatile memory (NVM) should keep the stored information without power supply for a long time. In 1967, D. Kahng and S. M. Sze invented the floating-gate nonvolatile semiconductor memory at Bell Labs. In recent years, the portable electronic products can provide the convenient life for human. Therefore, the popularity of portable equipment, such as mobile phone, digital camera, mp3 player, and personal digital assistant, the requirements of NVMs increase significantly in the semiconductor industry. An ideal NVM includes the properties of low operation voltage, simple structure, low power consumption, non-destructive readout, high operation speed, long retention time, high endurance, and small cell size. However, there is no such NVM meet the above properties up to now.

Nowadays, the mainstream of NVM is flash memory, included the NOR flash and NAND flash. The NOR flash has high operation speed, which is suitable for the computer coding, PC bios, DVD player, and mobile phone applications. On the other hand, the NAND flash with higher density is used for large data storage application, such as PDA, memory cards, MP3 players, digital cameras, and USB flash personal disc etc. A primary structure of flash memory is basic on a MOSFET with a modified stacking gate which composed by control gate, dielectric, floating gate and dielectric as a sandwich structure, shown in Fig. 1-1. The logic high or low is determined by charges injected in the floating-gate are maintained there, allowing the difference between threshold voltages of the cell transistor for NVM application.

However, the flash memory has some issues such as high operation voltage, low operation speed, poor retention time, and coupling interference effect during scaling down [1]-[2]. Therefore, some modified flash memories, such as charge-trapping (SONOS) flash and band-engineered SONOS flash are proposed to replace the tradition flash memory [3]-[4]. Moreover, many researchers want to find emerging next-generation NVM with the advantages of DRAM, SRAM, and flash memory. Some possible candidates for next-generation NVMs, including ferroelectric random access memory (FeRAM) [5]-[7], magnetroresistive random access memory (MRAM) [8]-[10], phase change random access memory (PCRAM) [11]-[15], and resistive random access memory (RRAM) are discussed in the next section.

1.2 Introduction to next-generation nonvolatile memories

1.2.1 Ferroelectric Random Access Memory

A ferroelectric material with a spontaneous polarization and the polarization can being altered by applying an electric field. A standard structure of the ferroelectric material is the ABO_3 structure (perovskite structures) as shown in Fig. 1-2, where the A, B, and O atoms are located at corner, body center, and face center of the cubic, respectively. When an electric field is applied to the ferroelectric material, the B atom with two thermodynamically stable positions is located depended on the polarity of the applied electric field. The polarization hysteresis curve of the ferroelectric material is shown in Fig. 1-3. The hysteresis phenomenon of ferroelectric material can be used for NVM applications called it FeRAM. The FeRAM can be subdivided into two types. One type is the metal-ferroelectric-semiconductor FET (MFSFET) structure as shown in Fig. 1-4. The structure is very similar to the MOSFET except the oxide film is replaced by the

ferroelectric film. The polarizations (+Pr or －Pr) of the ferroelectric film will affect the drain current of the transistor, and the memory effect of the MFSFET type FeRAM is nonvolatile and with nondestructive readout property. The other type is similar to DRAM, where the dielectric of the capacitor is replaced by the ferroelectric film. The polarizations of the ferroelectric film will also affect the current of the device. The memory effect of this type FeRAM is also nonvolatile, but the read process is destructive and needing a re-write process.

1.2.2 Magnetroresistive Random Access Memory

The standard MRAM cell is the magnetic tunneling junction which consists of two magnetic layers sandwiching a thin tunneling layer as shown in Fig. 1-5. The magnetization of one magnetic layer, also named reference layer, is fixed and kept in a specific direction. The other layer, also named storage layer, can be switched to parallel or antiparallel to the reference layer by applying a specific magnetic field. The logic high or low is determined by the resistance of parallel or antiparallel state. In read process, a small current flowing through the tunneling layer is detected to recognize the resistance states. The MRAM have a lot of merits, but the reliability of the tunneling layer and the device scaling limitation are the most important challenge of MRAM.

1.2.3 Phase Change Random Access Memory

A phase-change memory (PCRAM), also named ovonic unified memory (OUM), is reported by Neale et al. in 1970. The standard memory cell of PCRAM is shown in Fig. 1-6 [12], where the GeSbTe (GST) chalcogenide alloy material has been adopted as a primary material of the PCRAM. The PCRAM exhibits two different structural phases of

the GST, amorphous and polycrystalline, for data storage. In reset process, a high magnitude current pulse with short tailing edge is applied on the programmable volume of the phase change material. The temperature of the material exceeds the melting point which eliminates the polycrystalline order in the volume. When the reset pulse is terminated, the device quenches to "freeze in" the disordered structural state. This quench time about several nanoseconds is determined by the thermal environment of the device and the fall time of the reset pulse. In set process, a moderate magnitude current pulse with sufficient duration is applied to maintain the device temperature for crystal growth. The amorphous structural state (high resistance state) or the polycrystalline structural state (low resistance state) is read by applying a low magnitude and long duration current pulse. The time-temperature relationship of the PCRAM is shown in Fig. 1-7 [12]. During the set and reset processes, large Joule heating is applied on the phase change material, and hence, huge power is consumed. How to reduce the power consumption during the PCRAM operation is a significant challenge of the PCRAM.

1.2.4 Resistive Random Access Memory

The resistive random access memory which consists of two memory states, the low resistance state (LRS) and the high resistance state (HRS), which can be altered by applying bias voltage or pulse, and utilizes the two different resistance values to storage digital data. Table 1-1 performs the comparison with the Flash and next-generation NVMs [16]-[17]. This table shows that the RRAM with low operation voltage and power, high operation speed, high scalability, good endurance, small size, etc. The details of the RRAM are discussed in section.

1.3 Introduction to Resistive Random Access Memory

1.3.1 Forming process and resistive switching polarities

The forming process is the common phenomenon in the binary metal oxide films which is similar to the dielectric breakdown, named it "soft breakdown". Forming is possible with structures containing a wide variety of amorphous or microcrystalline insulators between a few tens and many hundreds of nanometers thick and a variety of metal electrodes, although the process occurs most readily when noble metals (such as Au) are used as the anode material. The forming voltage is strongly dependent upon the dielectric or its thickness. The cathode material does not affect the forming process or subsequent properties. Therefore, the anode of the resistive switching device plays an important role in the forming process and diffuses into the resistive switching film to change the resistivity considerably.

The resistive switching properties can be divided into three types based on the resistive switching polarities. First, the resistive switching is defined as unipolar resistive switching when being performed only by one polarity of the applied voltage bias, as indicated in Fig. 1-8 (a) [18]. Second, As for bipolar resistive switching, it depicts that the resistive switching phenomenon is observed as applying the specific polarity of the voltage and current biases to reach the ON-state, and back into the OFF-state by applying the other polarity of the voltage and current biases as shown in Fig. 1-8 (b) [18]. Third, Fig. 1-9 [19] shows the typical I-V curve of nonpolar resistive switching. Nonpolar switching means that the device can be switched to another state by applying an electric signal regardless of the directions.

1.3.2 Top electrodes

Because the RRAM stores the digital data by different resistance value, the resistive switching behavior might result from the resistance change at Metal-Insulator interface. Thus, the different work function, electronegativity, and oxygen affinity property of metal, even the interface reaction, and the interdiffusion all possibly have influence on the resistive switching behaviors. Therefore, to make RRAM more practical and reliable, it is very important to pick up the suitable combination of the electrodes.

1.3.3 Resistive switching films

The resistive switching phenomena have been found in many materials. The research mainstream is focused on several groups, including binary oxides, complex metal oxide, perovskite oxides, manganites, and other alloy or polymers.

The binary metal oxides such as NiO, TiO_2, HfO_2, and etc [20]-[22]. The complex metal materials such as $Gd_{1-x}Ca_xBaCo_2O_5$, $Ba_{0.7}Sr_{0.3}TiO_3$, and etc. The carrier-doped manganites with the perovskite structure, such as $Pr_{1-x}Ca_xMnO_3$ (PCMO), $La_{1-x}Ca_xMnO_3$ (LCMO), and etc.

Various processing techniques can be used for the preparation of composite and multilayer resistive switching thin films by modifying the apparatus and the conditions for deposition, such as atomic layer deposition (ALD), electron cyclotron resonance (ECR) sputtering, plasma-enhanced atomic layer deposition (PEALD), plasma-enhanced chemical vapor deposition (PECVD), pulsed laser deposition (PLD), metallorganic chemical vapor deposition (MOCVD), reactive DC sputtering, RF sputtering, sol-gel method, and solid-state reaction method.

Therefore, process parameters such as deposition temperature, O_2 partial pressure, and

working process are introduced to elucidate the influence on the resistive switching properties. In addition, the dopant species and the crystallinity of the resistive switching films also determine the resistive switching behaviors, which have been discussed as well.

1.4 Conduction mechanisms

The resistive switching mechanisms of each RRAM material are not clearly understood up to now. Therefore, the conduction mechanisms of each resistance state of the RRAM device are studied for further understanding of the resistive switching mechanisms in each RRAM material. In this section, six basic conduction mechanisms in insulator are summarized in Table 1-2 [94].

1.4.1 Schottky emission

The Schottky emission is caused by thermionic emission of carriers across the interface between metal and insulator [94]. Therefore, the Schottky emission is also named it thermionic emission. If carriers transport in an insulator is by this mechanism, a plot of $Ln|J/T^2|$ versus 1/T in a specific voltage is a straight line, and the slope can determine the permittivity of the insulator. Besides, a lot of $Ln|J|$ versus $V^{1/2}$ at a fixed temperature is also a straight line.

1.4.2 Frenkel-Poole emission

The Frenkel-Poole (F-P) emission is due to field-enhance thermal excitation of trapped electrons into the conduction band [94]. For the F-P emission, plots of $Ln|J|$ versus 1/T in a specific voltage and $Ln|J/V|$ versus $V^{1/2}$ at a fixed temperature are straight lines.

1.4.3 Tunnel or Field emission

The tunnel or field emission corresponds to electrons tunneling from the metal Fermi energy into the insulator conduction band or field ionization of trapped electrons into the conduction band [94]. This emission is strongly dependent on the applied voltage, but is essentially independent on the temperature. A plot of $Ln|J/V^2|$ versus $1/V$ is a straight line in this conduction mechanism.

1.4.4 Space-charge-limited current

The space-charge-limited current (SCLC) is caused by carriers injected into the insulator and no compensation charge is present [94]. The density of SCLC is direct proportion to V^2, and is essentially independent on the temperature.

1.4.5 Ohmic conduction

The Ohmic conduction is results from thermally excited electrons hopping from one isolated state to the next state [94]. If carriers transport in an insulator is by this conduction, plots of $Ln|J|$ versus $Ln|V|$ at fixed temperature and $Ln|J|$ versus $1/T$ in a specific voltage are straight lines with unity slope.

1.4.6 Ionic conduction

The ionic conduction is similar to a diffusion process. In this mechanism, the voltage and current dependence is the same with the Ohmic conduction at a fixed temperature, and a plot of $Ln|J \times T|$ versus $1/T$ in a specific voltage is a straight line with unity slope. In addition, each conduction mechanism may dominate in some voltage and temperature

ranges, and there are possibly two or more mechanisms causing the conduction in an insulator.

1.5 Filament model

The major possible models having been proposed by other research groups are sorted as the following, including filament model, charge tapping and detrapping model, phase change, and solid-state electrolyte. Each model may be applied for some combinations of electrodes and oxide materials. However, many models were proposed by many researchers up to now, but the mainstream of many models nowadays is filament model [23]-[29].

The filamentary model comes from the nature of oxide breakdown and integrity that the defects existing in an oxide bulk such as the interstitials and vacancies of oxygen and metals constitute the leakage current path, as depicted in Fig. 1-10 [30]. This model has been proposed since 1970's and is one of the earliest models in resistive switching. Recently, since nonvolatile memories have acquired a lot of attention, the further and more detailed studies have been carried out to investigate the possible resistive switching mechanisms. The most obvious evidences for the filamentary model are conductive atomic force microscopy (CAFM) mapping results and the cell-area-insensitivity of LRS and HRS, as shown Fig. 1-11 [31]. CAFM is one of the best tools to investigate the local conductivity throughout the film.

Another subject of debate this model is the switching process. It is reasonable to assume that the oxygen deficient region (filaments) of a film is much more conducting than the stoichiometric region irrespective of whatever the defect type is. Generally the mobility of oxygen ions in binary oxides is much higher than metal ions, and the formation of the filaments could be induced by the rejection of O^{2-} ions. During the filament formation

process, it is the electrical field effect that takes an essential part, because the insulating parts among the filaments are stressed by the highest electrical field accompanied with point discharge effect. As for the filament rupture, it is the current-induced effect that rules the process in which Joule heating effect resulting from the current flow through the tiny filaments generates heat and raises temperature up to hundreds of degree Celsius at the local spot, providing enough energy for oxygen ions to reflow and making the conductive regions of non-stoichiometry return to insulator to rupture the filaments.

Recently, the concept of tree-shaped filament structure has been proposed. The breakdown paths (filaments) are formed in a dielectric when the carriers are injected from a local point at the electrode interface. The initial cross-sectional area of the path for the carrier conduction is quite narrow, but with the propagation of the filaments the cross section largely increases by an increasing number of secondary formed paths. Therefore the region near the cathode might contain filaments with a larger conductivity compared to the region near the anode. That is to say the filament is thick at the cathode and thin at the anode if merely considering a single filament, which matters in terms of conductivity and has impact on Joule heating effect. It is at the thinnest part of a filament near the anode that most thermal energy accumulates and the filament formation and rupture occur. Experiments reported by K. M. Kim et al. show that only 3~10 nm of the filaments near the anode dominates the switching, and the schematics are shown in Fig. 1-12 [32].

Function	Flash	FeRAM	MRAM	PCRAM	RRAM
CMOS Integration	Good	Poor	Poor	Good	Good
Cell Size	$4F^2$	$20F^2$	$20F^2$	$6F^2$	$4F^2$
Program Voltage	High	Low	Low	Medium	Low
Program Current	~uA	~uA	~mA	~mA	<0.1mA
W/E Time	~ms	~40ns	<10ns	~100ns	<10ns
Retention Time	>10y	>10y	>10y	>10y	>10y
Endurance	$>10^5$	$>10^{12}$	$>10^{12}$	$>>10^6$	$>>10^6$

Table 1-1 Comparison with the Flash memory and next-generation NVMs.

mechanism	expression	voltage and temperature dependence
Schottky emission	$J = A^* T^2 \exp\left[\frac{-q\left(\phi_B - \sqrt{qE/4\pi\varepsilon_i}\right)}{kT}\right]$	$J \sim T^2 \exp\left(+a\sqrt{V}/T - q\phi_B/kT\right)$
F-P emission	$J \sim E \exp\left[\frac{-q\left(\phi_B - \sqrt{qE/\pi\varepsilon_i}\right)}{kT}\right]$	$J \sim V \exp\left(+2a\sqrt{V}/T - q\phi_B/kT\right)$
tunnel or field emission	$J \sim E^2 \exp\left[-\frac{4\sqrt{2m^*}\left(q\phi_B\right)^{3/2}}{3q\hbar E}\right]$	$J \sim V^2 \exp\left(-1/V\right)$
SCLC	$J = \frac{9\varepsilon_i \mu V^2}{8d^3}$	$J \sim V^2$
Ohmic conduction	$J \sim E \exp\left(-\Delta E_{ae}/kT\right)$	$J \sim V \exp\left(-1/T\right)$
ionic conduction	$J \sim \frac{E}{T} \exp\left(-\Delta E_{ai}/kT\right)$	$J \sim \frac{V}{T} \exp\left(-1/T\right)$

Table 1-2 Basic conduction mechanisms in insulator.

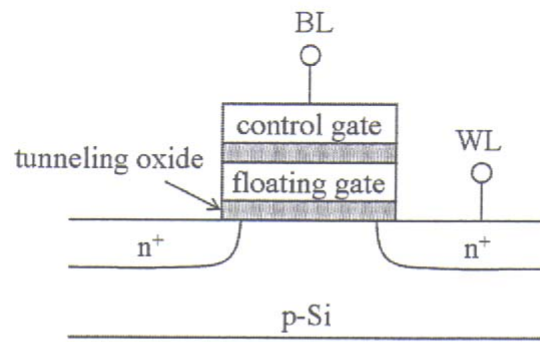

Fig. 1-1 Typical floating-gate flash memory.

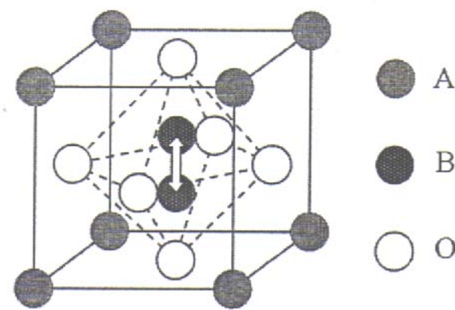

Fig. 1-2 ABO_3 structure (perovskite structures).

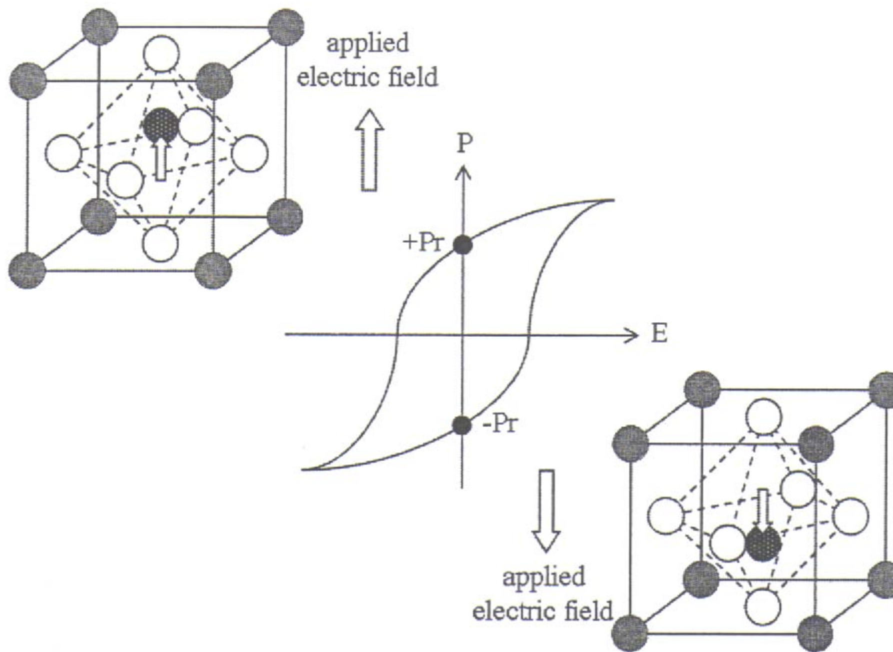

Fig. 1-3 Polarization hysteresis curve of the FeRAM material.

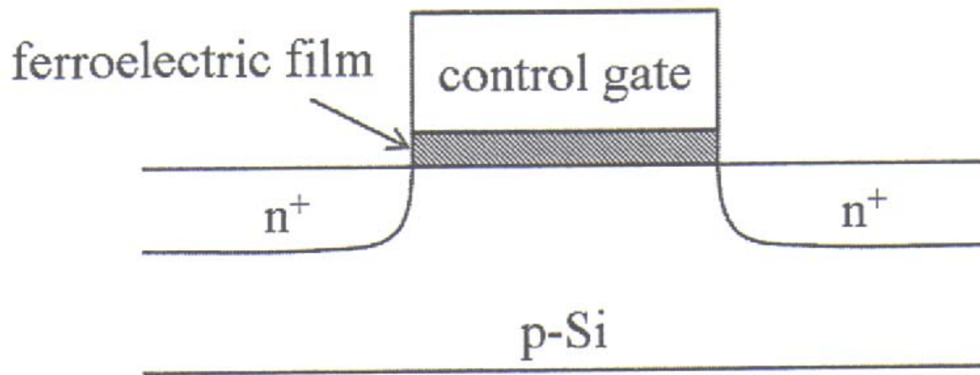

Fig. 1-4 MFSFET structure of the FeRAM.

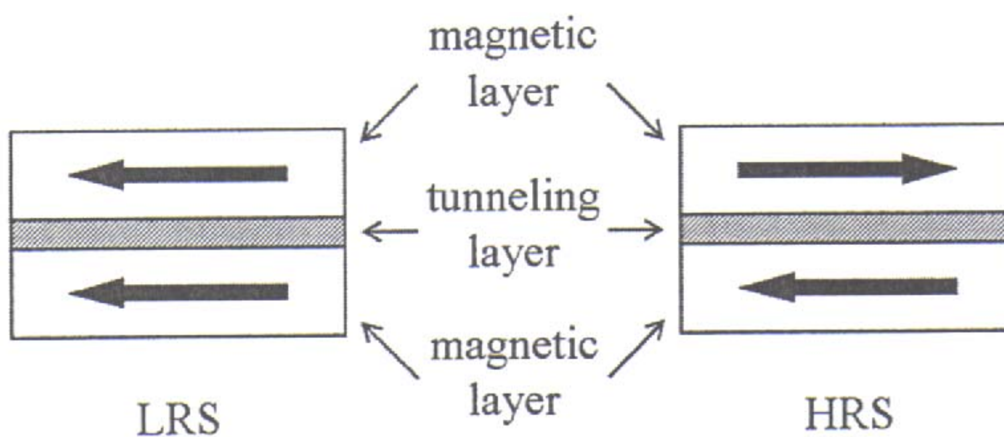

Fig. 1-5 Parallel state (low resistance state) and antiparallel state (high resistance state) of the MRAM.

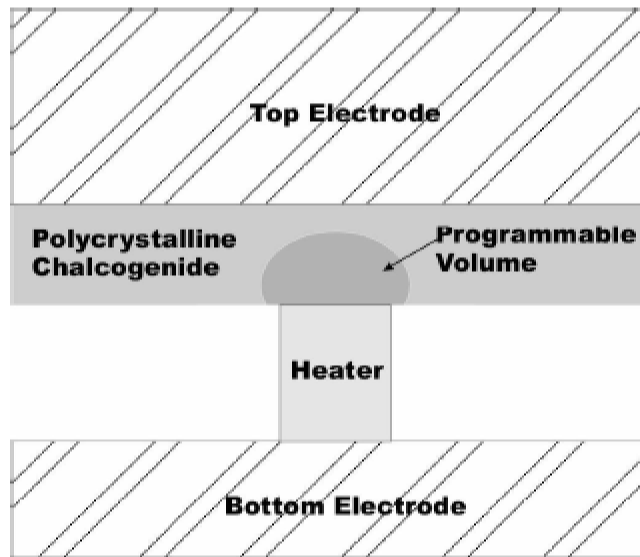

Fig. 1-6 Basic memory cell of the PCRAM [12].

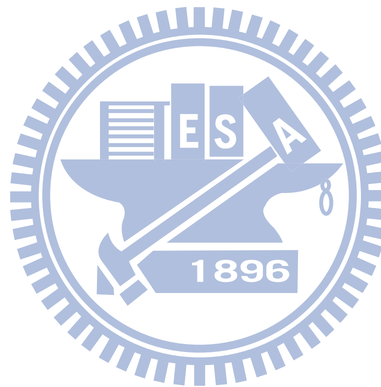

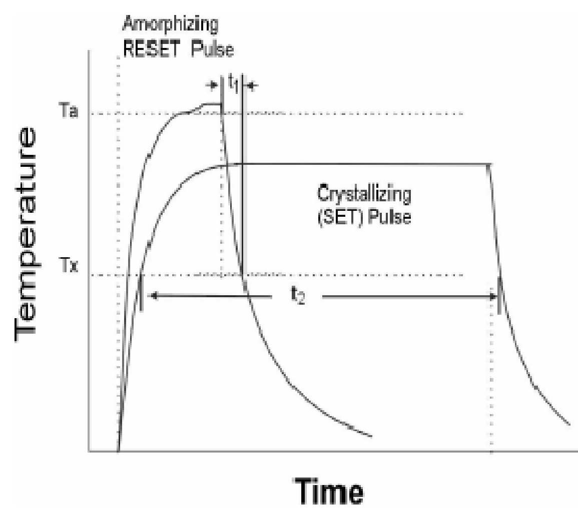

Fig. 1-7 Time-temperature relationship of the PCRAM [12].

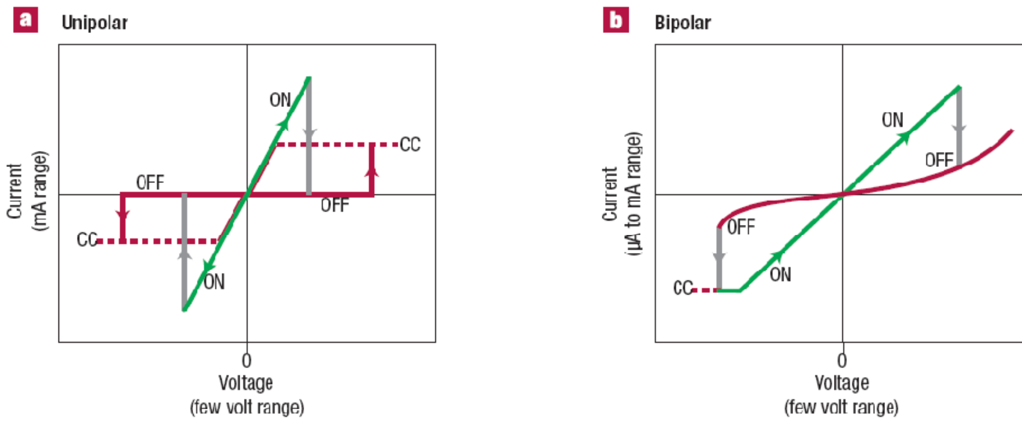

Fig. 1-8 (a) Typical I-V curves of the unipolar resistive switching. (b) Typical I-V curves of the bipolar resistive switching [18].

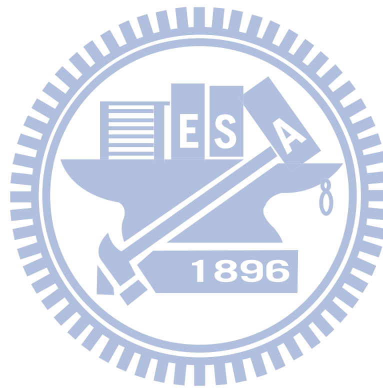

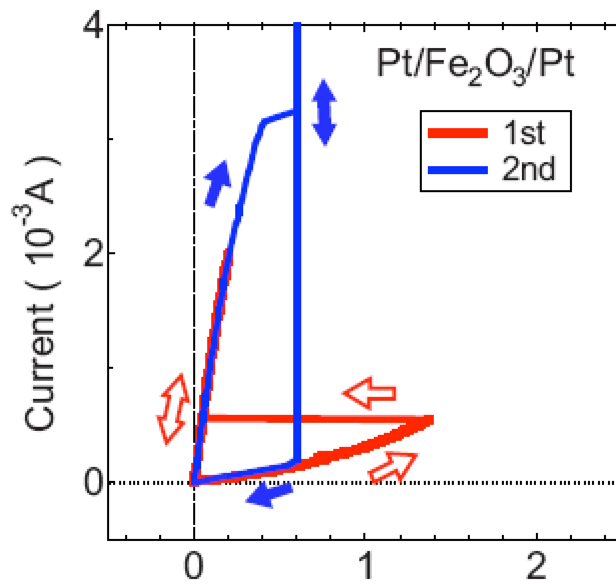

Fig. 1-9 Typical I-V curve of the nonpolar resistive switching [19].

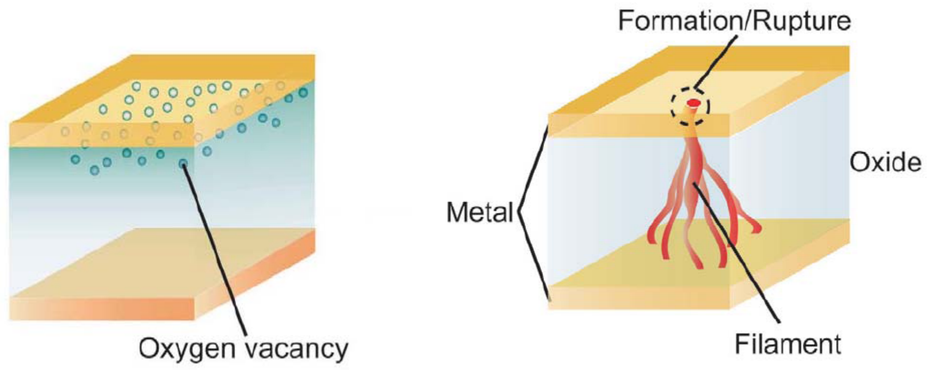

Fig. 1-10 Schematic of the filament in an oxide [30].

(a)

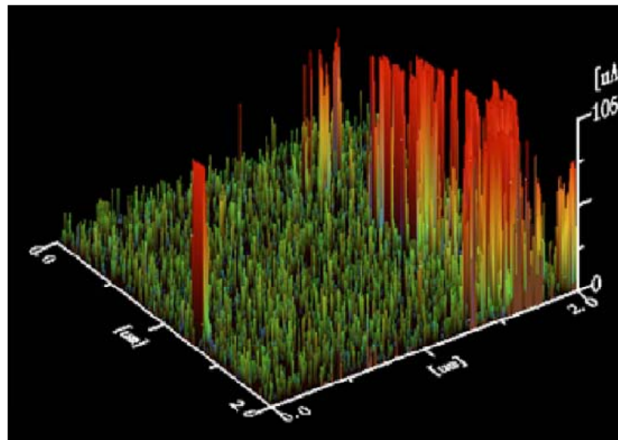

(b)

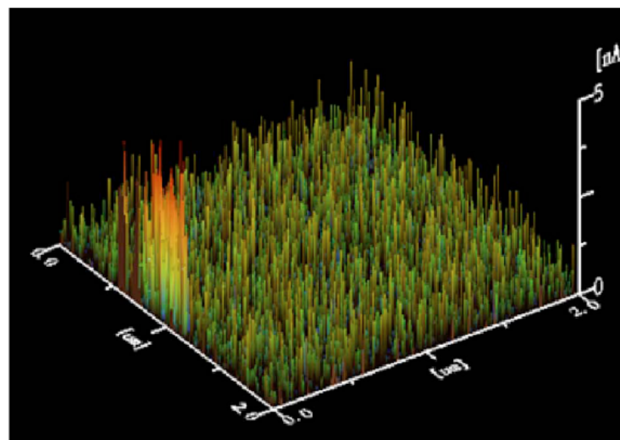

Fig. 1-11 CAFM results for RRAM in (a) LRS and (b) HRS [31].

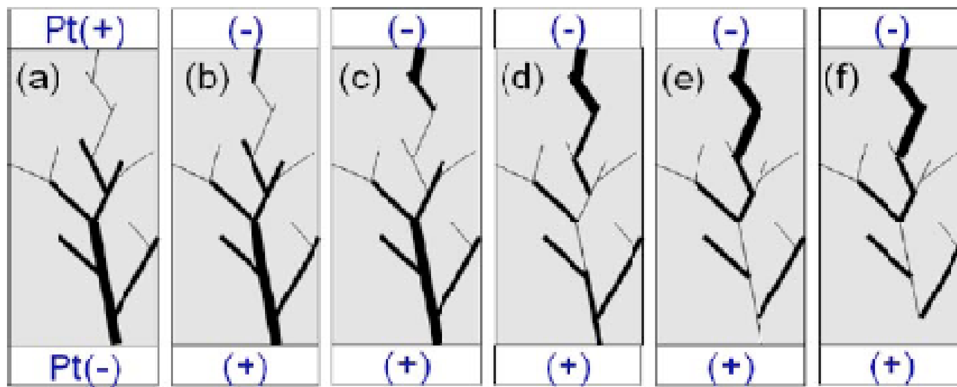

Fig. 1-12 Schematic diagram for switching from LRS to HRS. (a) LRS formed by positive bias on TE. [(b)-(e)] Nucleation and propagation of a filament when negative bias is applied on TE. (f) HRS is attained [32].

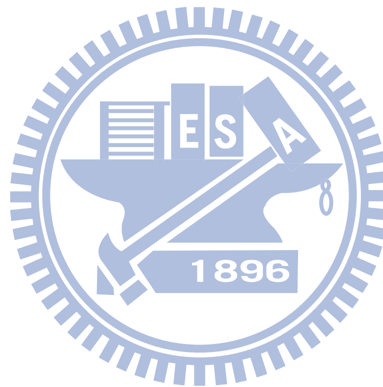

Chapter 2 Experiment Details

2.1 Experimental procedure

Resistive memory device were fabricated as follows [33]-[36]. TiN metal as a bottom electrode was deposited on $Ti/SiO_2/Si$ wafer by sputtering. Then, nonstoichiometric HfO_x films with a thickness of 20 nm were deposited by ALD (ASM, Polygon 8200) at temperature of 300 ^{o}C. Hafnium tetrachloride ($HfCl_4$) and water (H_2O) were used as reactants for HfO_x deposition, and changed the aspect ratio to 2:5. The primitive chemical-formula as follows [37]-[39].

$$HfCl_4 + 4H_2O \rightarrow Hf(OH)_4 + HCl\uparrow \qquad (2\text{-}1)$$

$$Hf(OH)_4 \text{ heating} \rightarrow HfO_2 + H_2O \qquad (2\text{-}2)$$

After stacking HfO_x thin films on the bottom electrodes, various kind of metals as top electrodes were deposited by sputtering using a shadow mask at room temperature, such as Pt, Pd, Cu, Ni, Ti, Al, and etc. The thickness of metals were about 30-100 nm. To study the area dependence of the electrical properties, the circular top electrodes were formed with diameters of 100 μm. The structure of device shown in Fig. 2-1. The surface morphology of $HfO_x/TiN/Ti/SiO_2/Si$ samples was examined by atomic force microscopy (AFM) in trapping mode, and the composition depth profiles of HfO_x films were carried out by X-ray photon-electron spectroscopy (XPS).

As shown in Fig. 2-2, and Fig. 2-3, the rms surface roughness over a scanning area of $10\times10\,\mu m^2$ is around 1.5 nm. The depth profile of the chemical composition of HfO_x films measured by XPS is shown Fig. 2-4, and Fig. 2-5. The atomic ratio of oxygen to hafnium (O:Hf) inside the HfO_x film is found to be about 1.5, which suggests that the

HfO_x film is nonstoichiometric. The binding energy of HfO_x films measured by XPS is shown Fig. 2-6. The primitive binding energy of HfO_2 is 16.7 eV. The peak of plot is shift, and peak of $Hf_{7/2}$ and $Hf_{5/2}$ is not very clear, which was demonstrated the resistive switching films is nonstoichiometric HfO_x films. In addition, residual chloride in our HfO_x film, which was used in the ALD process as a chloride precursor ($HfCl_4$), was not detected by XPS measurement.

2.2 Material analyses

Many material analyses are used to assist us in understanding the related and the corresponding electrical properties to investigate the dopant effects, the top electrode effects, and the resistive switching mechanism. Atomic force microscopy, X-ray photoelectron spectrometer, Focus Ion Beam, and Transmission electron microscopy are used in the thesis, which are going to be introduced in the following content.

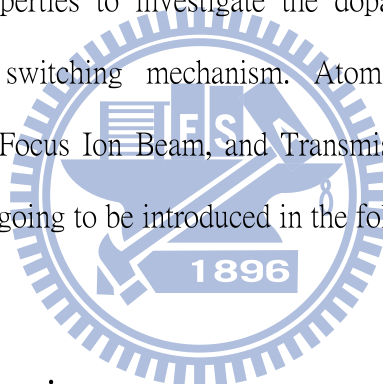

2.2.1 Atomic force microscopy

The surface roughness and surface morphology of the bottom electrodes and the resistive switching thin films are characterized by the atomic force microscopy in tapping mode. The average roughness (R_a) and the root mean square (RMS) roughness of the device are automatically recorded and calculated by the software.

2.2.2 X-ray photoelectron spectroscopy

When the light illuminates the matter, the inner electrons are going to be excited and ionized. The ionized electrons, which close to the surface of the matter, have the ability to

escape into vacuum, named photoelectron, and the phenomenon is called photoelectric effect. Due to the different components and chemical states of the matters, photoelectrons have characteristic kinetic energy, which can be used to identify the composed elements and the chemical states of surface atoms. When the excitation source is soft x-ray, the photoemission spectroscopy is termed by X-ray photoelectron spectroscopy.

2.2.3 Focus ion beam

FIB is a scientific instrument that resembles a scanning electron microscope. However, the SEM uses a focused beam of electrons to image the sample in the chamber, whereas a FIB instead uses a focused beam of gallium ions. Gallium is chosen because it is easy to build a gallium liquid metal ion source (LMIS). In a Gallium LMIS, gallium metal is placed in contact with a tungsten needle and heated. Gallium wets the tungsten, and a huge electric field (greater than 10^8V per centimeter) causes ionization and field emission of the gallium atoms.

Unlike an electron microscope, the FIB is inherently destructive to the specimen. When the high-energy gallium ions strike the sample, they will sputter atoms from the surface. Gallium atoms will also be implanted into the top few nanometers of the surface, and the surface will be made amorphous.

Because of the sputtering capability, the FIB is used as a micro-machining tool, to modify or machine materials at the micro- and nano-scale.

The FIB is commonly used to prepare samples for the transmission electron microscope. The TEM requires very thin samples, typically ~100 nanometers. The nanometer-scale resolution of the FIB allows the exact thin region to be chosen.

2.2.4 Transmission electron microscopy and Energy dispersive spectroscopy

Transmission electron microscopy (TEM) is a microscopy technique whereby a beam of electrons is transmitted through an ultra thin specimen, interacting with the specimen as it passes through it. An image is formed from the electrons transmitted through the specimen, magnified and focused by an objective lens and appears on an imaging screen, a fluorescent screen in most TEMs, plus a monitor, or on a layer of photographic film, or to be detected by a sensor such as a CCD camera.

In material science/metallurgy the speciments tend to be naturally resistant to vacuum, but must be prepared as a thin foil, or etched so some portion of the specimen is thin enough for the beam to penetrate. Preparation techniques to obtain an electron transparent region include ion beam milling and wedge polishing. The focused ion beam (FIB) is a relatively new technique to prepare thin samples for TEM examination from larger specimens. Because the FIB can be used to micro-machine samples very precisely, it is possible to mill very thin membranes from a specific area of a sample, such as a semiconductor or metal.

By the way, TEM and EDS can be analyzed at the same time. Energy dispersive spectroscopy (EDS) analysis, it is released X-ray that the components percentage of the sample is analyzed by electron hit the surface of TEM sample.

2.3 Electrical measurements

The most important parts of all are the electrical measurements. The electrical properties of the devices from I-V curve are demonstrated. The electrical measurement system consisted of a probe station, an Agilent 4156C semiconductor parameter analyzer,

and GPIB controller.

Our electrical measurement was sorted into three items: current-voltage measurement by DC voltage sweeping, endurance measurement, and data retention time measurement. The three initial items are tested for criteria of our memory devices.

2.3.1 Current-voltage measurement

The measurement is performed by Agilent 4156C which provides a DC voltage sweeping between two specific voltages to observe the resistive switching. We could observe the relations between the bias voltage and the current of the high/low resistive states.

2.3.2 Endurance measurement

Before used in commercial applications, it is important to investigate that how many times that the memory devices can be operated before failure. That is so called endurance measurement. A memory device is expected with excellent endurance characteristics due to the requirements for users.

2.3.3 Data retention time measurement

Retention time is how long the stored data can be maintained, and the data is not able to be distinguished beyond retention time. The data retention time measurement is performed by reading the stored data after certain periods to find out if there occurs data loss or not. The data retention time measurement performed at high temperature can accelerate the degradation of the device to investigate the thermal stability of the memory

devices.

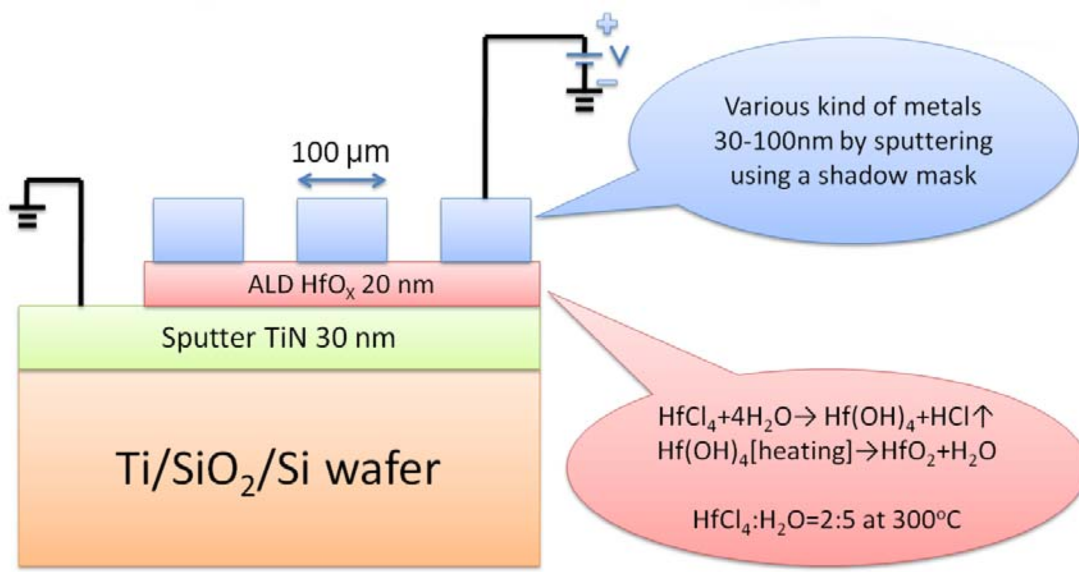

Fig. 2-1 The device structure of our sample.

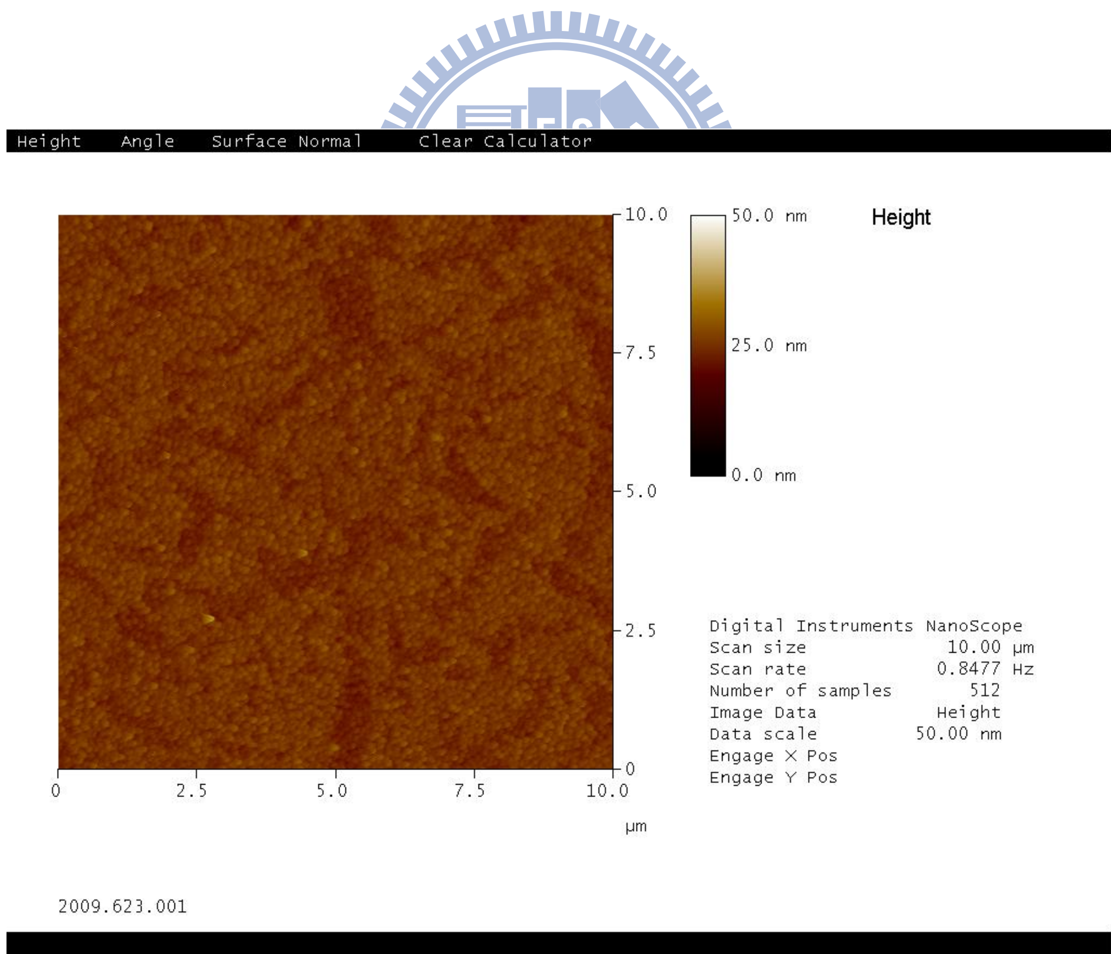

Fig. 2-2 AFM image of HfO_x/TiN/Ti/SiO_2/Si structure.

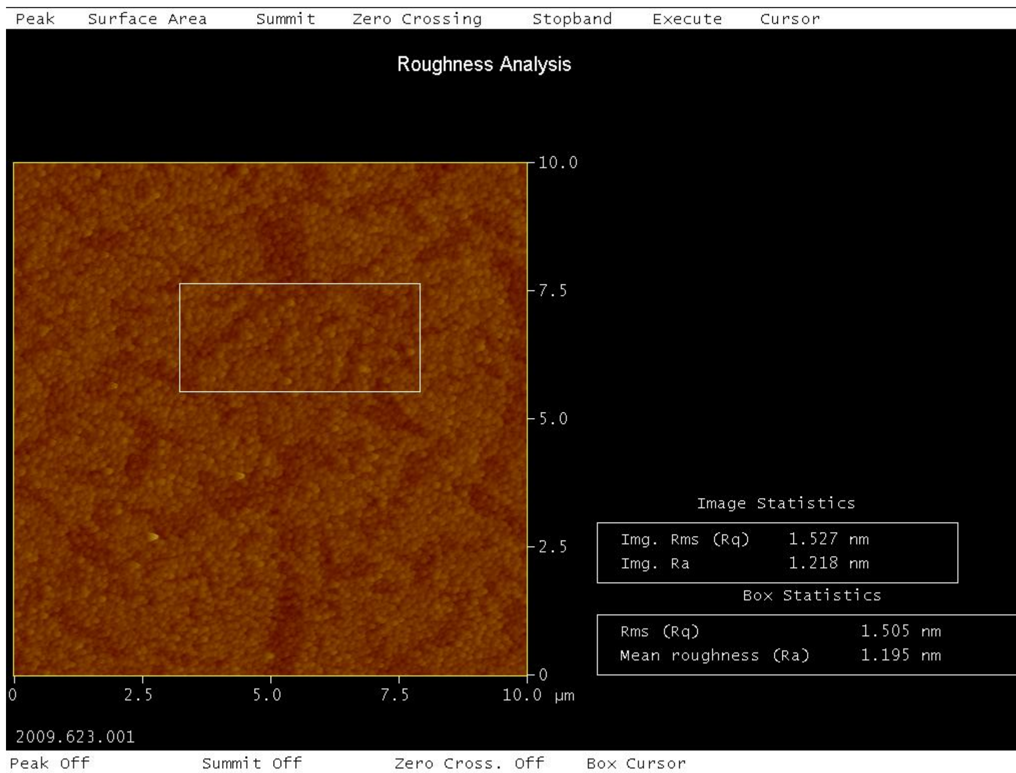

Fig. 2-3 The rms surface roughness of $HfO_x/TiN/Ti/SiO_2/Si$ structure.

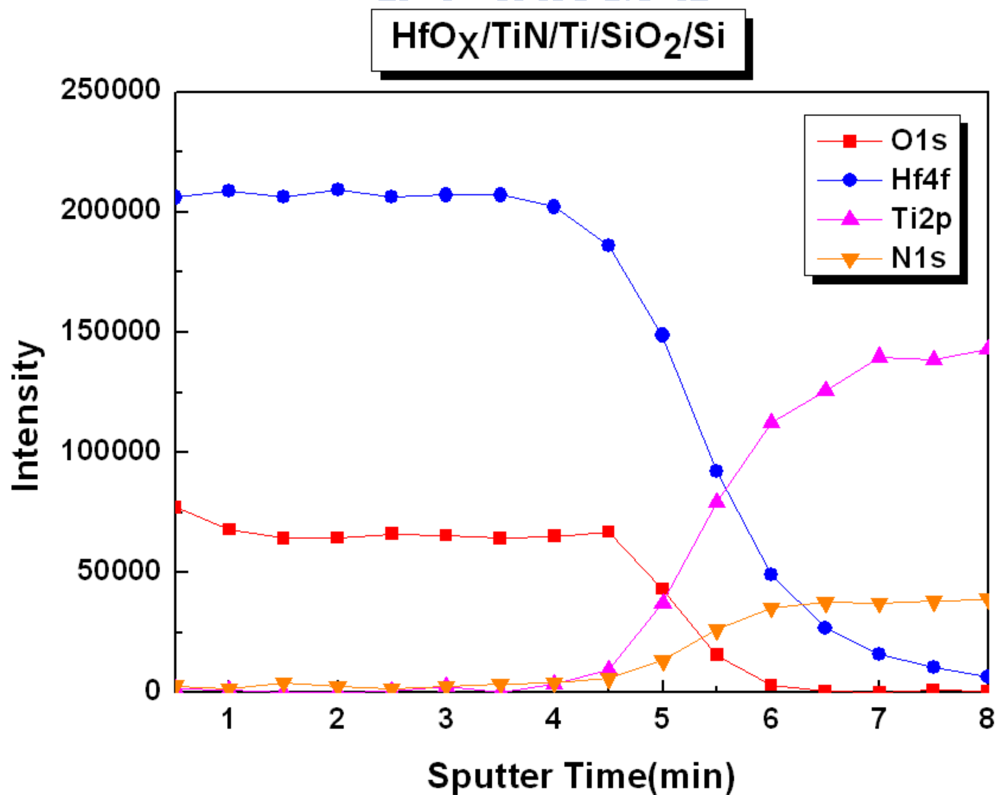

Fig. 2-4 XPS intensity of $HfO_x/TiN/Ti/SiO_2/Si$ structure.

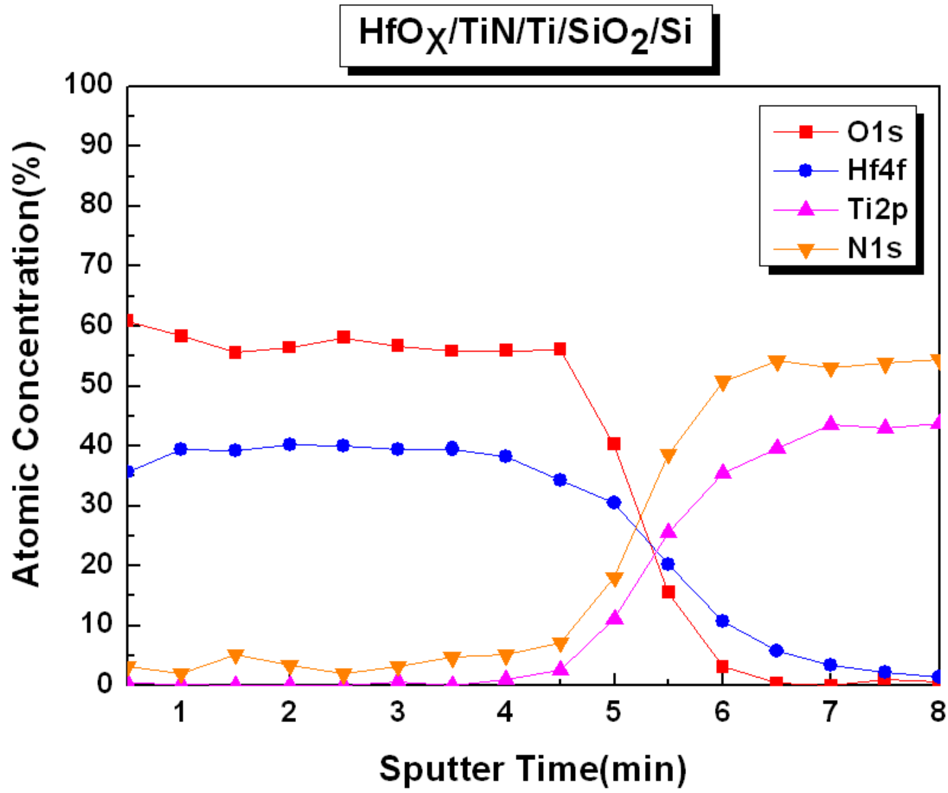

Fig. 2-5 XPS atomic concentration of $HfO_x/TiN/Ti/SiO_2/Si$ structure.

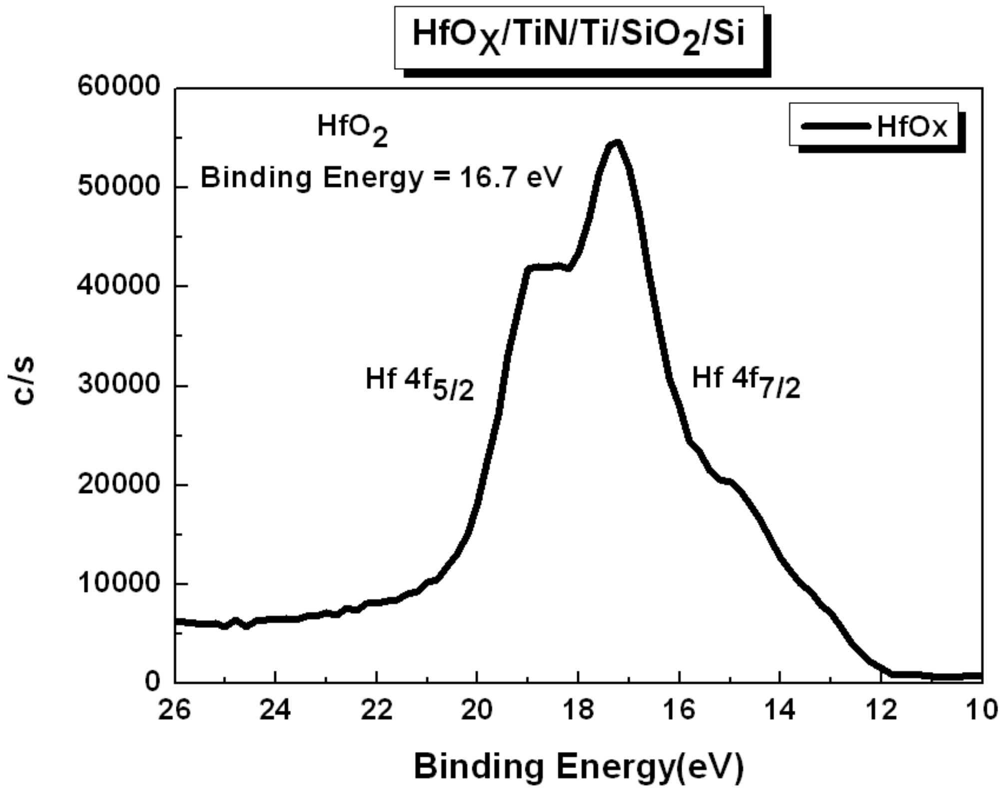

Fig. 2-6 XPS binding energy of HfO_x films.

Chapter 3 Results and Discussion

3.1 Defined some resistive switching parameters

3.1.1 Resistive switching parameters

First, we have been defining some resistive switching parameters. In Fig. 3-1, the unipolar resistive switching is performed by sweeping current bias. The forming process is the common phenomenon in the binary metal oxide films which is similar to the dielectric breakdown, named it "soft breakdown". In general, exhibits two memory states: the low resistance state (LRS), also named high conducting state (ON-state) and the high resistance state (HRS), also named low conducting state (OFF-state), which can be altered by applying bias voltage, and utilizes the two different resistance values to storage digital data. R_{HRS} (R_{off}) is defined the resistance of HRS. R_{LRS} (R_{on}) is defined the resistance of LRS. ON process is defined as the transformation from LRS into HRS. OFF process is defined as the transformation from HRS into LRS. V_{SET} (V_{on}) is the voltage which is the highest slope of current-voltage curve. During ON process, a sudden increase in current occurs at V_{SET} and limited at compliance current. V_{RESET} (V_{OFF}) is the voltage which the lowest slope of current-voltage curve. During OFF process, a sudden decrease in current occurs at V_{RESET}.

3.1.2 Compliance current

An important part of RRAM is the compliance current [40]-[44]. Compliance current imposed by the measure instruments or the electrical circuit is imposed on the resistive switching memory device to avoid the device breakdown. To investigate the influence of

compliance current during resistive switching, the compliance currents are varied from μA to mA as shown in Fig. 3-2. As the compliance current of resistive switching reaches 5 μA, the V_{SET} and V_{RESET} values increases and overlap each other, and various resistance of HRS increases. This phenomenon might be attributed to that because the smaller compliance current forms few filaments which are very weak. The weak filaments are created that is easy to rupture all the filaments at the same time during OFF process, and the weak filaments are more easier to form in other place of HfO_x films which leads to the V_{SET} and V_{RESET} values increases and overlap each other, and resistance of HRS is larger various, as shown in Fig. 3-2 (a). As the compliance current of resistive switching reaches 5 mA, the V_{SET} and V_{RESET} values decreases and don' t overlap each other, and various resistance of HRS decreases. This phenomenon might be attributed to that because the larger compliance current forms many filaments which are very strong. The strong filaments are created that is hard to rupture all the filaments at the same time during OFF process, and the strong filaments are more easier to form in the residual partial filaments of HfO_x films which leads to the V_{SET} and V_{RESET} values decreases and don' t overlap each other, and resistance of HRS is smaller various, as shown in Fig. 3-2 (b).

3.2 Various metal of top electrodes

In many reports, we know that top electrodes and resistive switching films are great influence on the RRAM [45]-[50]. Therefore, in order to reduce variables, we fixed resistive switching films for HfO_x films, then to change the different electrode. In this section, we performed the resistive switching in various top electrodes/HfO_x/TiN/Ti/SiO_2/Si devices where various top electrodes where Pt, Pd, Cu, Ni, Ti, and Al.

3.2.1 Electrical properties of various top electrodes

At this section, we would show the basic memory device electrical properties of various top electrodes, including resistive switching characteristics, distribution of V_{SET} and V_{RESET}, resistance of HRS and LRS.

In Pt/HfO_x/TiN device, first, is using the dc voltage sweep method with a current compliance of 5 mA. In Fig. 3-3 shows the typical I-V curve. Distribution of V_{SET} and V_{RESET} are shown in Fig. 3-4. Resistance of HRS and LRS by 0.08 V read bias are shown in Fig. 3-5. Second, the compliance current changed 50 μA, and shows the typical I-V curve in Fig. 3-6. Distribution of V_{SET} and V_{RESET} are shown in Fig. 3-7. Resistance of HRS and LRS by 0.08 V read bias are shown in Fig. 3-8. Form the results, we demonstrates when Pt as top electrode, which can use the dc voltage sweep with different compliance current. As mentioned in the previous section, smaller compliance current leads to the V_{SET} and V_{RESET} values increases and overlap each other, and resistance of HRS is larger various, but the endurance is more than 1200 cycles. On the contrary the lager compliance current leading to the V_{SET} and V_{RESET} values decreases and don't overlap each other, and various resistance of HRS decreases, but the endurance is less than 15 cycles.

In Pd/HfO_x/TiN device, first, is using the dc voltage sweep method with a current compliance of 5 mA. In Fig. 3-9 shows the typical I-V curve. Distribution of V_{SET} and V_{RESET} are shown in Fig. 3-10. Resistance of HRS and LRS by 0.08 V read bias are shown in Fig. 3-11. Second, the compliance current changed 50 μA, and shows the typical I-V curve in Fig. 3-12. Distribution of V_{SET} and V_{RESET} are shown in Fig. 3-13. Resistance of HRS and LRS by 0.08 V read bias are shown in Fig. 3-14. Form the results, we demonstrates when Pd as top electrode, which can use the dc voltage sweep with different compliance current. As mentioned in the previous section, smaller compliance current leading to the V_{SET} and V_{RESET} values increases and overlap each other, and resistance of

HRS is larger various, but the endurance is more than 200 cycles. On the contrary the lager compliance current leading to the V_{SET} and V_{RESET} values decreases and don’t overlap each other, and various resistance of HRS decreases, but the endurance is less than 30 cycles.

In Cu/HfO_x/TiN device, is using the dc voltage sweep method with a current compliance of 5 mA. In Fig. 3-15 shows the typical I-V curve. Distribution of V_{SET} and V_{RESET} are shown in Fig. 3-16. Resistance of HRS and LRS by 0.08 V read bias are shown in Fig. 3-17. Form the results, we demonstrates when Cu as top electrode, which only use the dc voltage sweep with mA compliance current. As mentioned in the previous section, lager compliance current leading to the V_{SET} and V_{RESET} values decreases and don’t overlap each other, and various resistance of HRS decreases, but the endurance is less than 10 cycles.

In Ni/HfO_x/TiN device, is using the dc voltage sweep method with a current compliance of 5 mA. In Fig. 3-18 shows the typical I-V curve. Distribution of V_{SET} and V_{RESET} are shown in Fig. 3-19. Resistance of HRS and LRS by 0.08 V read bias are shown in Fig. 3-20. Form the results, we demonstrates when Ni as top electrode, which only use the dc voltage sweep with mA compliance current. As mentioned in the previous section, lager compliance current leading to the V_{SET} and V_{RESET} values decreases and don’t overlap each other, various resistance of HRS decreases, and the endurance is more than 250 cycles.

In Ti/HfO_x/TiN device, is using the dc voltage sweep method with a current compliance of 3 mA. In Fig. 3-21 shows the typical I-V curve. Distribution of V_{SET} and V_{RESET} are shown in Fig. 3-22. Resistance of HRS and LRS by 0.08 V read bias are shown in Fig. 3-23. Form the results, we demonstrates when Ti as top electrode, which only use the dc voltage sweep with mA compliance current. As mentioned in the previous section, lager compliance current leading to the V_{SET} and V_{RESET} values decreases and don’t overlap

each other, and various resistance of HRS decreases, but the endurance is less than 50 cycles.

In Al/HfO_x/TiN device, forming process is formed as shown in Fig. 3-24. After forming process, the device couldn't cause resistive switching as shown in Fig. 3-25. That is to say the resistive switching phenomenon couldn't be observed for Al/HfO_x/TiN device.

3.2.2 Work function of various metals

According to textbooks, the values of work function φ of various metals are as follows; φ_{Pt}=5.65 eV, φ_{Pd}=5.12 eV, φ_{Ni}=5.15 eV, φ_{Cu}=4.65 eV, φ_{Ti}=4.33 eV, and φ_{Al}=4.28 eV.

In the early reports, such as Sawa et al., which proposed that a Schottky barrier, the origin of the nonlinearity of the I-V curve, is formed by a low work function metal and p-type semiconductor PCMO, and the resistive switching mechanism on based Schottky barrier barrier modulation was suggested [51]. Afterward, Seo et al., demonstrated that the effective electric field across the NiO film was high enough to cause resistive switching phenomenon while Ohmic contact or a low Schottky barrier formed between the metal-insulator interface. There is no resistive switching phenomenon with Ti top electrode due to the considerable voltage drop across the well-established Schottky barrier at the Ti/NiO interface [52].

In particular, our sample of various top electrodes did not show similar resistive switching characteristics as reported previously. Table 3-1 performs the comparison with the work function and resistive switching parameters of various metals. We demonstrates larger work function metal, which has better electrical properties, and can resistive switching for different compliance current, but there are different electrical properties on

different compliance current. The work function could not be clear to explain this phenomenon.

3.2.3 Free energy of various metals

Recently, electronegativity and free energy is often used to explain the mechanism RRAM. Hasan et al. proposed that under a positive bias, electromigration of oxygen ions forms thicker oxide, which dissociates under a negative bias, causes high and low resistance states, respectively [53]-[54]. Afterward, Lee et al. proposed that the importance of the reaction at the metal/NiO interface is demonstrated in relation to the free energy of oxide formation of electrode metals and Ni [47], [55]-[57].

Figure 3-26 shows Ellingham diagram of representative high-κ dielectrics showing the free energy of formation as a function of temperature, and Fig. 3-27 shows Ellingham diagram plotting the standard free energies of the formation of oxides of the metals. The free energy of oxidation of Al is close to the free energy of oxidation of Hf. Therefore, the Al/HfO_x/TiN device showed no resistive switching characteristics. Because Al attracted and trapped more oxygen ions from HfO_x films to form interface layer [58]-[68], which resulted the filaments were not ruptured.

The Ti top electrode was investigated, as Ti has slightly larger free energy of oxidation than free energy of oxidation of Hf. Therefore, the Ti/HfO_x/TiN device showed resistive switching characteristics, but the endurance is bad. Because Ti still attracted and trapped some oxygen ions from HfO_x films to form thin interface layer. When RESET process, the filaments were not ruptured clearly. Therefore, resistance of HRS and ratio decrease.

The Ni top electrode was also investigated, as Ni has higher free energy of oxidation than free energy of oxidation of Hf. Therefore, the Ni/HfO_x/TiN device showed good

resistive switching characteristics. Because Ni did not attract and trap oxygen ions from HfO_x films.

The Cu top electrode was also investigated, as Cu has higher free energy of oxidation than free energy of oxidation of Hf. However, the Cu/HfO_x/TiN device showed bad resistive switching characteristics. Because Cu is a highly diffusive element in semiconductor materials due to its high diffusion coefficient, they could migrate into the NiO bulk from the top electrode and affect the resistive switching characteristics. The formula as follows.

$$D=D_0 \exp(-Q/KT) \qquad (3\text{-}1)$$

The Pt and Pd top electrodes were also investigated, as Pt and Pd have very high free energy of oxidation than free energy of oxidation of Hf. Therefore, the Pt/HfO_x/TiN and Pd/HfO_x/TiN device showed good resistive switching characteristics, and could sweep with different compliance current. However, sweep with larger compliance current resulted bad endurance. Because Pt and Pd have too higher free energy, when applied a dc voltage, the oxygen ions is direct from HfO_x films to air. Table 3-2 performs the comparison with the free energy of oxide formation of electrode metals and resistive switching parameters of various metals.

In order to confirm our thoughts, we used Pd as top electrode, and injected N_2 6 sccm 30 second. In Fig. 3-28 shows the typical I-V curve. Distribution of V_{SET} and V_{RESET} are shown in Fig. 3-29. Resistance of HRS and LRS by 0.08 V read bias are shown in Fig. 3-30. Form the results, we demonstrates the Pd/HfO_x/TiN with N_2 showed better resistive switching characteristics than the Pd/HfO_x/TiN without N_2. The endurance is significant addition. Because N_2 can block oxygen ions from HfO_x films to air.

Afterward, we used TiN as top electrode under a mixed gas atmosphere with a partial pressure of P(Ar) : P(N_2) = 24 : 9.6. In Fig. 3-31 shows the typical I-V curve. Distribution

of V_{SET} and V_{RESET} are shown in Fig. 3-32. Resistance of HRS and LRS by 0.08 V read bias are shown in Fig. 3-33. Form the results, we demonstrates the TiN/HfO_x/TiN showed better resistive switching characteristics than the Ti/HfO_x/TiN. The endurance is significant addition. Because TiN did not attract and trap oxygen ions from HfO_x films. Table 3-3 performs the comparison with the Pd/HfO_x/TiN with N_2 versus without N_2 and the Ti/HfO_x/TiN versus TiN/HfO_x/TiN.

3.3 Resistive switching characteristics of Pd/Al/HfO_x/TiN structure

In previous discussions, we demonstrates reactive metal (lower free energy of oxidation of the metal) is easier combined with oxygen from resistive switching films and forms metal oxide, which resulted the filaments were not ruptured and no resistive switching characteristics. However, the inert metal (higher free energy of oxidation of the metal) is hard easier combined with oxygen from resistive switching films. Therefore, the inert metal as top electrode has good resistive switching characteristics, but can’t resistive switching in larger compliance current. Because inert metal have too higher free energy, when applied a dc voltage, the oxygen ions is direct from HfO_x films to air. In this paper, we have studied to use two-layer metal as top metal, the first layer is inert metal and the second layer is thin reactive metal, such as Pd/Al, Pt/Ti, etc. Because thin reactive metal can trap oxygen ions to form thin interface layer and avoid oxygen ions from HfO_x films to air, and Inert metal is protection reactive metal which avoid to direct contact with air.

3.3.1 Electrical properties

First, we fixed the thickness of Pd for 30nm, and to change the thickness of Al. In Pd/Al(20 Å)/HfO_x/TiN device, is using the dc voltage sweep method with a current compliance of 5 mA. In Fig. 3-34 shows the typical I-V curve. Distribution of V_{SET} and V_{RESET} are shown in Fig. 3-35. Resistance of HRS and LRS by 0.08 V read bias are shown in Fig. 3-36. The Pd/Al(20 Å)/HfO_x/TiN device shown good resistive switching characteristics. The V_{SET} and V_{RESET} values don't overlap each other, and the endurance is more than 300 cycles.

In Pd/Al(50 Å)/HfO_x/TiN device, is using the dc voltage sweep method with a current compliance of 5 mA. In Fig. 3-37 shows the typical I-V curve. Distribution of V_{SET} and V_{RESET} are shown in Fig. 3-38. Resistance of HRS and LRS by 0.08 V read bias are shown in Fig. 3-39. The Pd/Al(50 Å)/HfO_x/TiN device shown good resistive switching characteristics. The V_{SET} and V_{RESET} values don't overlap each other, and the endurance is more than 550 cycles.

In Pd/Al(75 Å)/HfO_x/TiN device, is using the dc voltage sweep method with a current compliance of 5 mA. In Fig. 3-40 shows the typical I-V curve. Distribution of V_{SET} and V_{RESET} are shown in Fig. 3-41. Resistance of HRS and LRS by 0.08 V read bias are shown in Fig. 3-42. The Pd/Al(75 Å)/HfO_x/TiN device shown good resistive switching characteristics. The V_{SET} and V_{RESET} values don't overlap each other, the endurance is more than 200 cycles, but the yield decreases.

In Pd/Al(100 Å)/HfO_x/TiN device, is using the dc voltage sweep method with a current compliance of 5 mA. In Fig. 3-43 shows the typical I-V curve. Distribution of V_{SET} and V_{RESET} are shown in Fig. 3-44. Resistance of HRS and LRS by 0.08 V read bias are shown in Fig. 3-45. The Pd/Al(100 Å)/HfO_x/TiN device shown good resistive switching characteristics. The V_{SET} and V_{RESET} values don't overlap each other, the endurance is

more than 450 cycles, but the yield decreases.

In Pd/Al(150 Å)/HfO_x/TiN device, is using the dc voltage sweep method with a current compliance of 5 mA. In Fig. 3-46 shows the typical I-V curve for SET process. In Fig. 3-47 shows the typical I-V curve for RESET process. The Pd/Al(150 Å)/HfO_x/TiN device shown bad resistive switching characteristics, the endurance is less than 3 cycles.

In Table 3-4 performs the comparison with the different thickness of Al of Pd/Al/HfO_x/TiN structure and resistive switching parameters of the devices. Form the results, we demonstrates Pd/Al/HfO_x/TiN structure which has good resistive switching characteristics, but thickness of Al is thicker to result that the yield and resistance decrease [69]-[70]. Because thickness of Al is thicker, which forms thicker AlO_x at Al/HfO_x interface to result the filaments were not ruptured.

In order to confirm our thoughts, we etched aboriginal Al/HfO_x/TiN device for etching Al solution. The proportion of chemical solution is H_3PO_4 : HNO_3 : CH_3COOH : H_2O = 50 : 2 : 10 : 9. Afterward, we etched thickness of Al of the device to 30 Å. In Al(30 Å)/HfO_x/TiN device, is using the dc voltage sweep method with a current compliance of 5 mA. In Fig. 3-48 shows the typical I-V curve. Distribution of V_{SET} and V_{RESET} are shown in Fig. 3-49. Resistance of HRS and LRS by 0.08 V read bias are shown in Fig. 3-50. The Al(30 Å)/HfO_x/TiN device has resistive switching phenomenon. Afterward, we used direct sputtering Al 30 Å as top electrode. In Al(30 Å)/HfO_x/TiN device, is using the dc voltage sweep method with a current compliance of 5 mA. In Fig. 3-51 shows the typical I-V curve. Distribution of V_{SET} and V_{RESET} are shown in Fig. 3-52. Resistance of HRS and LRS by 0.08 V read bias are shown in Fig. 3-53. The Al(30 Å)/HfO_x/TiN device has resistive switching phenomenon.

Form the results, we demonstrates thickness of Al is thicker to result that the yield decreases, and thickness of Al is thin, which has resistive switching phenomenon.

However, thickness of Al is too thin to result oxygen ions through AlO_x from HfO_x films to air. Therefore, we chosen Pd/Al(35 Å)/HfO_x/TiN structure. In Pd/Al(35 Å)/HfO_x/TiN device, is using the dc voltage sweep method with a current compliance of 5 mA and 10mA. In Fig. 3-54 and Fig. 3-55 shows the typical I-V curve. Distribution of V_{SET} and V_{RESET} are shown in Fig. 3-56 and Fig. 3-57. Resistance of HRS and LRS by 0.08 V read bias are shown in Fig. 3-58. In Pd/Al(35 Å)/HfO_x/TiN device shown very good resistive switching characteristics. The V_{SET} and V_{RESET} values don' t overlap each other, and the endurance is more than 4000 cycles.

3.3.2 Retention property

For a nonvolatile memory, the data storage time, called retention time, is an important indicator [71]-[77]. It means that how long the stored resistance values can be remained. In order to accelerate the degradation of Pd/HfO_x/TiN structure, the retention test is also tested under the 85 ℃. As showed in Fig. 3-59, the retention time of the two states is at 1000 seconds and the resistance ratio only over 1 by 0.08 V read bias. Afterward, in order to accelerate the degradation of Pd/Al(35 Å)/HfO_x/TiN structure, the retention test is also tested under the 175 ℃, as show in Fig. 3-60. Retention time at the high temperature is at least over 5×10^4 seconds, and the resistance ratio still remains over 50.

3.3.3 Thermal stability

Current transport mechanisms for the LRS and the HRS were analyzed by measuring the I-V curve at the temperature ranging from 25 to 175 ℃. For the LRS, the I-V curve follows Ohm' s law and the resistivity of the HfO_x films shows slightly negative temperature dependence, as shown in Fig. 3-61. Metallic filaments in HfO_x films induced

by the set process may be responsible for this observation. On the other hand, the I-V curve of the HRS, as shown in Fig. 3-62, has positive and weak temperature dependence at low bias. This positive temperature dependence for the HRS current suggests that the dominant current transport mechanism for the Pd/Al/HfO_x/TiN structure during set process may be tunneling, Schottky emission, or Pool-Frenkel emission. However, we ruled out Schottky emission and Pool-Frenkel emission as possible candidates due to the very weak temperature dependence of the HRS current [36], [78]-[84].

3.3.4 Curve fitting of current-voltage plots

Figure 3-63 and Fig. 3-64 show the plot of ln |J| versus ln |V| of our Pd/Al(35 Å)/HfO_x/TiN structure. In the LRS current and HRS current at small bias region, the curve present Ohmic behavior whose slopes are close to unity. The ln $|J/V^2|$ versus 1/V curve is presented in Fig. 3-65. The linear line with a negative slope at the large bias region of the plot shows that the HRS current at large bias is due to the Fowler-Nordheim (FN) tunneling [36], [85]-[93].

In the fitting curve, the filament model for the resistive switching in the Pd/Al(35 Å)/HfO_x/TiN structure can be described as follows: When HfO_x films is destroyed during the forming process, the conductive path is created. An Ohmic current-voltage behavior is observed for devices. As the device was switched back to the HRS, the HfO_x films near the anode is recovered by the partial rupture of filaments near anode/ HfO_x films interface.

3.3.5 Material analyses

In order to analyze Al/HfO_x interface and provide extra information for the elucidation of the switching mechanism, XPS, EDS, and TEM are taken to inspect the

atomic percentage, binding energy in the samples and the cross section view. The further details are described as below.

The depth profile of the chemical composition of Pd/Al/HfO_x structure measured by XPS is shown in Fig. 3-66 and Fig. 3-67. We could see that O_2 and Al at the same depth, which is formed AlO_x at interface. The binding energy of Pd/Al/HfO_x structure measured by XPS is shown Fig. 3-68. The primitive binding energy of Al_2O_3 is 74.4 eV. The peak of plot is close to 74.4 eV, which was demonstrated the AlO_x is formed at interface.

Figure 3-69 is the TEM micrograth of Pd/Al/HfO_x/TiN/Ti/SiO_2/Si structure. Fig. 3-70 is high resolution TEM image of Al/HfO_x interface, which shows Al thickness from 3.5 nm to 9 nm. Therefore, we could demonstrate AlO_x which was formed at Al/HfO_x interface.

Figure 3-71 is EDS analysis of the Al layer, which shows the Al layer has oxygen content. Therefore, we could demonstrate AlO_x which was formed at Al/HfO_x interface.

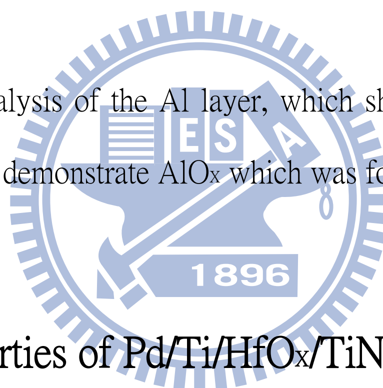

3.3.6 Electrical properties of Pd/Ti/HfO_x/TiN structure

In order to validate our argument, we decided to change the reactive metal. The structure is Pd/Ti(30 Å)/HfO_x/TiN. In the device, is using the dc voltage sweep method with a current compliance of 5 mA. In Fig. 3-72 shows the typical I-V curve. Distribution of V_{SET} and V_{RESET} are shown in Fig. 3-73. Resistance of HRS and LRS by 0.08 V read bias are shown in Fig. 3-74. The Pd/Ti(30 Å)/HfO_x/TiN device shown good resistive switching characteristics. The V_{SET} and V_{RESET} values don't overlap each other, and the endurance is more than 350 cycles.

3.4 Resistive switching characteristics of Pt/Ti/HfO_x/TiN structure

3.4.1 Electrical properties

In order to validate our argument again, we decided to change the inert metal. The structure is Pt/Ti(30 Å)/HfO_x/TiN. In the device, is using the dc voltage sweep method with a current compliance of 5 mA. In Fig. 3-75 shows the typical I-V curve. Distribution of V_{SET} and V_{RESET} are shown in Fig. 3-76. Resistance of HRS and LRS by 0.08 V read bias are shown in Fig. 3-77. The Pt/Ti(30 Å)/HfO_x/TiN device shown good resistive switching characteristics. The V_{SET} and V_{RESET} values don' t overlap each other, and the endurance is more than 800 cycles.

3.4.2 Retention property

For a nonvolatile memory, the data storage time, called retention time, is an important indicator. It means that how long the stored resistance values can be remained. In order to accelerate the degradation of Pt/Ti(30 Å)/HfO_x/TiN structure, the retention test is also tested under the 85 ℃, as show in Fig. 3-78. Retention time at the high temperature is at least over 10^5 seconds, and the resistance ratio still remains over 100.

3.4.3 Curve fitting of current-voltage plots

Figure 3-79 and Fig. 3-80 show the plot of ln |J| versus ln |V| of our Pt/Ti(30 Å)/HfO_x/TiN structure. In the LRS current and HRS current at small bias region, the curve present Ohmic behavior whose slopes are close to unity. The ln $|J/V^2|$ versus 1/V curve is presented in Fig. 3-81. The linear line with a negative slope at the large bias region of the

plot shows that the HRS current at large bias is due to the Fowler-Nordheim (FN) tunneling.

3.4.4 Material analyses

In order to analyze Ti/HfO_x interface and provide extra information for the elucidation of the switching mechanism, XPS is taken to inspect the atomic percentage, binding energy in the sample. The further details are described as below.

The depth profile of the chemical composition of Pt/Ti/HfO_x structure measured by XPS is shown in Fig. 3-82 and Fig. 3-83. We could see that O_2 and Ti at the same depth, which is formed TiO_x at interface. The binding energy of Pt/Ti/HfO_x structure measured by XPS is shown Fig. 3-84. The primitive binding energy of TiO_2 is 458.7 eV. The peak of plot is close to 458.7 eV, which was demonstrated the TiO_x is formed at interface.

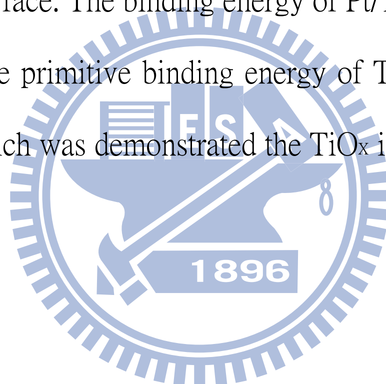

Metal	Pt	Pd	Ni	Cu	Ti	Al
V_{SET} (V)	μ A: 2.4~4.4 mA: 1.52~3.2	μ A: 2.72~3.92 mA: 0.96~1.76	1.2~2.32	1.28~2	1.12~2.8	X
V_{RESET} (V)	μ A: 1.12~3.6 mA: 0.8~1.12	μ A: 1.68~3.04 mA: 0.48~0.72	0.4~0.88	0.48~0.96	0.48~0.88	X
Average R_{HRS} (Ohm)	μ A: 15274427465 mA: 15430474	μ A: 1030318585 mA: 49097	22342	5502	18143	X
Average R_{LRS} (Ohm)	μ A: 114171 mA: 108	μ A: 349478 mA: 77	51	171	131	X
Average Ratio	μ A: 133786 mA: 142875	μ A: 2948 mA: 638	438	32	139	X
Endurance (Cycles)	μ A: >1200 mA: 5~15	μ A: 200~400 mA: 15~30	250~600	5~10	30~50	X
Work function (eV)	5.65	5.12	5.15	4.65	4.33	4.28

Table 3-1 Comparison with the work function and resistive switching parameters of various metals.

Metal	Pt	Pd	Cu	Ni	Ti	Al
V_{SET} (V)	μ A: 2.4~4.4 mA: 1.52~3.2	μ A: 2.72~3.92 mA: 0.96~1.76	1.28~2	1.2~2.32	1.12~2.8	X
V_{RESET} (V)	μ A: 1.12~3.6 mA: 0.8~1.12	μ A: 1.68~3.04 mA: 0.48~0.72	0.48~0.96	0.4~0.88	0.48~0.88	X
Average R_{HRS} (Ohm)	μ A: 15274427465 mA: 15430474	μ A: 1030318585 mA: 49097	5502	22342	18143	X
Average R_{LRS} (Ohm)	μ A: 114171 mA: 108	μ A: 349478 mA: 77	171	51	131	X
Average Ratio	μ A: 133786 mA: 142875	μ A: 2948 mA: 638	32	438	139	X
Endurance (Cycles)	μ A: >1200 mA: 5~15	μ A: 200~400 mA: 15~30	5~10	250~600	30~50	X
Free energies of the formation of oxides (KJ/mole)	High	High	Medium	Medium	Low	Low

Table 3-2 Comparison with the free energy of oxide formation of electrode metals and resistive switching parameters of various metals.

Metal	Pd	Pd (N_2 6 sccm 30s)	Ti	TiN
V_{SET} (V)	0.96~1.76	1.2~2.32	1.12~2.8	1.2~4.4
V_{RESET} (V)	0.48~0.72	0.4~0.88	0.48~0.88	0.4~1.2
Average R_{HRS} (Ohm)	49097	82107	18143	5984679
Average R_{LRS} (Ohm)	77	50	131	67
Average Ratio	638	1642	139	89324
Endurance (Cycles)	15~30	60~85	30~50	150~200
Free energies of the formation of oxides (KJ/mole)	High	High	Low	Low

Table 3-3 Comparison with the Pd/HfO_x/TiN with N_2 versus without N_2 and the Ti/HfO_x/TiN versus TiN/HfO_x/TiN.

Metal	Pd	Al	Pd/Al(20 Å)	Pd/Al(50 Å)	Pd/Al(75 Å)	Pd/Al(100 Å)	Pd/Al(150 Å)
V_{SET} (V)	0.96~1.76	X	0.96~2.08	0.96~2.16	1.04~2.04	0.8~2.24	X
V_{RESET} (V)	0.48~0.72	X	0.32~0.8	0.4~0.96	0.4~0.8	0.32~0.8	X
Average R_{HRS} (Ohm)	49097	X	25066	13680	10497	6891	X
Average R_{LRS} (Ohm)	77	X	47	62	56	69	X
Average Ratio	638	X	533	221	447	99	X
Endurance (Cycles)	15~30	X	> 300	> 550	> 200	> 450	< 3
Yield	Medium	X	High	High	Medium	Low	X

Table 3-4 Comparison with the different thickness of Al of Pd/Al/HfO_x/TiN structure and resistive switching parameters of the deivces.

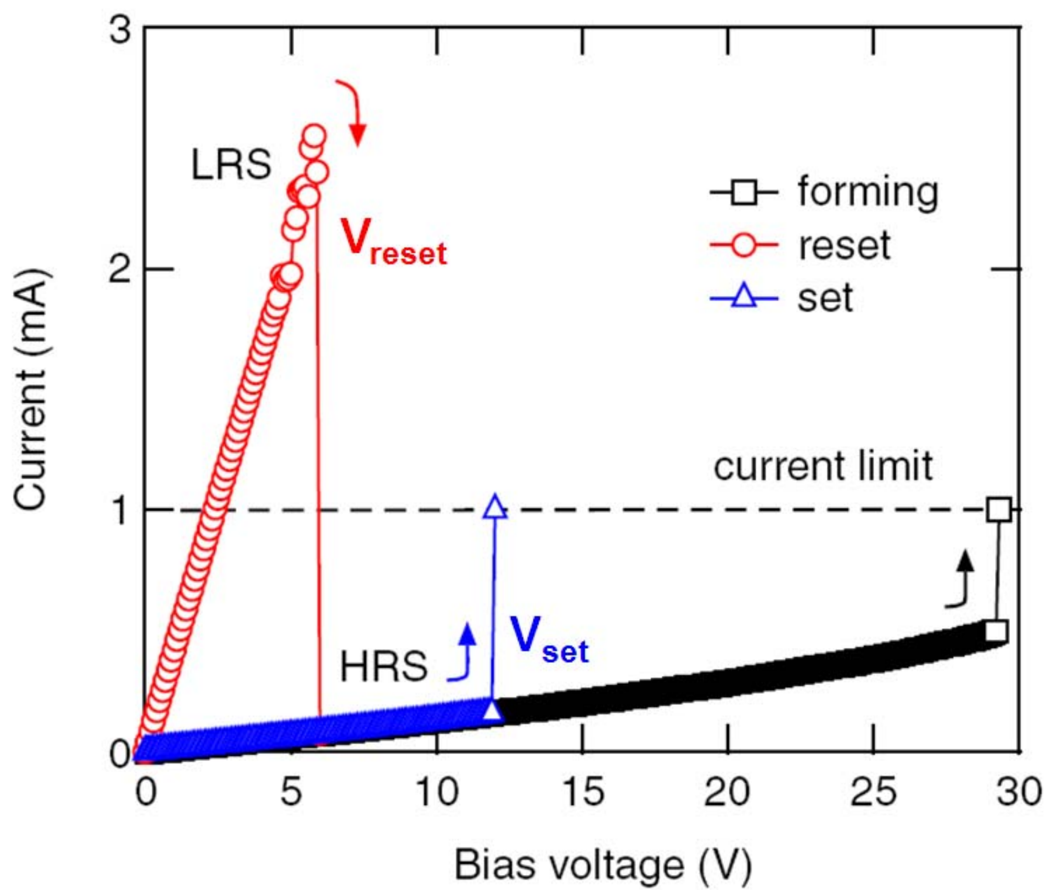

Fig. 3-1 Typical I-V characteristics of unipolar resistive switching.

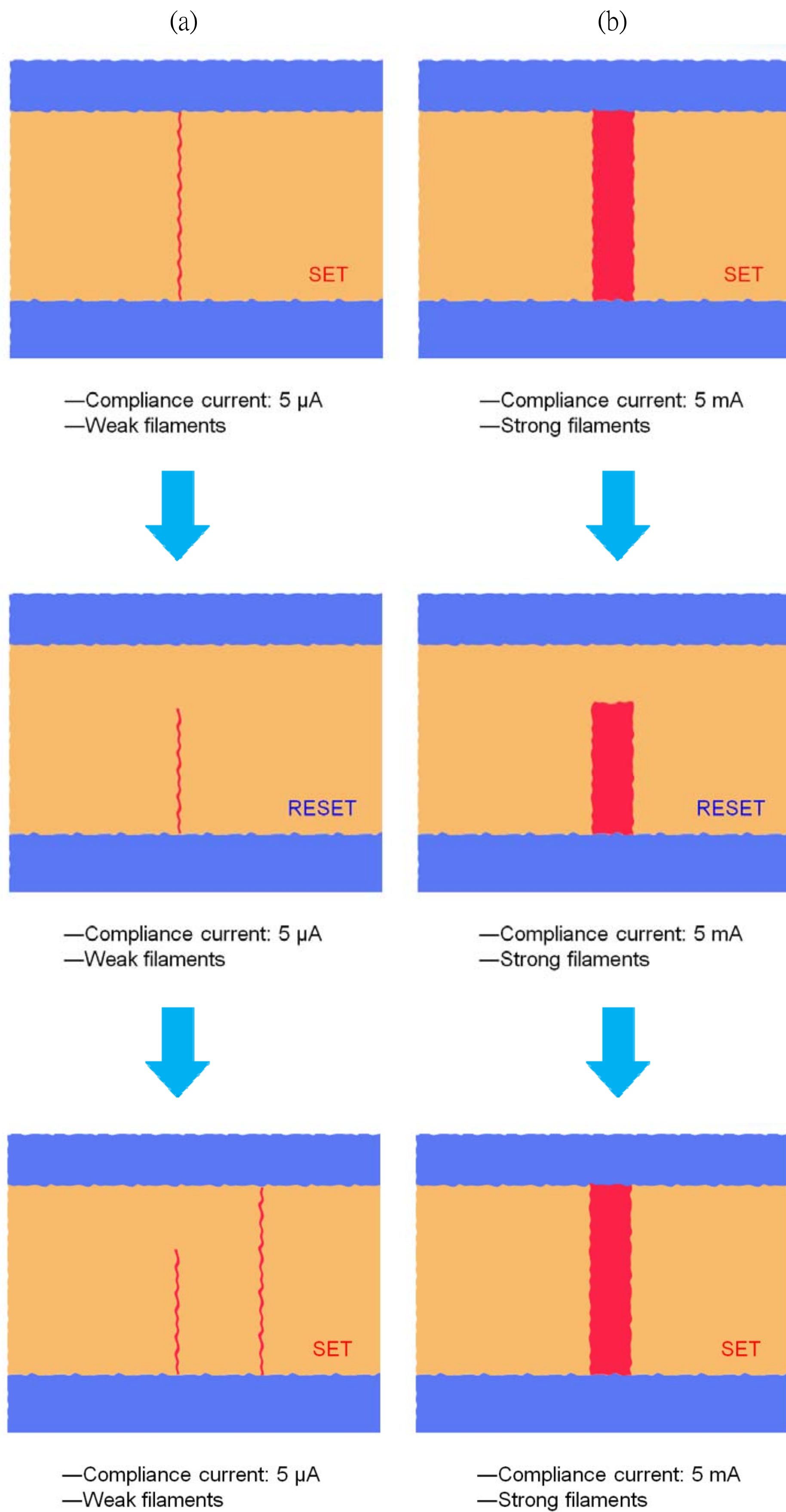

Fig. 3-2 Various compliance current of RRAM. (a) 5 μA (b) 5 mA.

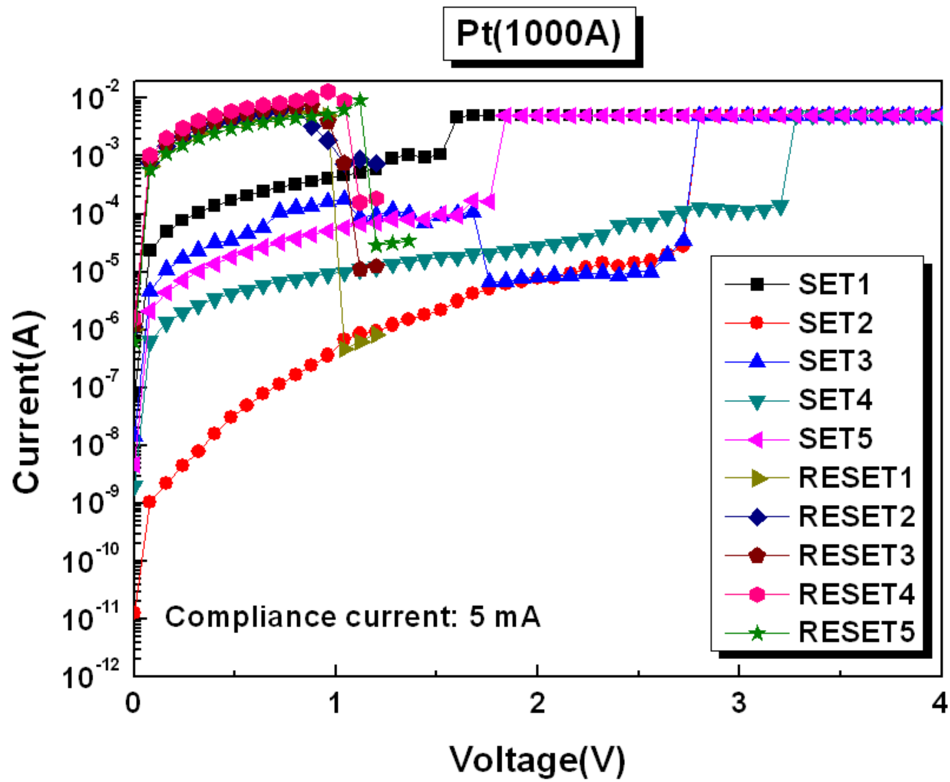

Fig. 3-3 The typical I-V curve of Pt/HfO_x/TiN structure (5 mA).

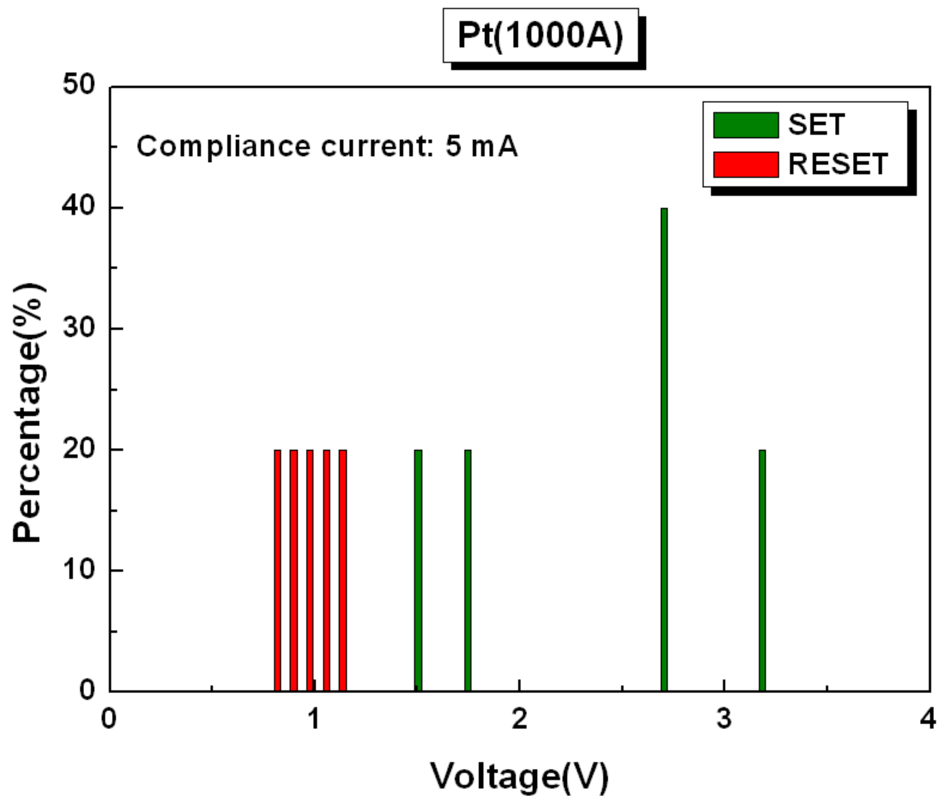

Fig. 3-4 Distribution of V_{SET} and V_{RESET} of Pt/HfO_x/TiN structure (5 mA).

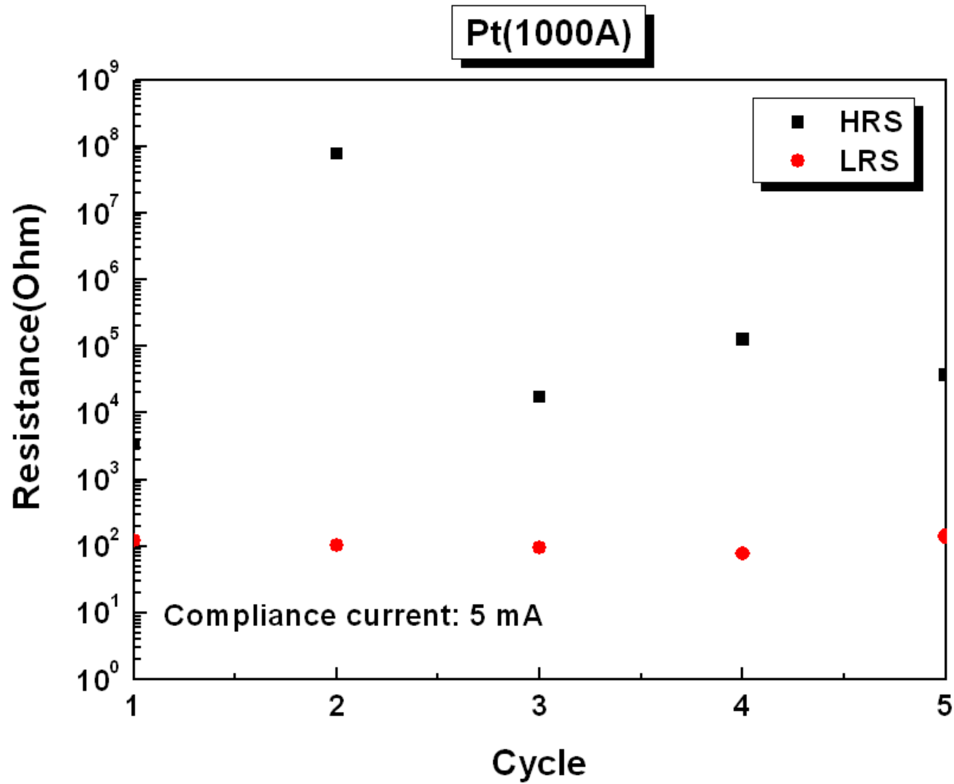

Fig. 3-5 Resistance of HRS and LRS of Pt/HfOx/TiN structure by 0.08 V read bias (5 mA).

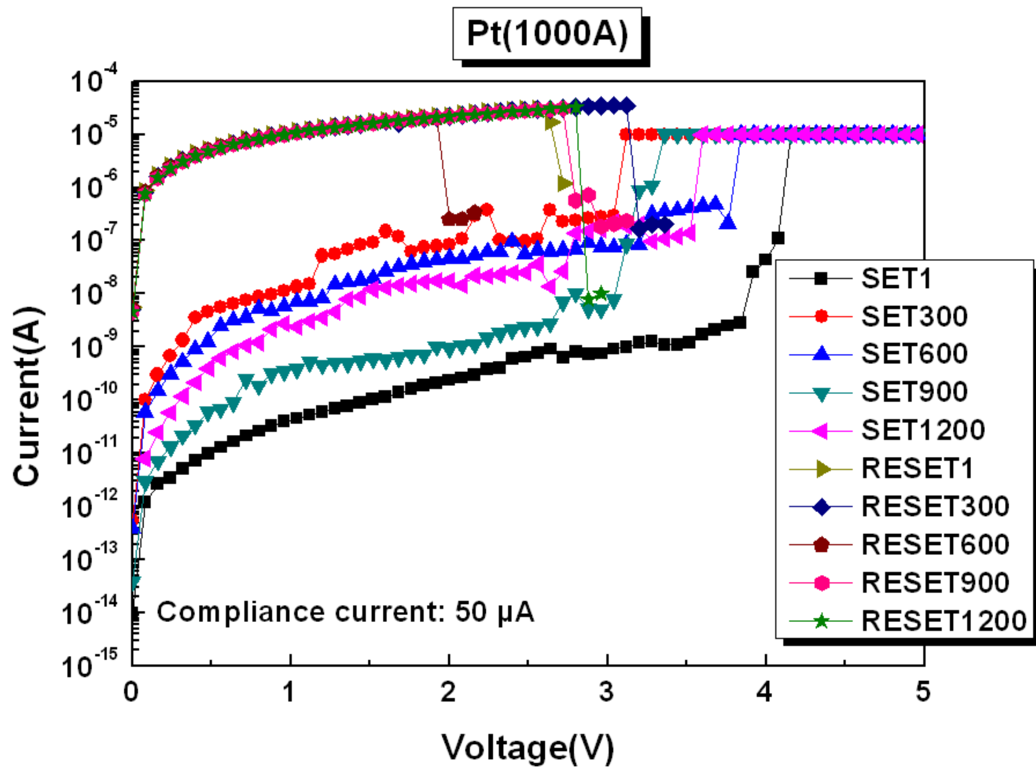

Fig. 3-6 The typical I-V curve of Pt/HfOx/TiN structure (50 μA).

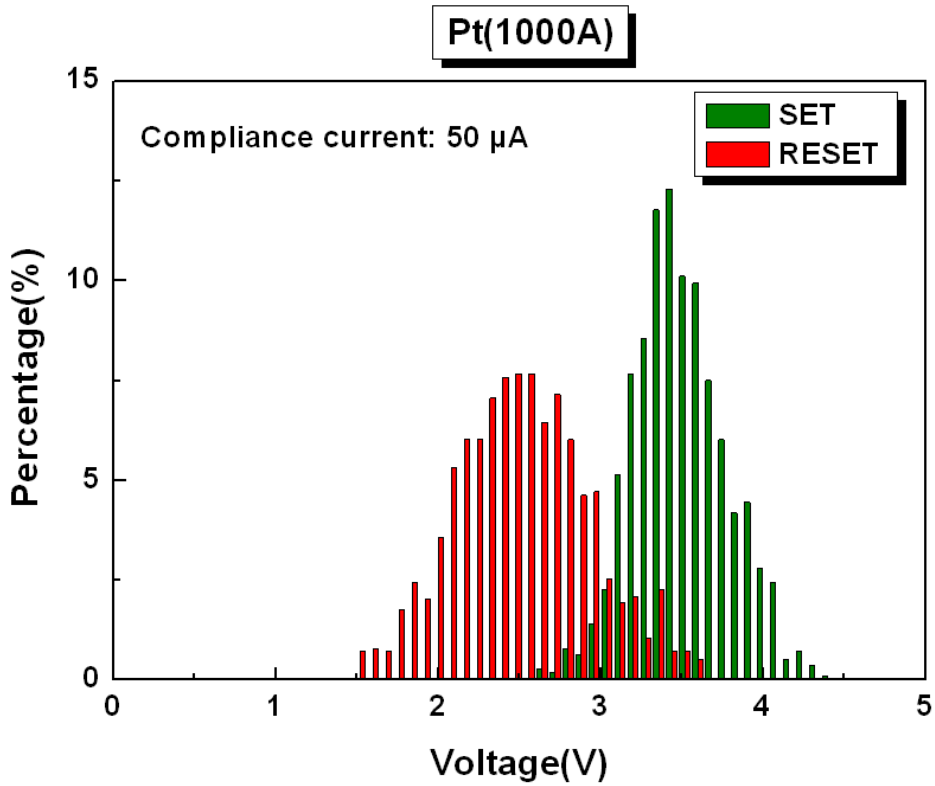

Fig. 3-7 Distribution of V_{SET} and V_{RESET} of Pt/HfOx/TiN structure (50 μA).

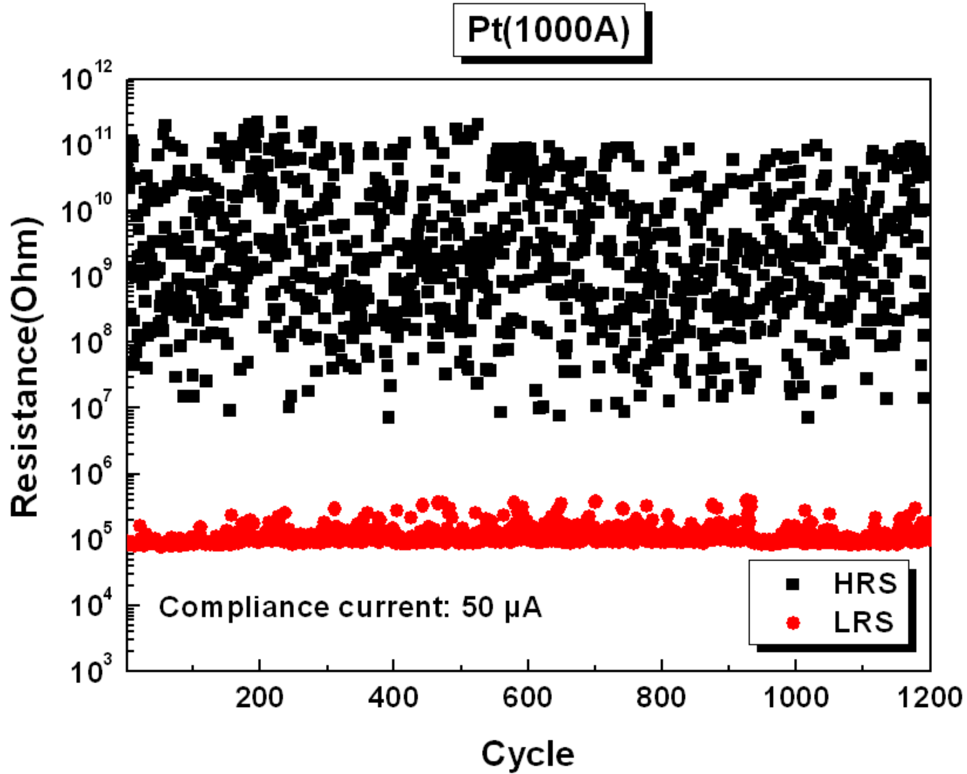

Fig. 3-8 Resistance of HRS and LRS of Pt/HfOx/TiN structure by 0.08 V read bias (50 μA).

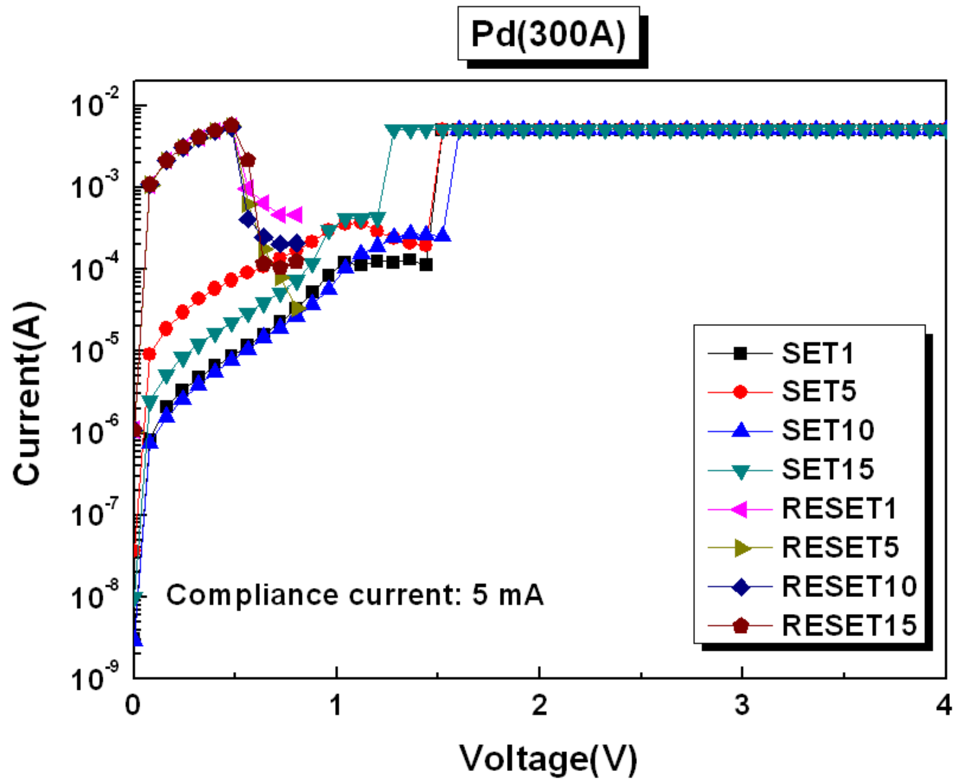

Fig. 3-9 The typical I-V curve of Pd/HfOx/TiN structure (5 mA).

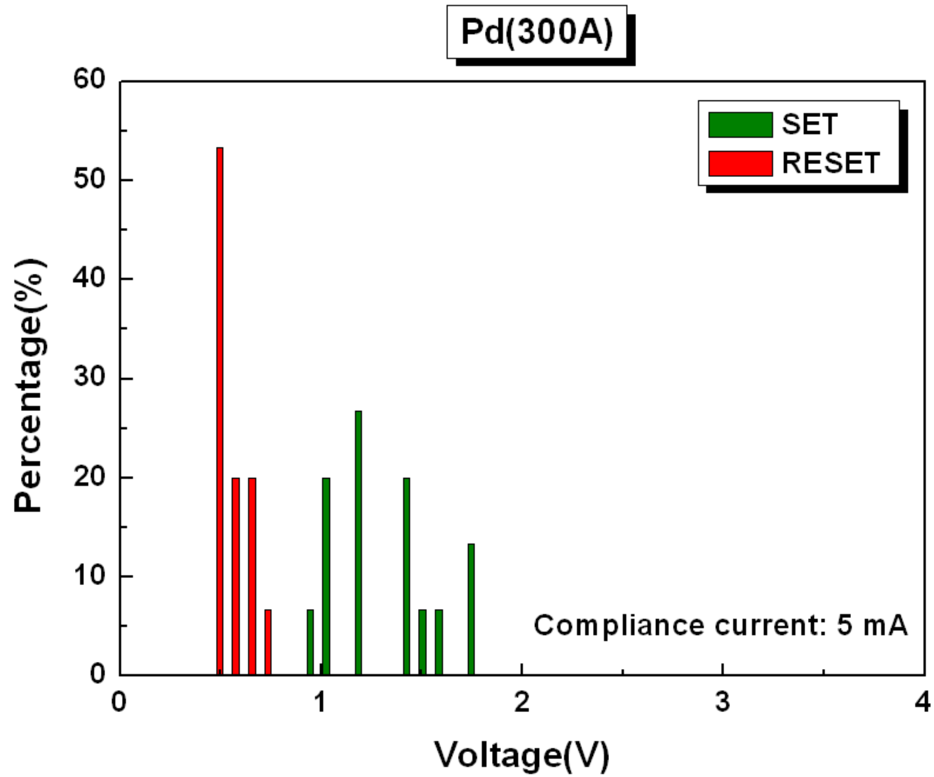

Fig. 3-10 Distribution of V_{SET} and V_{RESET} of Pd/HfOx/TiN structure (5 mA).

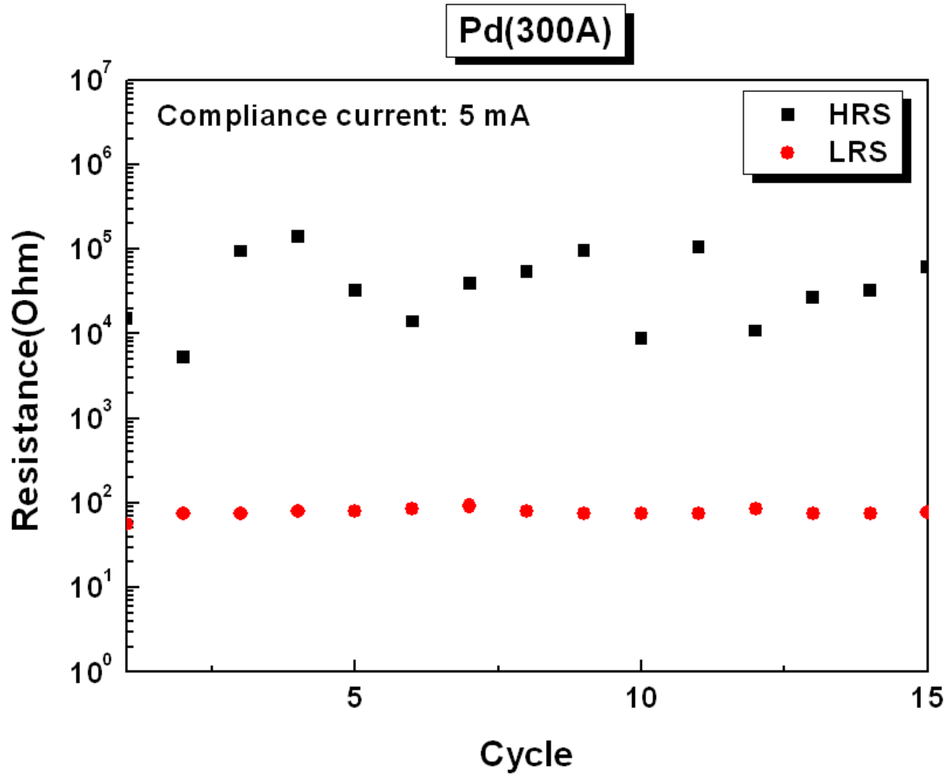

Fig. 3-11 Resistance of HRS and LRS of Pd/HfO_x/TiN structure by 0.08 V read bias (5 mA).

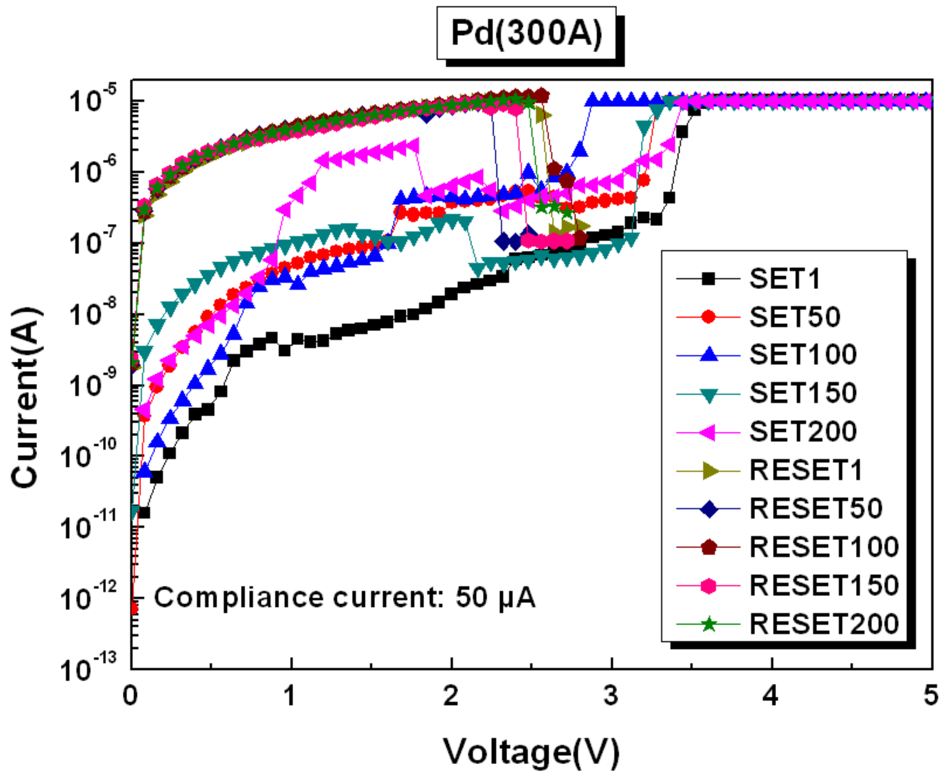

Fig. 3-12 The typical I-V curve of Pd/HfO_x/TiN structure (50 μA).

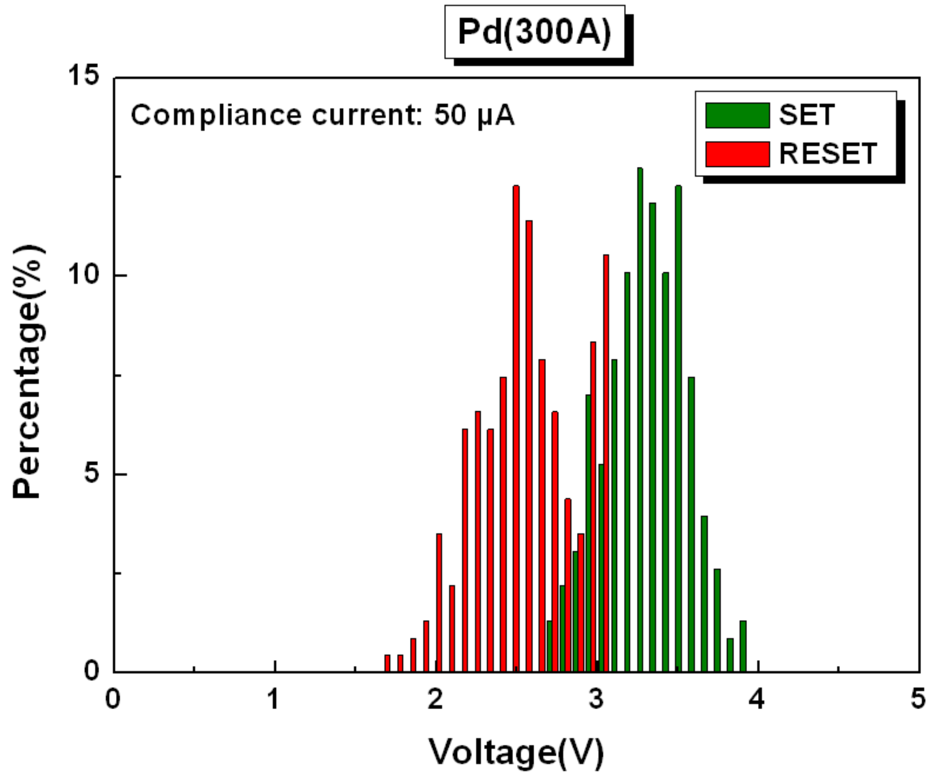

Fig. 3-13 Distribution of V_{SET} and V_{RESET} of Pd/HfOx/TiN structure (50 μA).

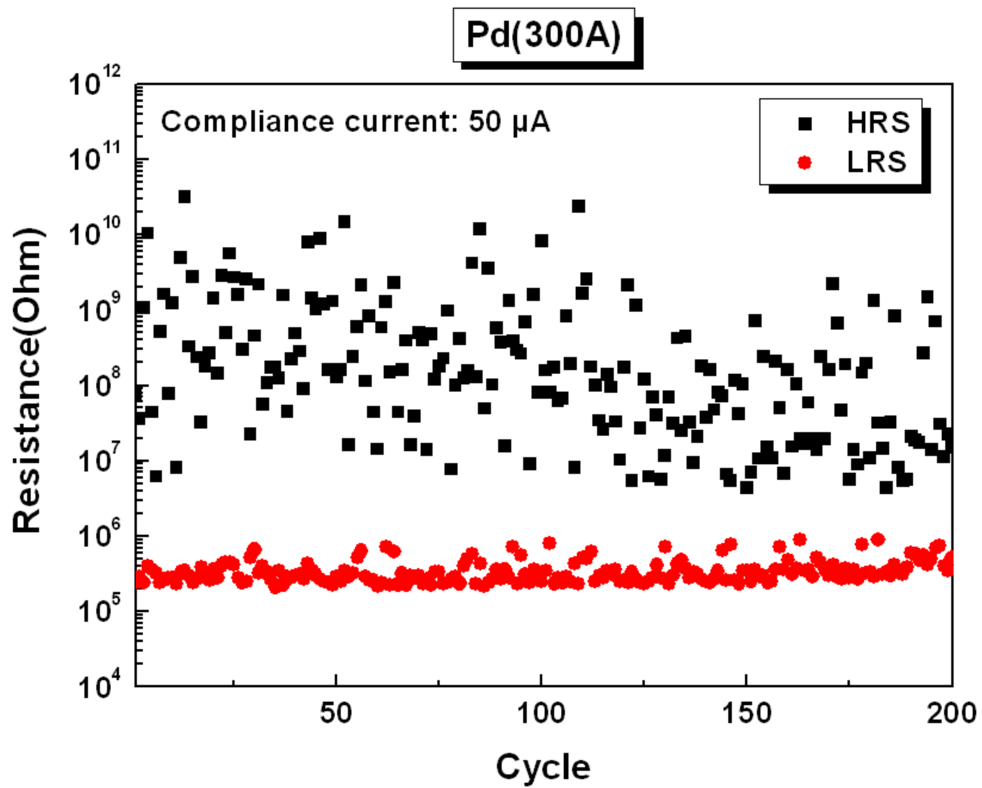

Fig. 3-14 Resistance of HRS and LRS of Pd/HfOx/TiN structure by 0.08 V read bias (50 μA).

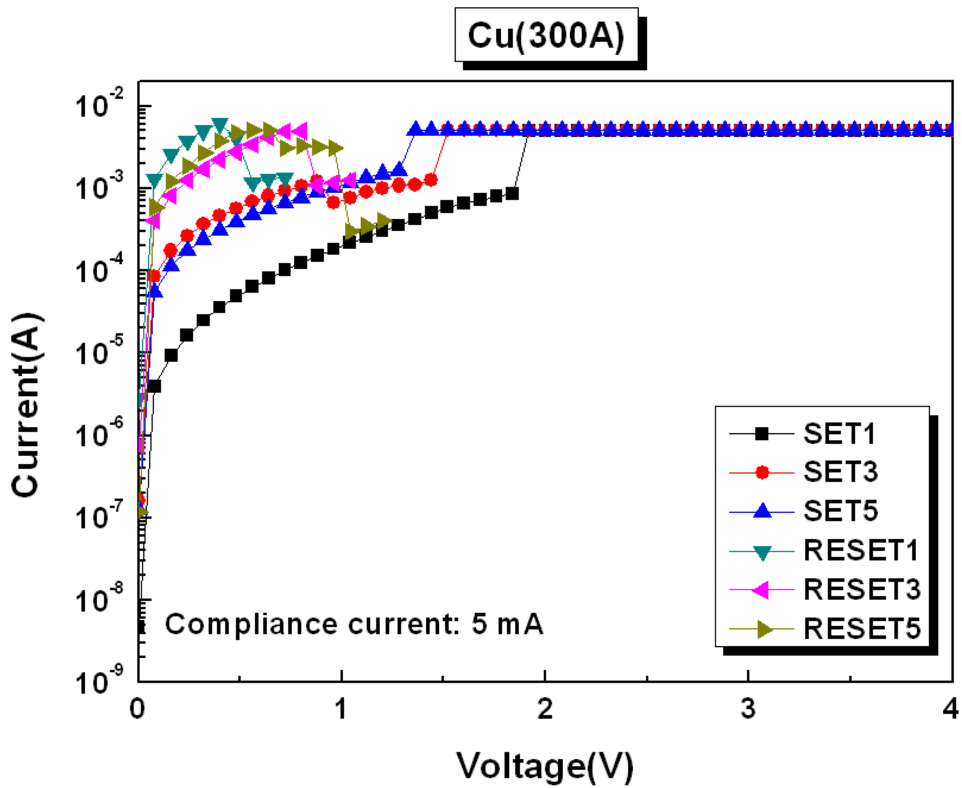

Fig. 3-15 The typical I-V curve of Cu/HfOx/TiN structure.

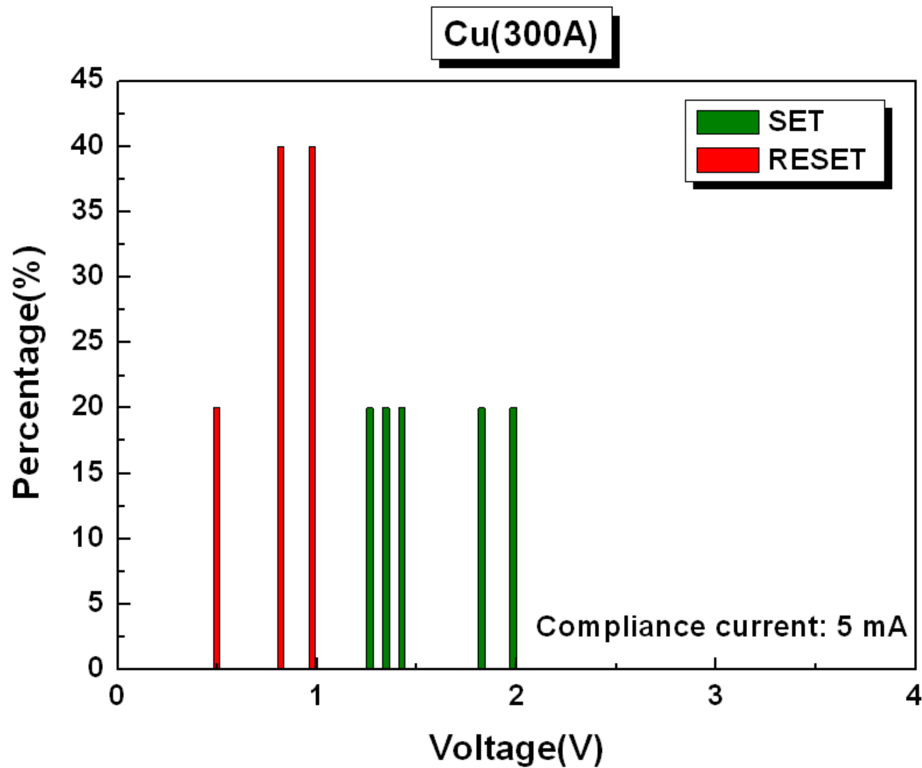

Fig. 3-16 Distribution of V_{SET} and V_{RESET} of Cu/HfOx/TiN structure.

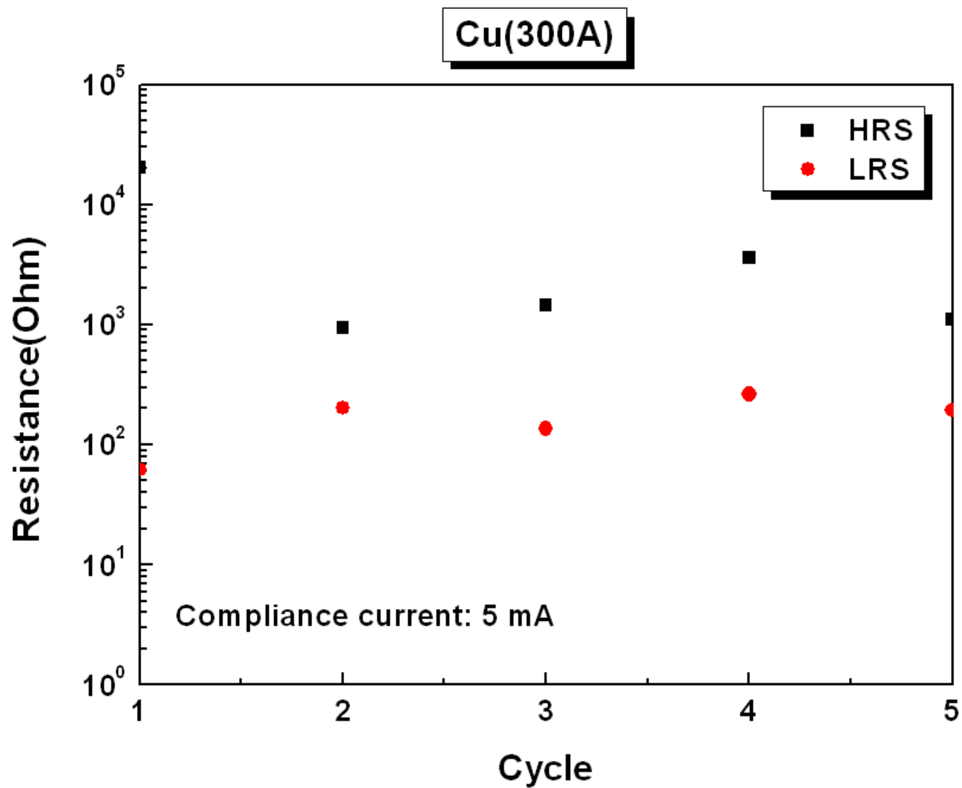

Fig. 3-17 Resistance of HRS and LRS of Cu/HfO_x/TiN structure by 0.08 V read bias.

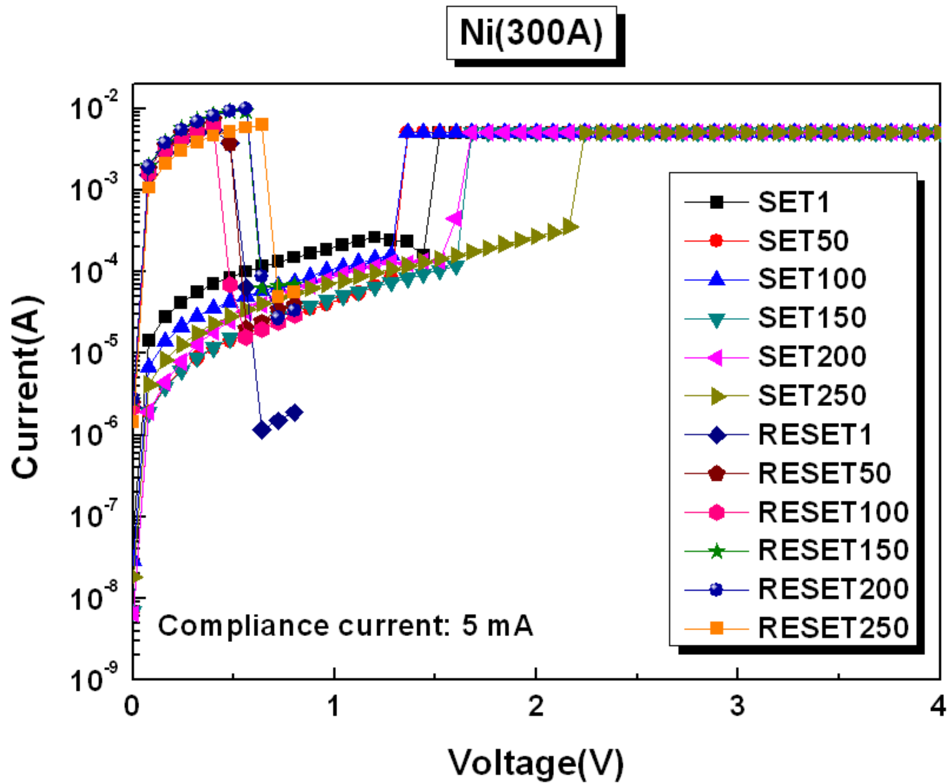

Fig. 3-18 The typical I-V curve of Ni/HfO_x/TiN structure.

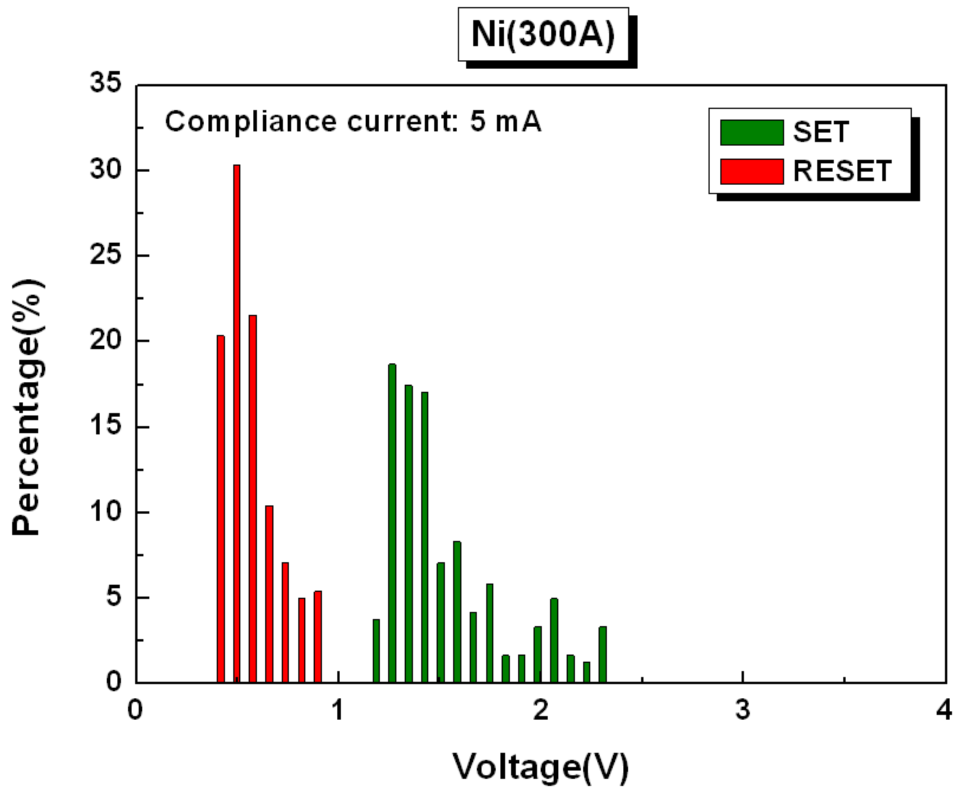

Fig. 3-19 Distribution of V_{SET} and V_{RESET} of Ni/HfOx/TiN structure.

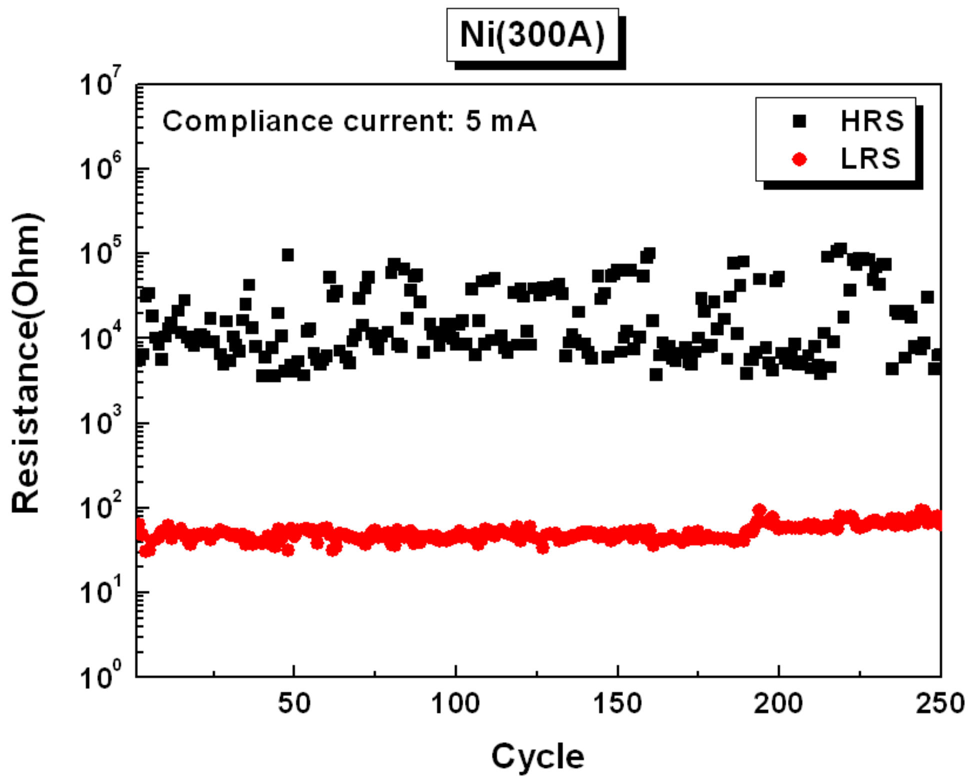

Fig. 3-20 Resistance of HRS and LRS of Ni/HfOx/TiN structure by 0.08 V read bias.

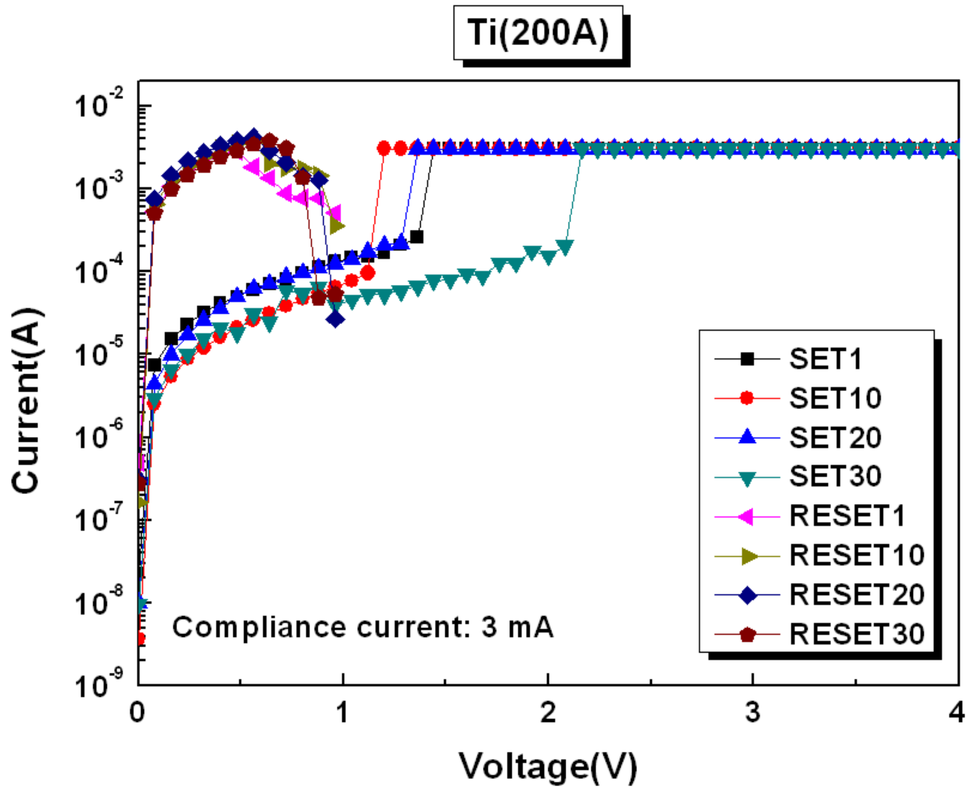

Fig. 3-21 The typical I-V curve of Ti/HfO_x/TiN structure.

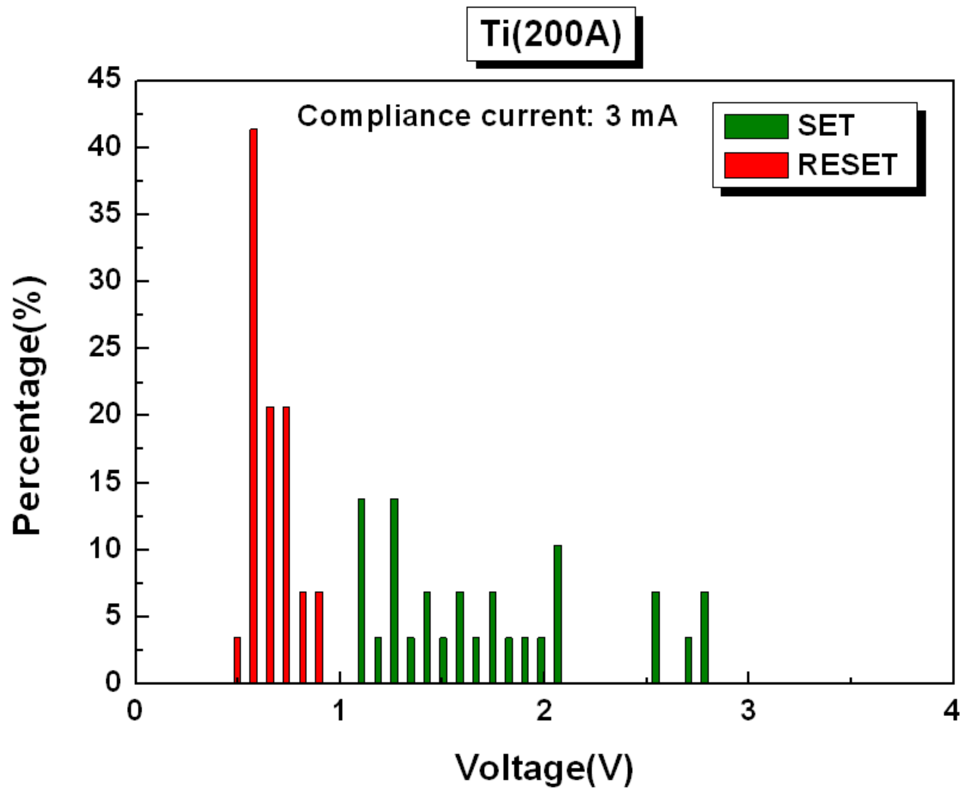

Fig. 3-22 Distribution of V_{SET} and V_{RESET} of Ti/HfO_x/TiN structure.

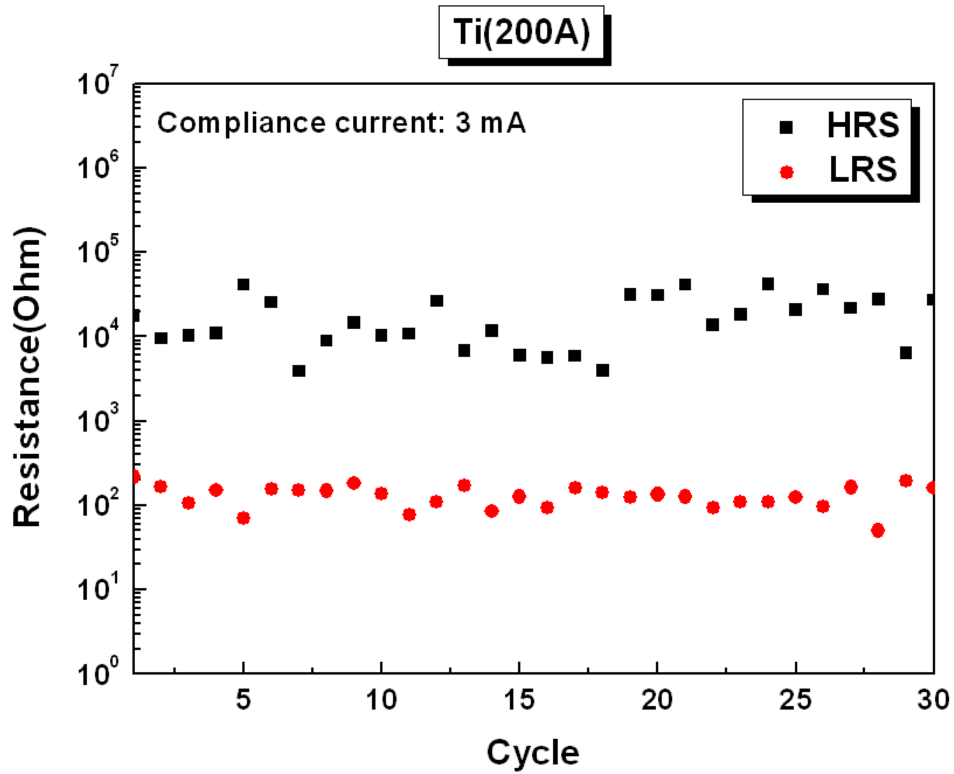

Fig. 3-23 Resistance of HRS and LRS of Ti/HfOx/TiN structure by 0.08 V read bias.

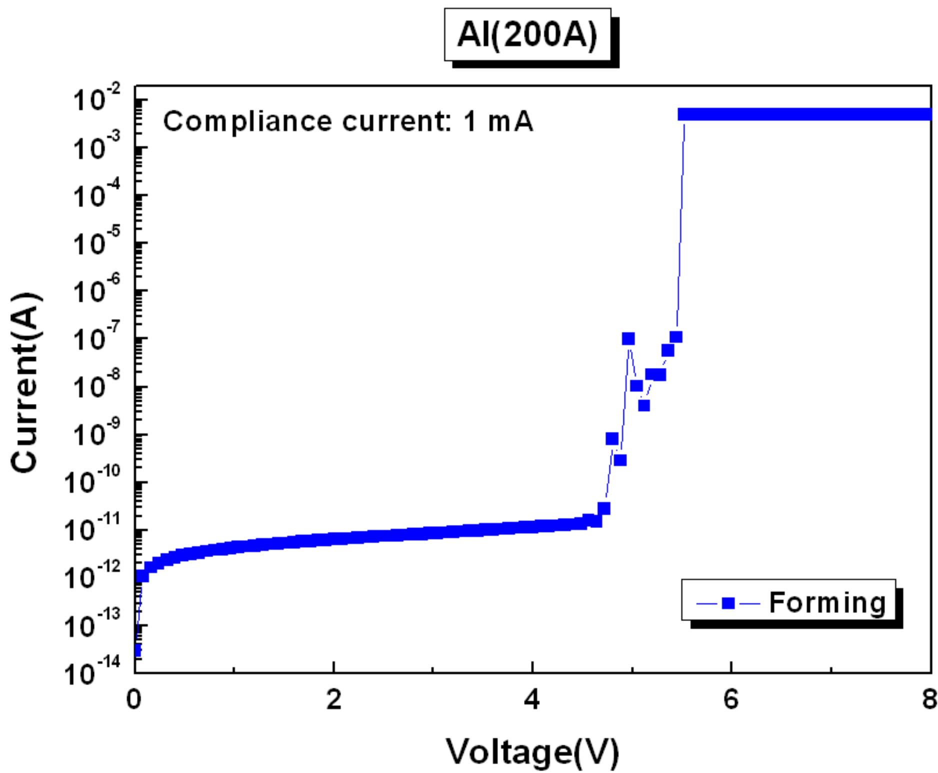

Fig. 3-24 Forming process of Al/HfOx/TiN structure.

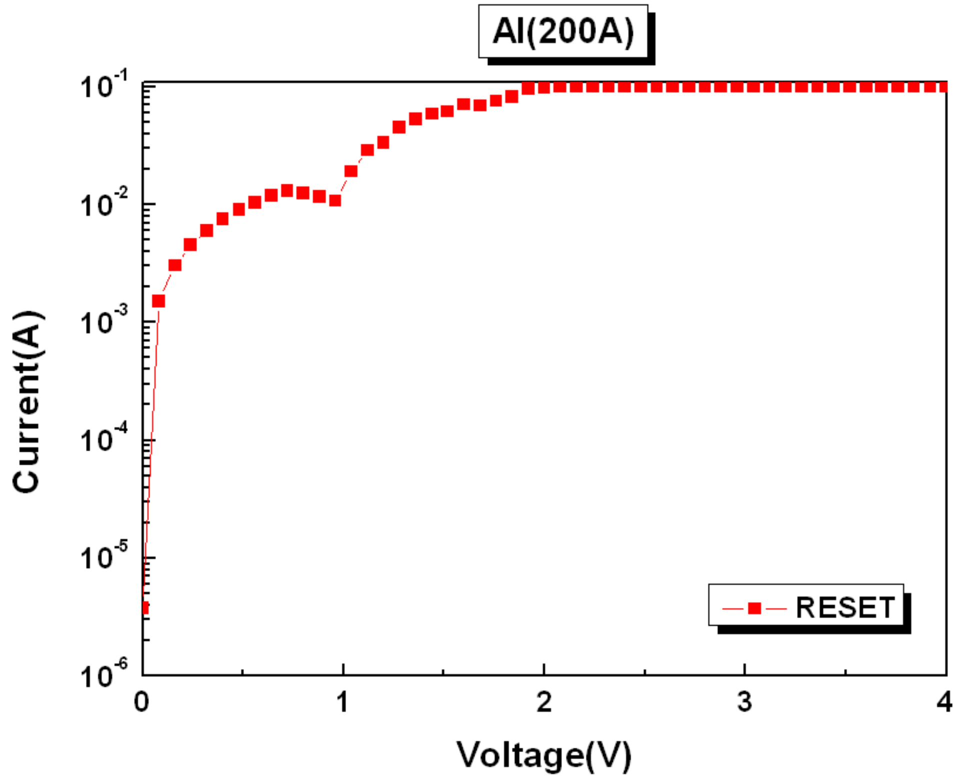

Fig. 3-25 RESET process of Al/HfOx/TiN structure.

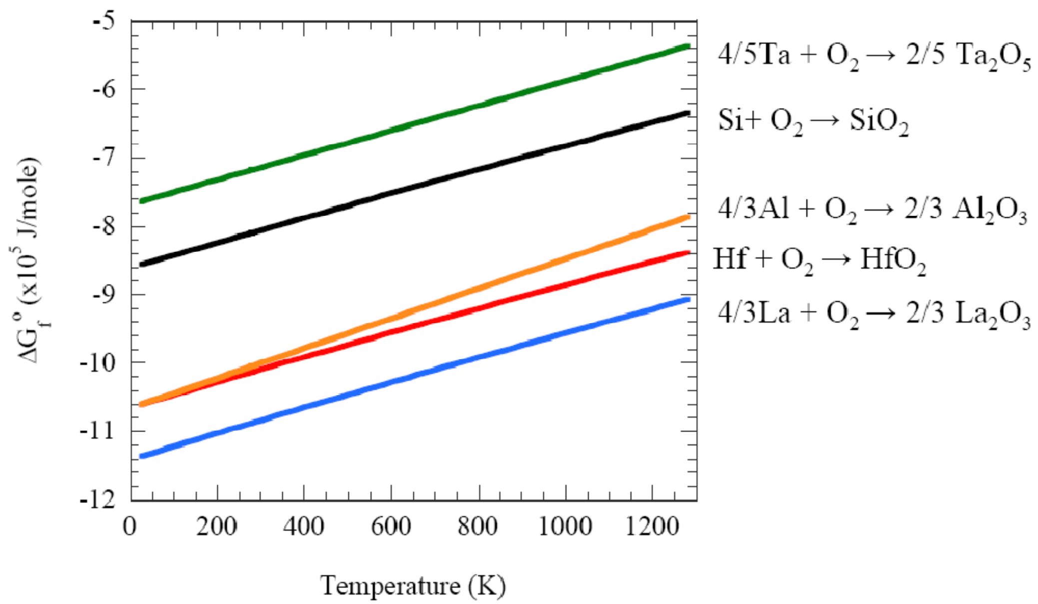

Fig. 3-26 Ellingham diagram of representative high-κ dielectrics showing the free energy of formation as a function of temperature.

Ellingham Diagrams

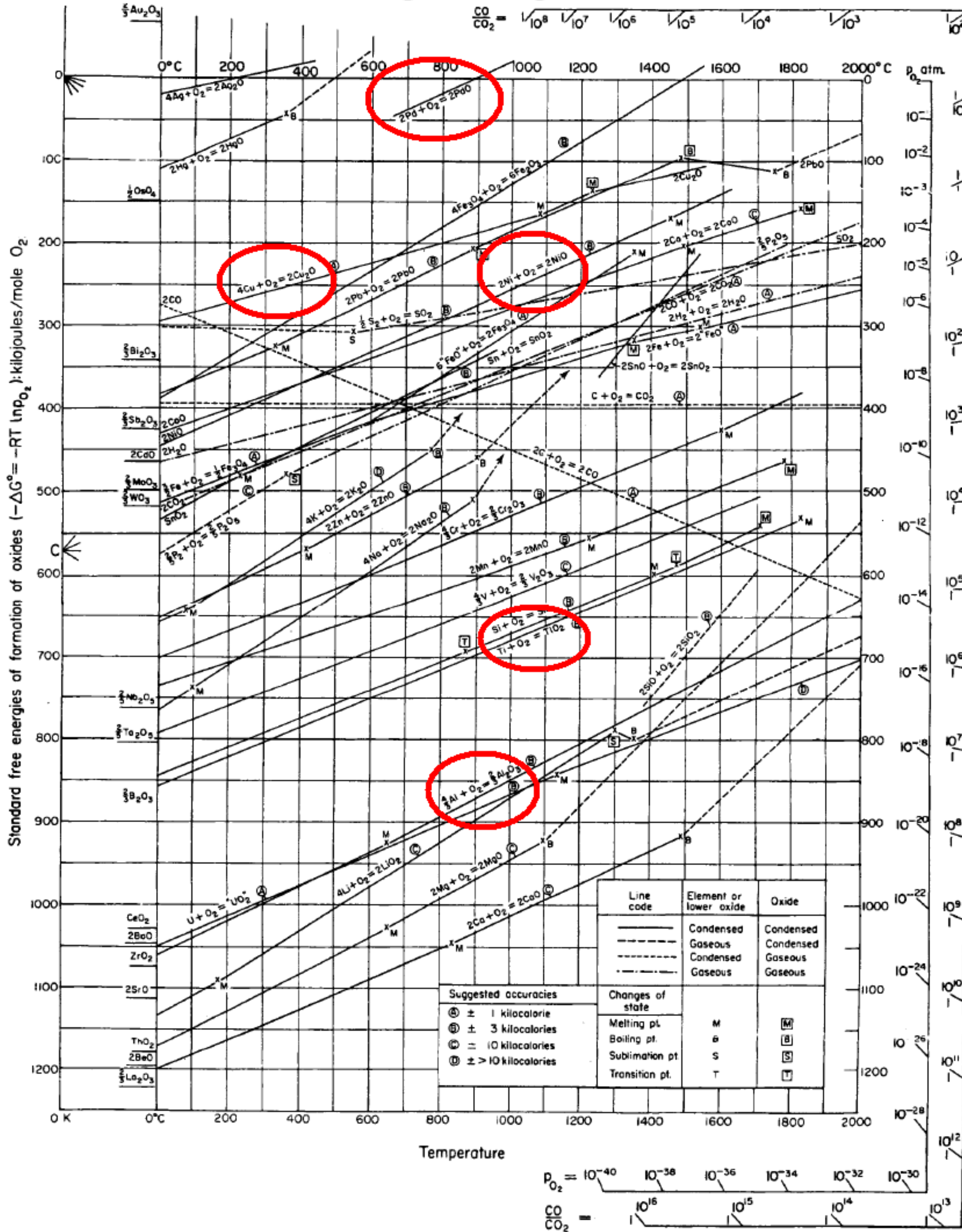

Fig. 3-27 Ellingham diagram plotting the standard free energies of the formation of oxides of the metals.

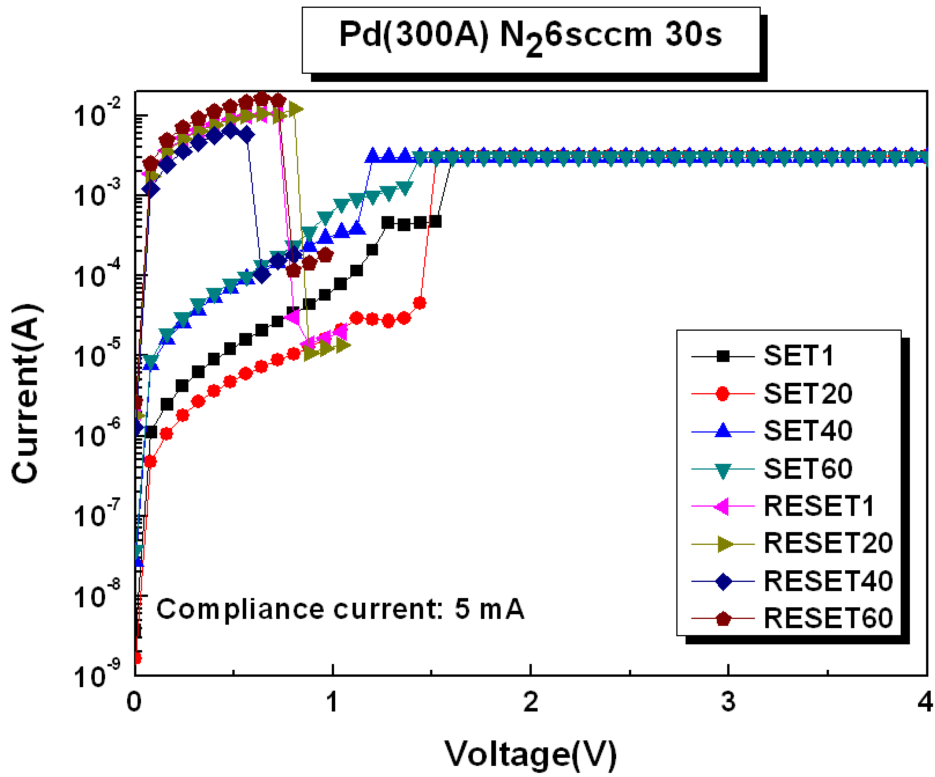

Fig. 3-28 The typical I-V curve of Pd/HfO_x/TiN structure with N_2 6 sccm 30 second.

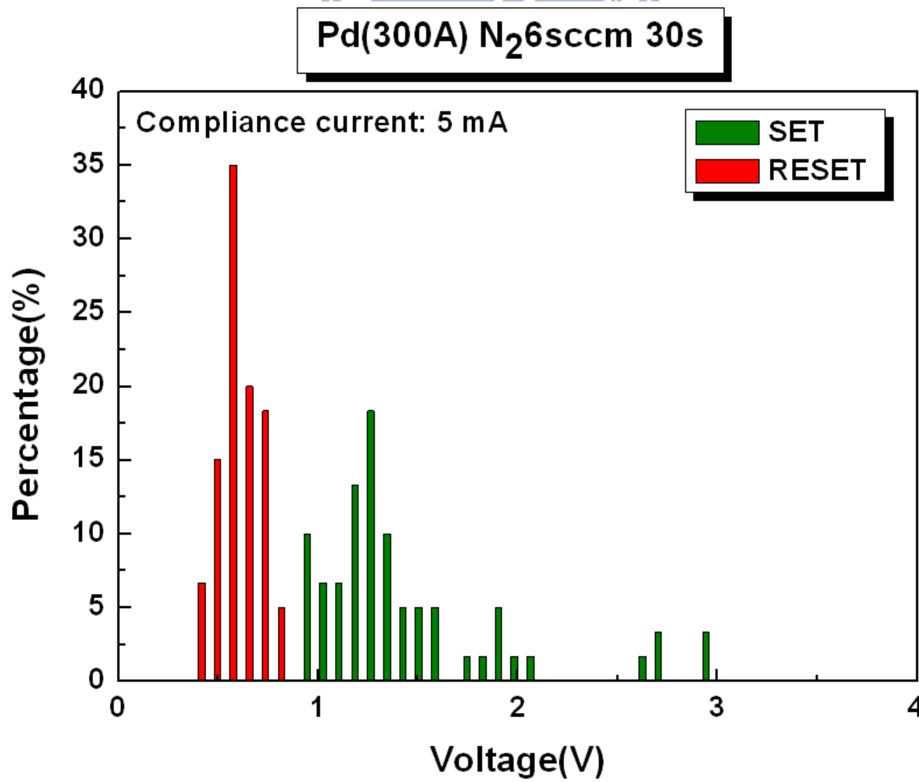

Fig. 3-29 Distribution of V_{SET} and V_{RESET} of Pd/HfO_x/TiN structure with N_2 6 sccm 30 second.

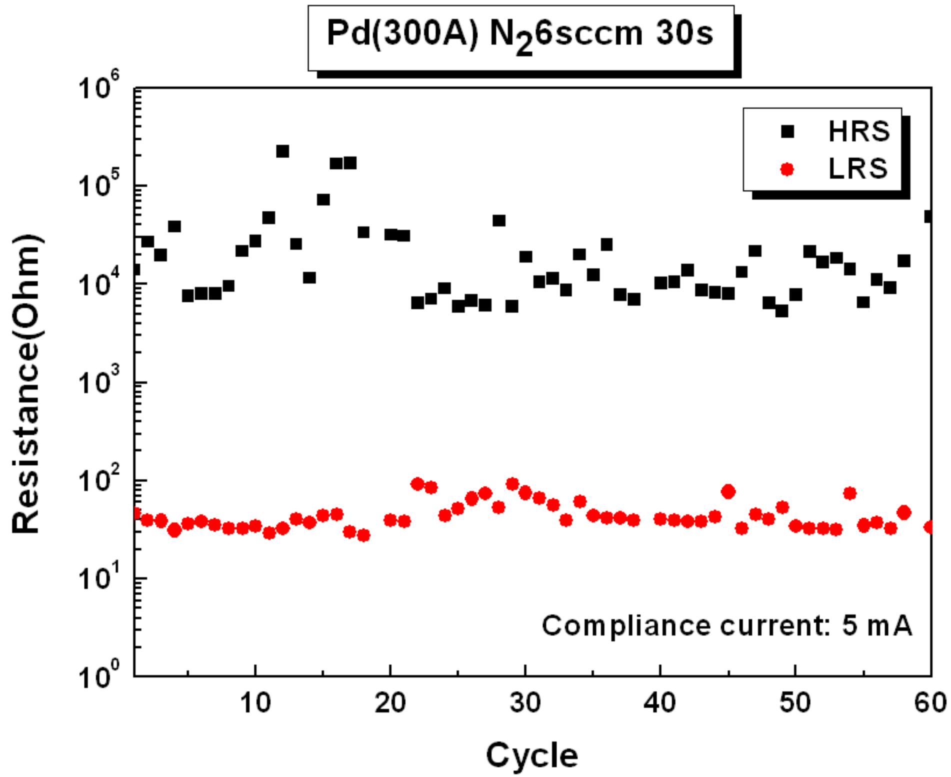

Fig. 3-30 Resistance of HRS and LRS of Pd/HfOx/TiN structure with N_2 6 sccm 30 second by 0.08 V read bias.

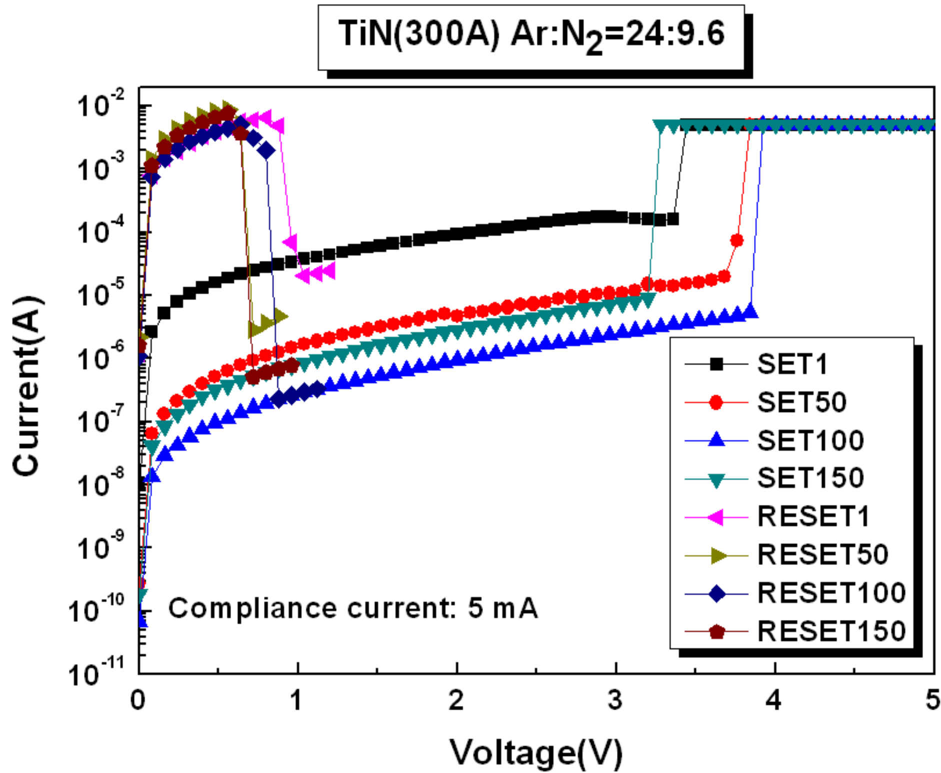

Fig. 3-31 The typical I-V curve of TiN/HfOx/TiN structure.

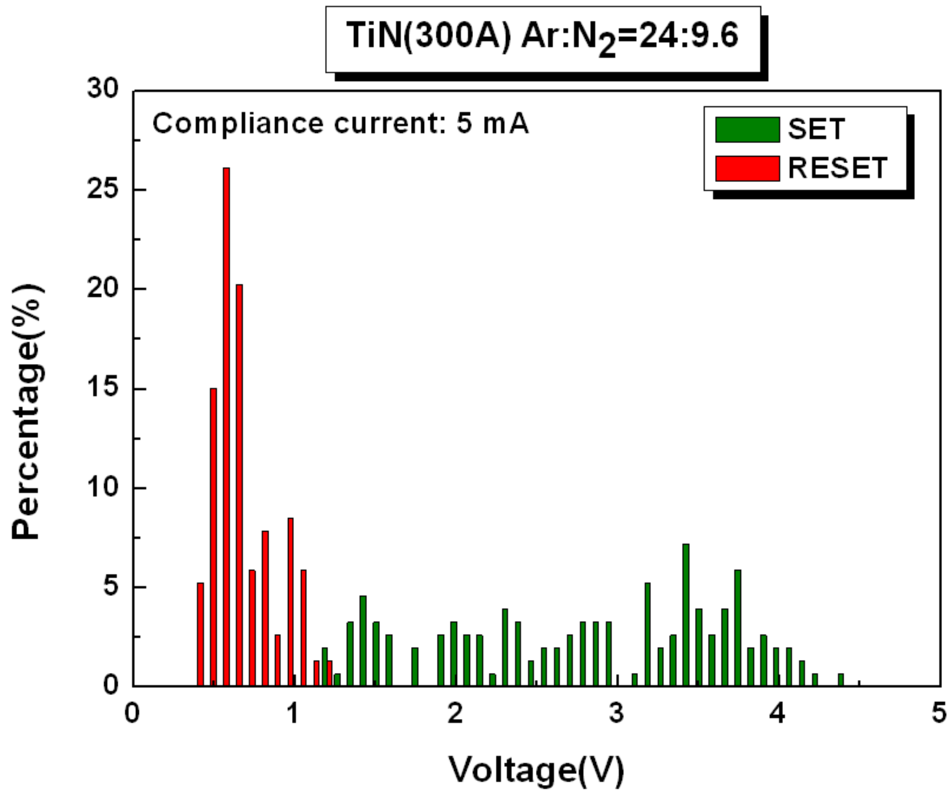

Fig. 3-32 Distribution of V_{SET} and V_{RESET} of TiN/HfO_x/TiN structure.

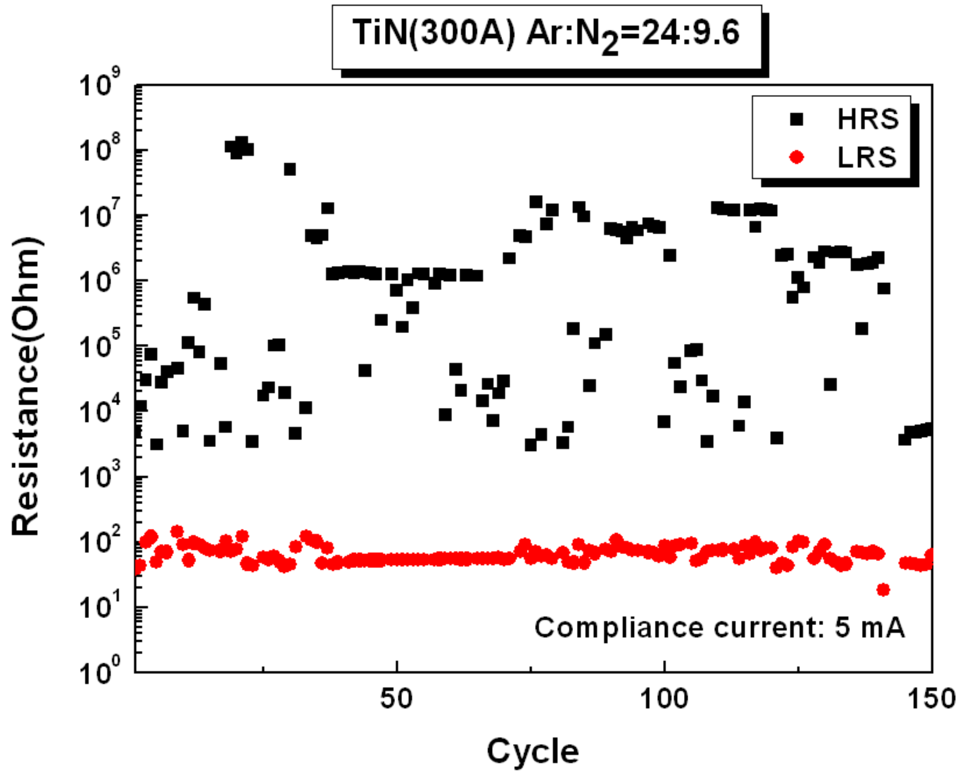

Fig. 3-33 Resistance of HRS and LRS of TiN/HfO_x/TiN structure by 0.08 V read bias.

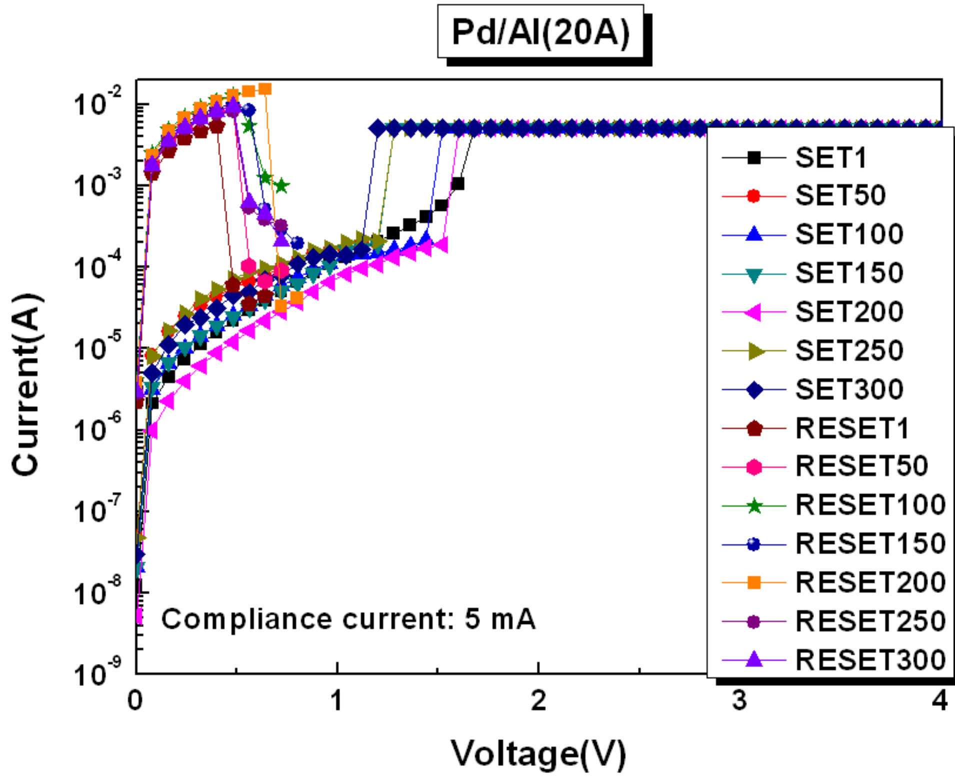

Fig. 3-34 The typical I-V curve of Pd/Al(20 Å)/HfO_x/TiN structure.

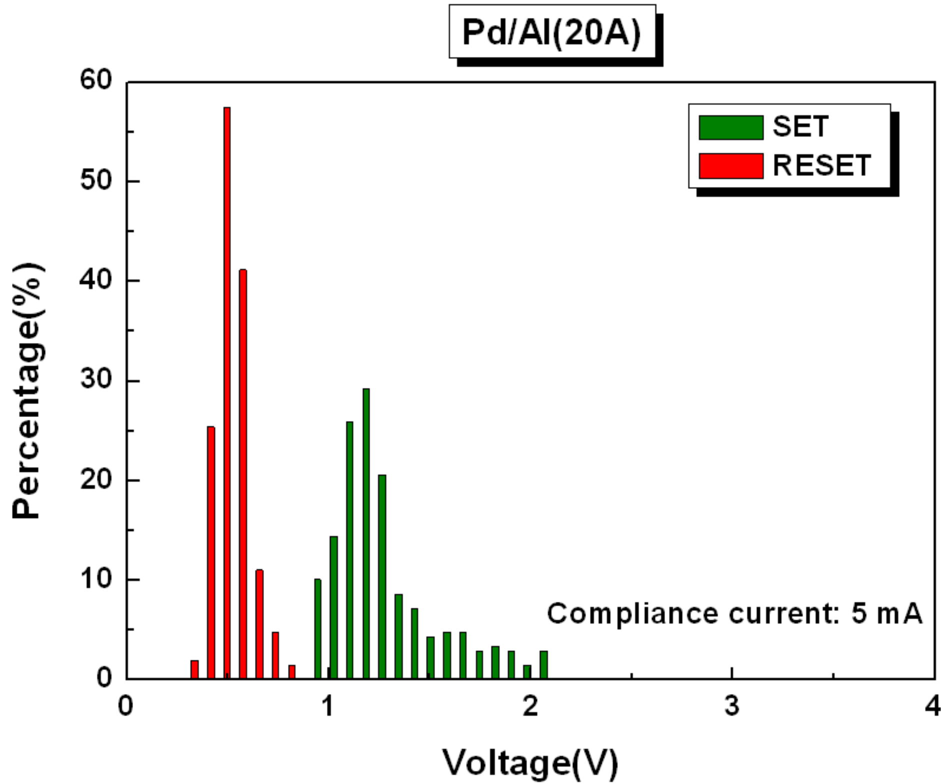

Fig. 3-35 Distribution of V_{SET} and V_{RESET} of Pd/Al(20 Å)/HfO_x/TiN structure.

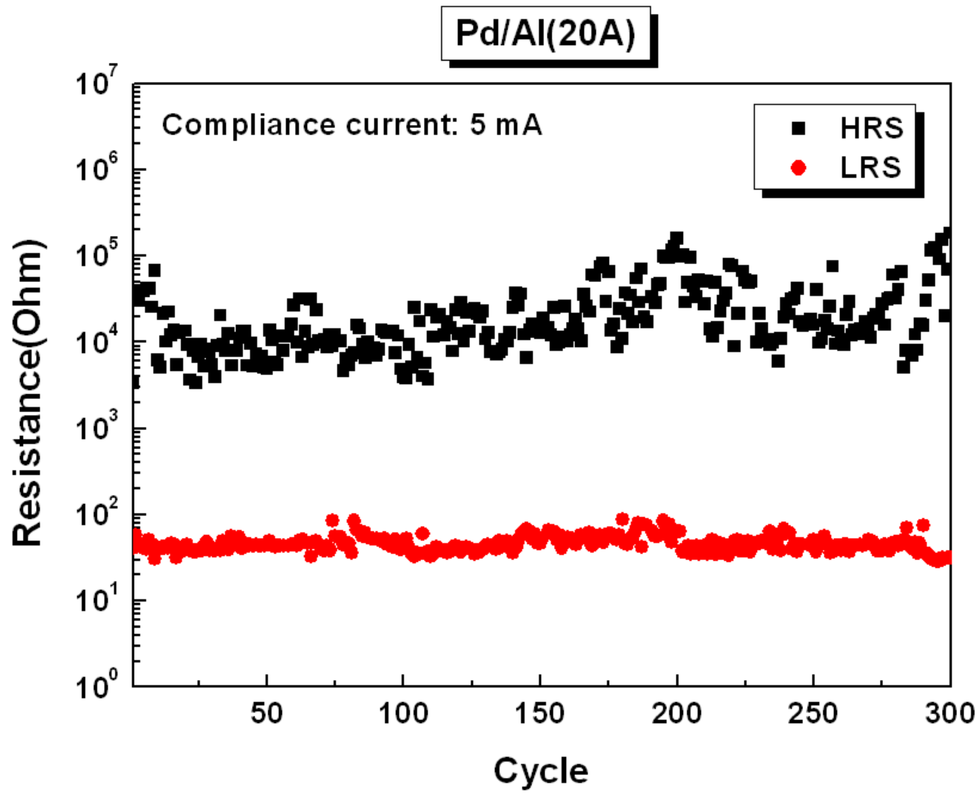

Fig. 3-36 Resistance of HRS and LRS of Pd/Al(20 Å)/HfO_x/TiN structure by 0.08 V read bias.

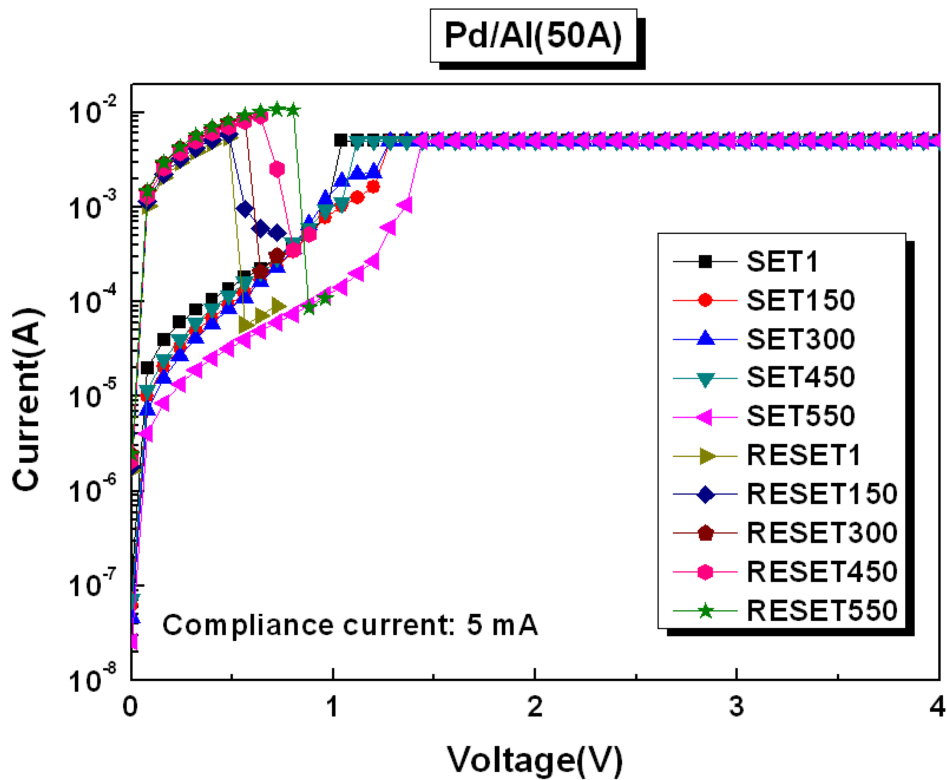

Fig. 3-37 The typical I-V curve of Pd/Al(50 Å)/HfO_x/TiN structure.

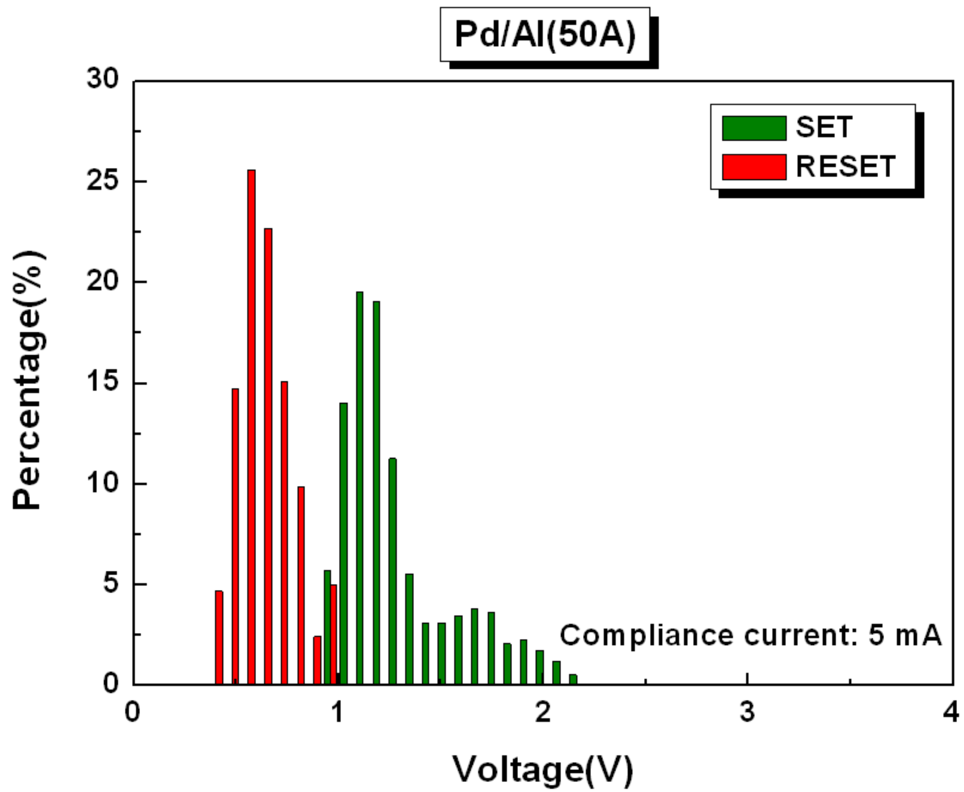

Fig. 3-38 Distribution of V_{SET} and V_{RESET} of Pd/Al(50 Å)/HfO_x/TiN structure.

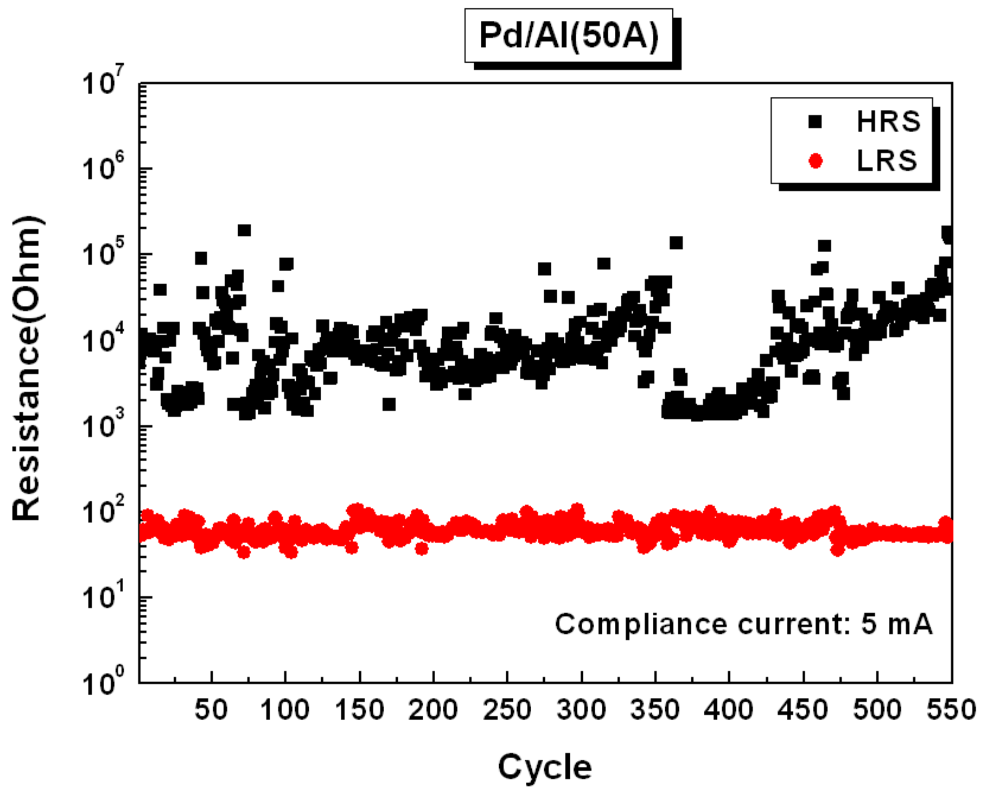

Fig. 3-39 Resistance of HRS and LRS of Pd/Al(50 Å)/HfO_x/TiN structure by 0.08 V read bias.

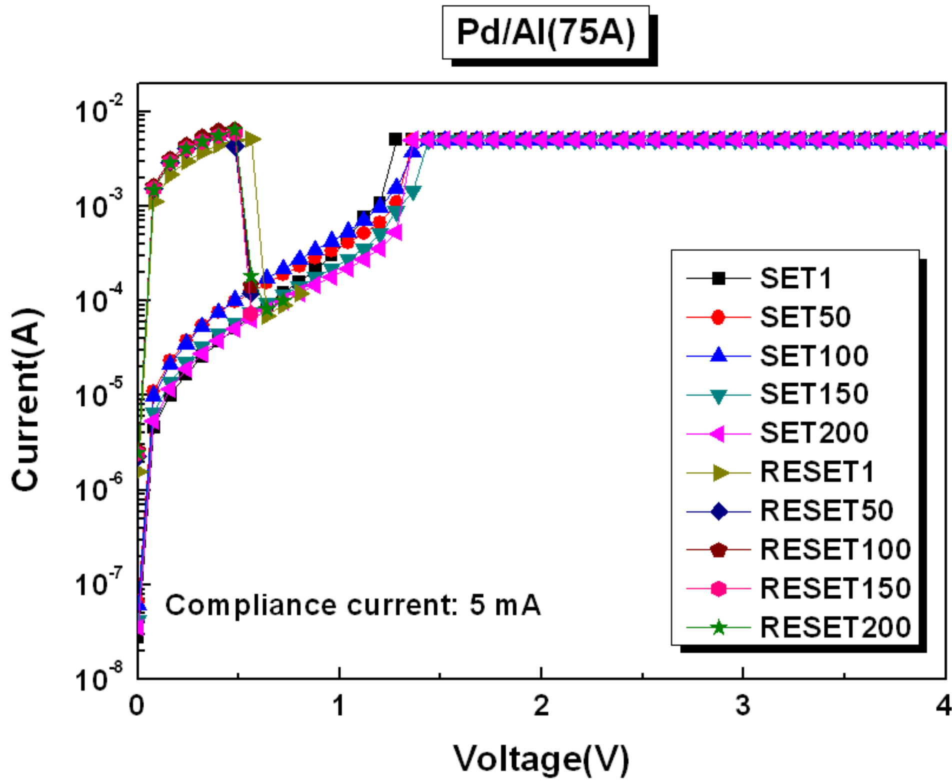

Fig. 3-40 The typical I-V curve of Pd/Al(75 Å)/HfO_x/TiN structure.

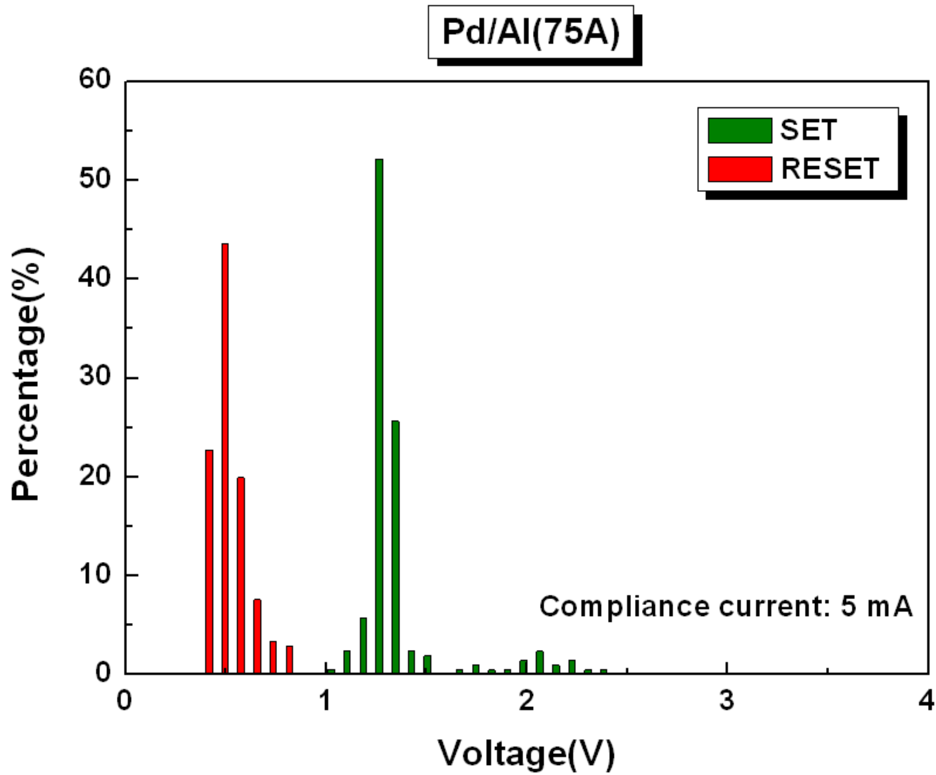

Fig. 3-41 Distribution of V_{SET} and V_{RESET} of Pd/Al(75 Å)/HfO_x/TiN structure.

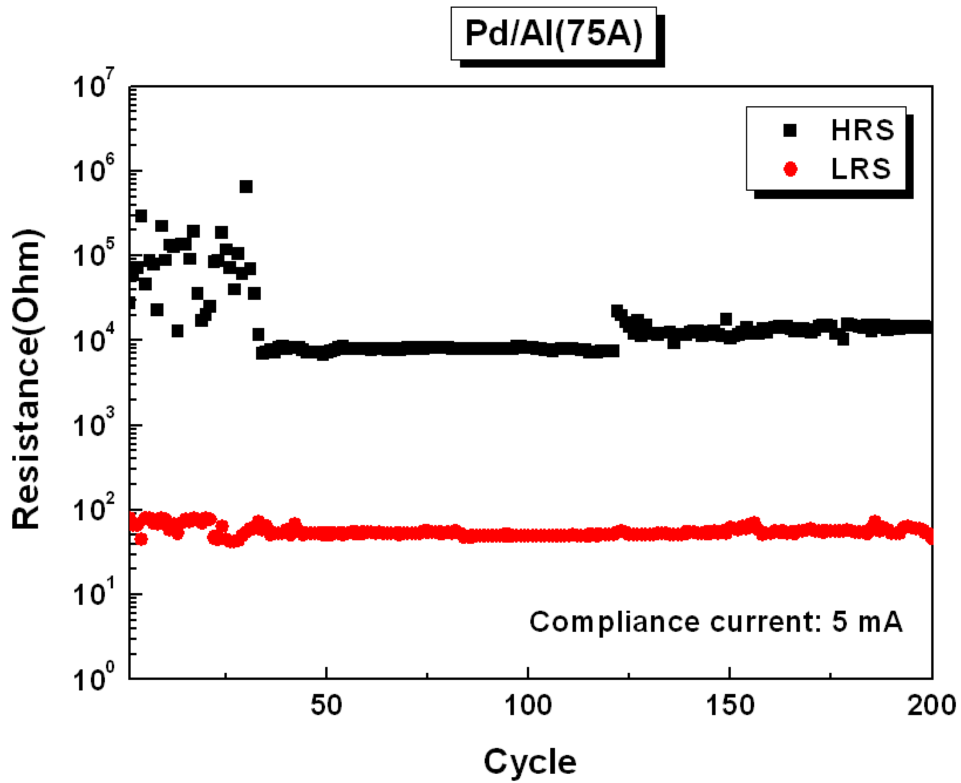

Fig. 3-42 Resistance of HRS and LRS of Pd/Al(75 Å)/HfO_x/TiN structure by 0.08 V read bias.

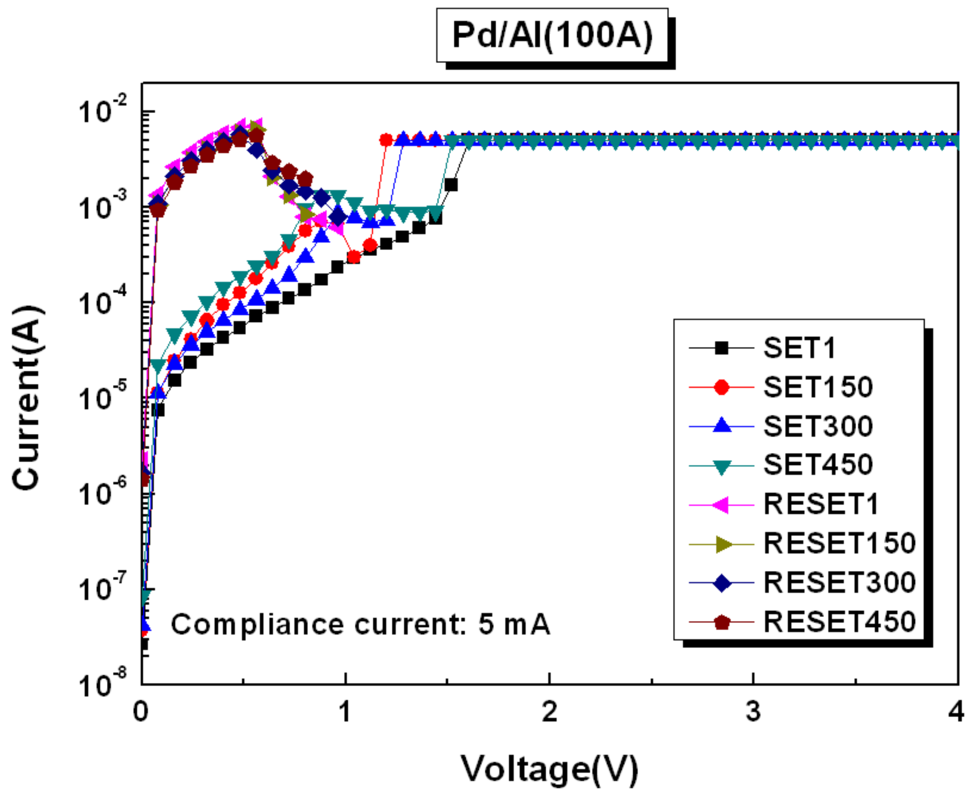

Fig. 3-43 The typical I-V curve of Pd/Al(100 Å)/HfO_x/TiN structure.

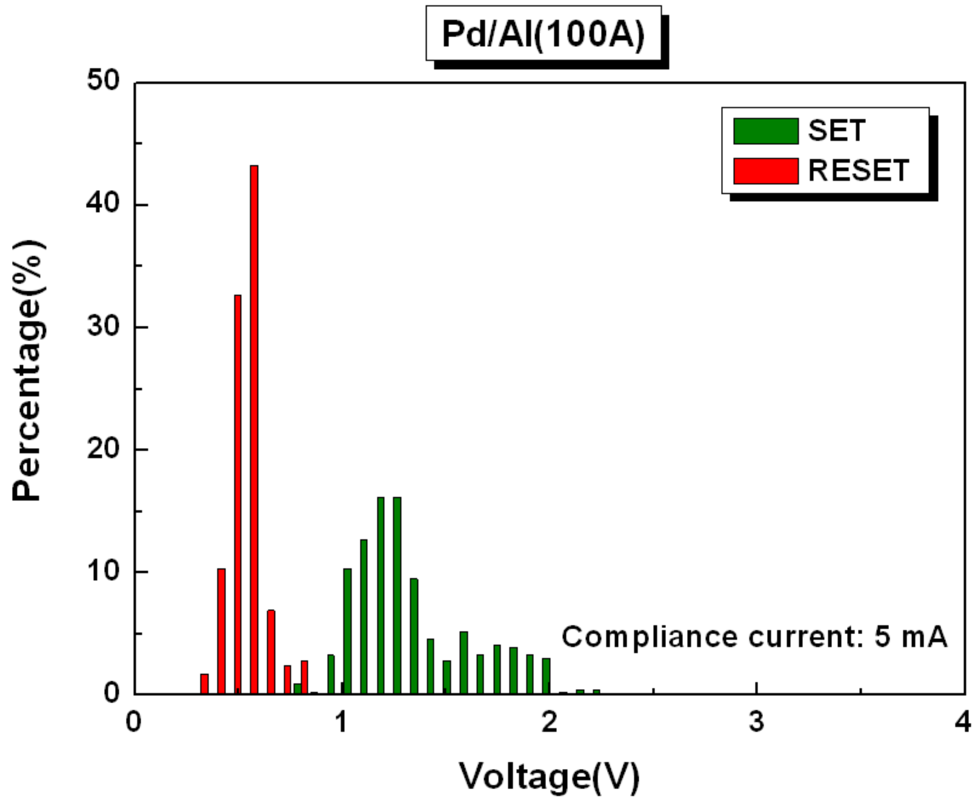

Fig. 3-44 Distribution of V_{SET} and V_{RESET} of Pd/Al(100 Å)/HfO_x/TiN structure.

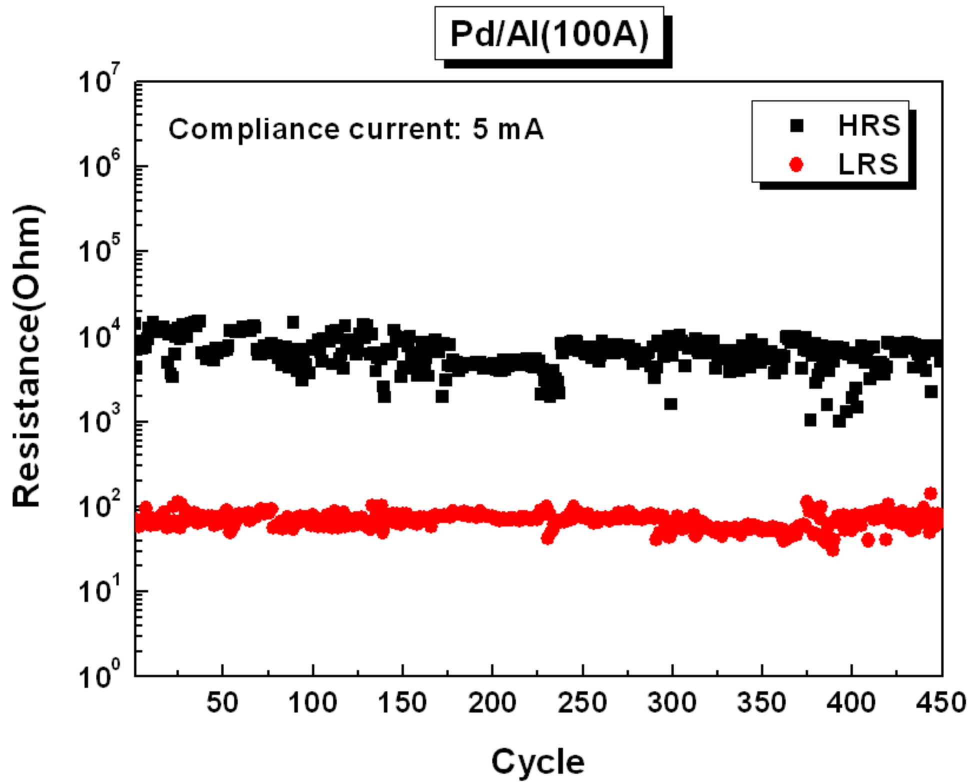

Fig. 3-45 Resistance of HRS and LRS of Pd/Al(100 Å)/HfO_x/TiN structure by 0.08 V read bias.

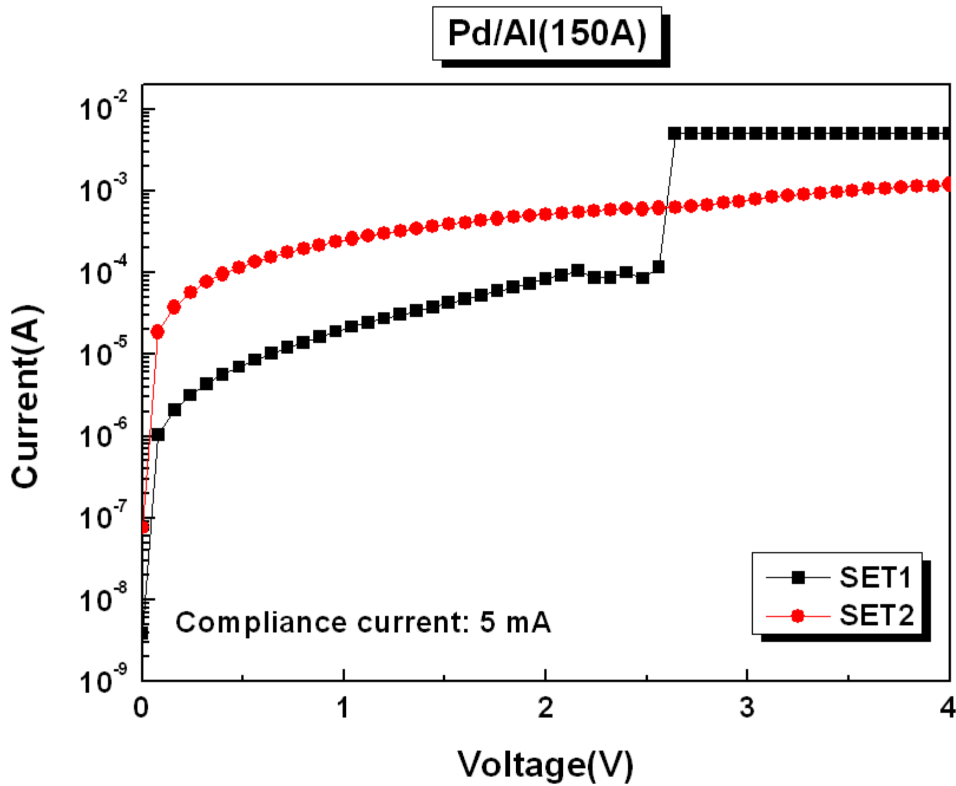

Fig. 3-46 The typical I-V curve of Pd/Al(150 Å)/HfO_x/TiN structure for SET process.

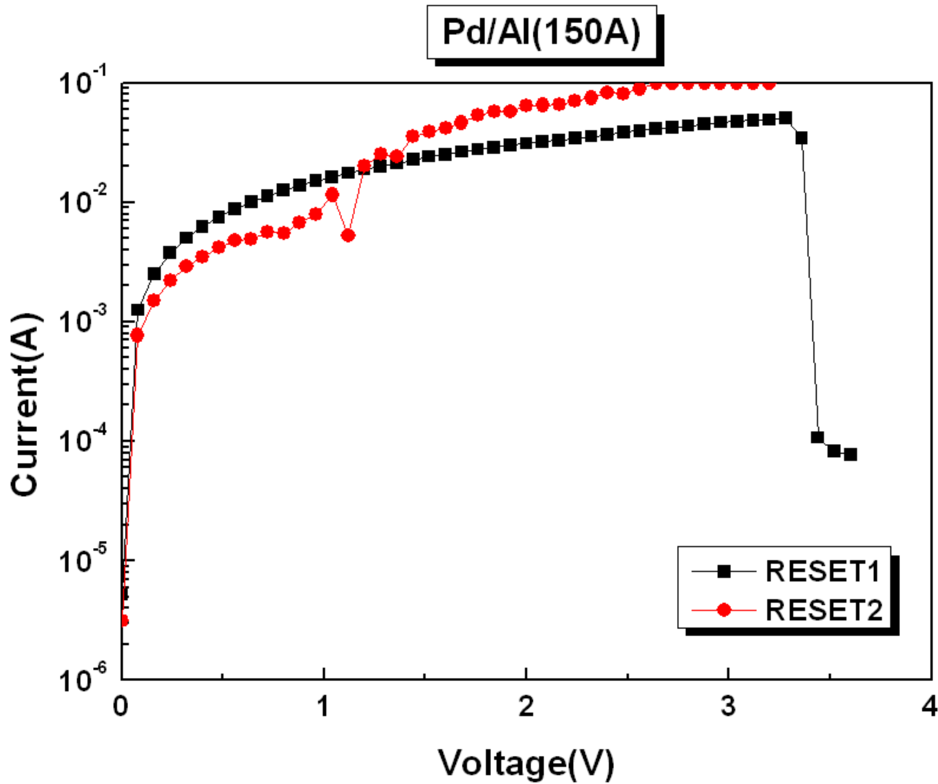

Fig. 3-47 The typical I-V curve of Pd/Al(150 Å)/HfO_x/TiN structure for RESET process.

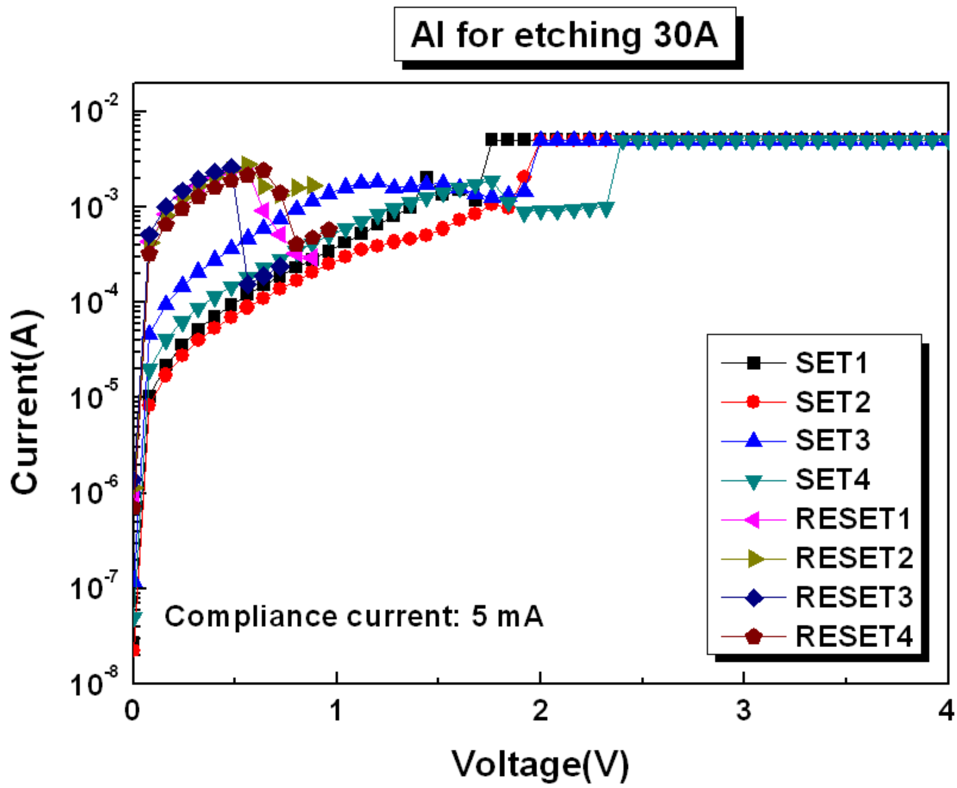

Fig. 3-48 The typical I-V curve of Al/HfO_x/TiN structure for etching Al to 30 Å.

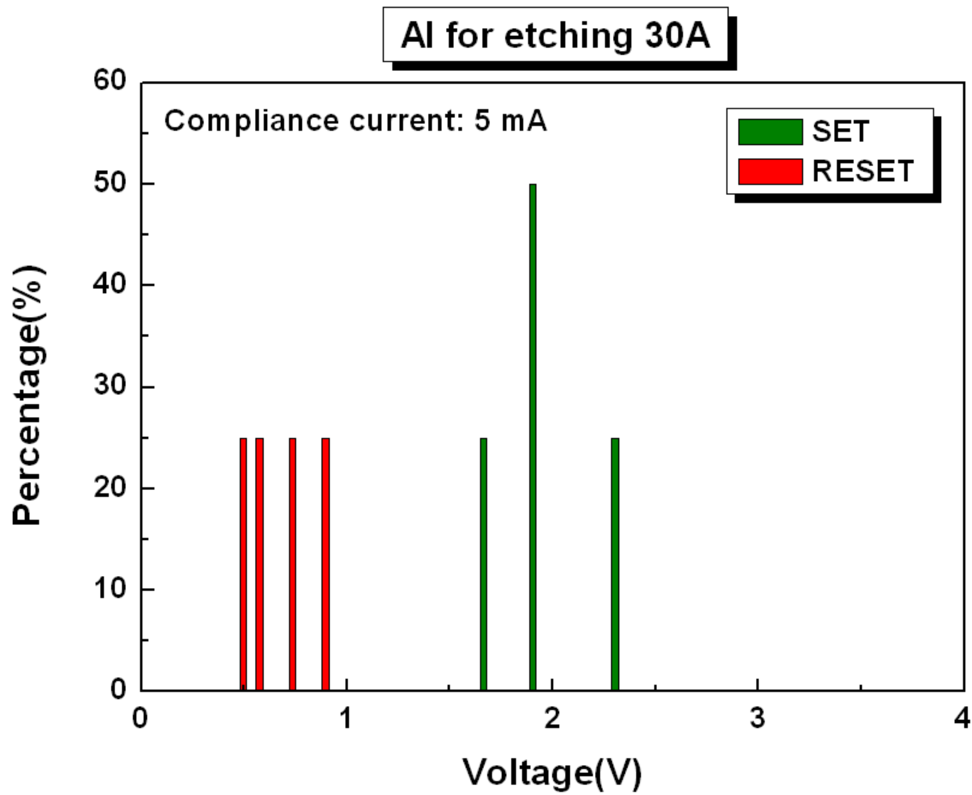

Fig. 3-49 Distribution of V_{SET} and V_{RESET} of Al/HfO_x/TiN structure for etching Al to 30 Å.

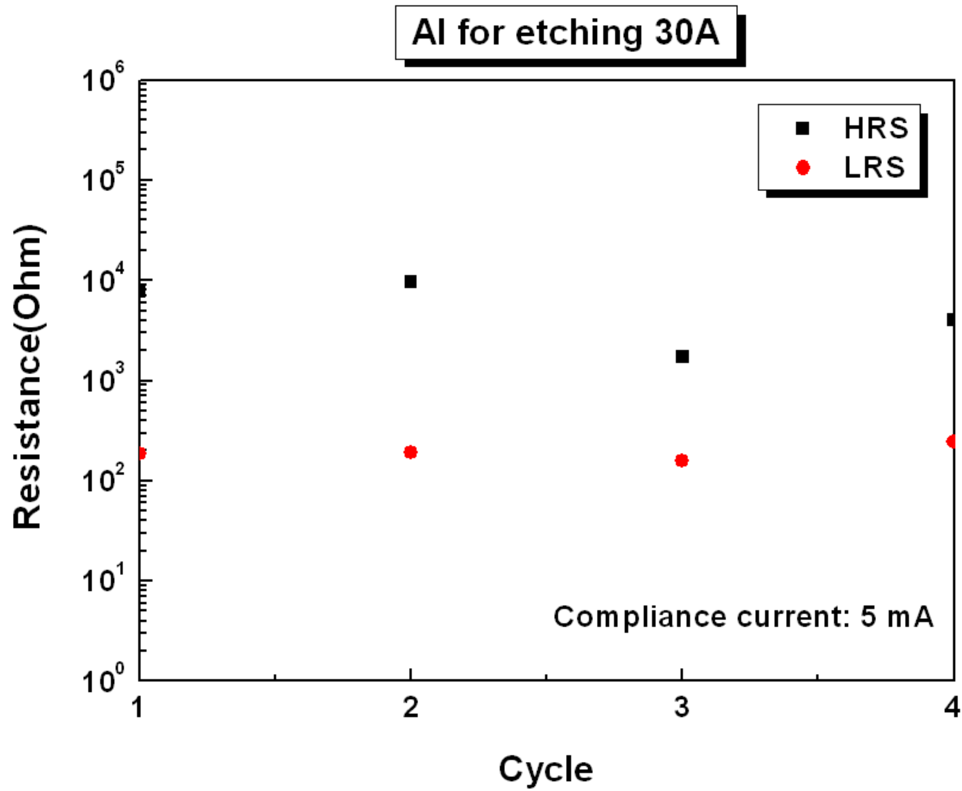

Fig. 3-50 Resistance of HRS and LRS of Al/HfOx/TiN structure for etching Al to 30 Å by 0.08 V read bias.

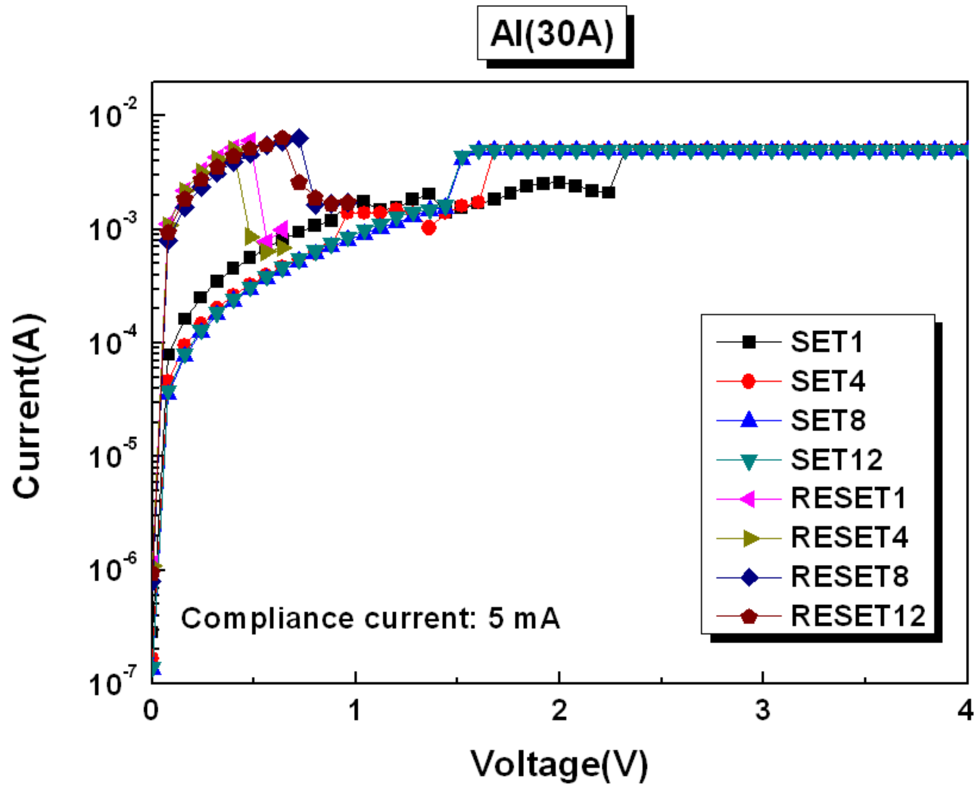

Fig. 3-51 The typical I-V curve of Al(30 Å)/HfOx/TiN structure.

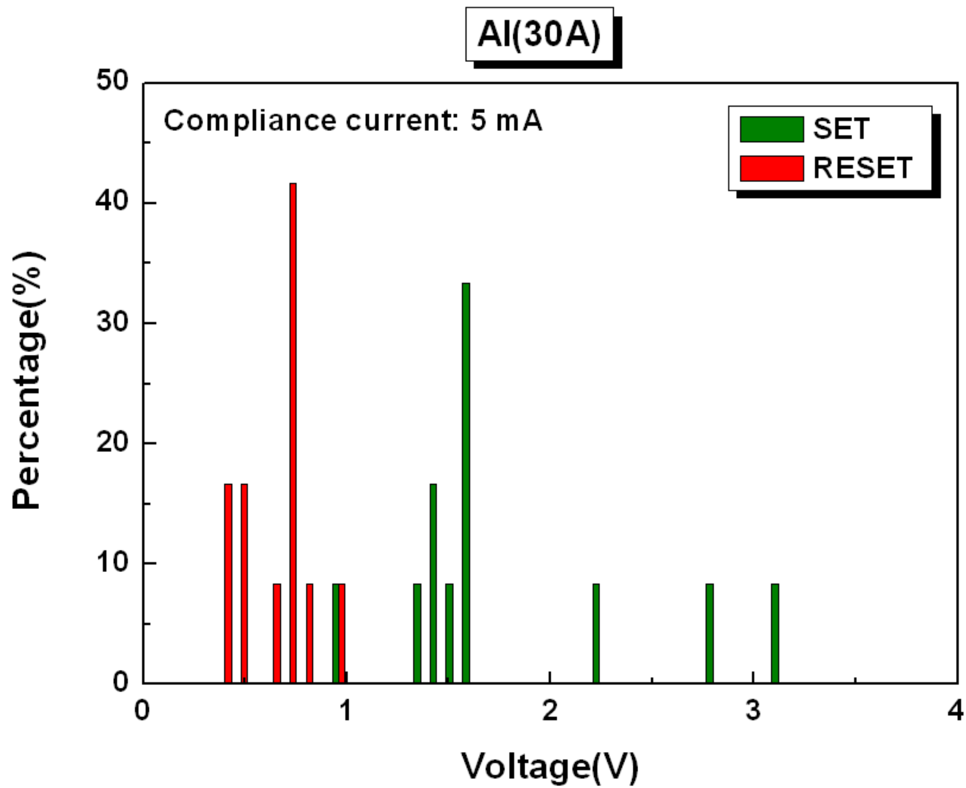

Fig. 3-52 Distribution of V_{SET} and V_{RESET} of Al(30 Å)/HfO_x/TiN structure.

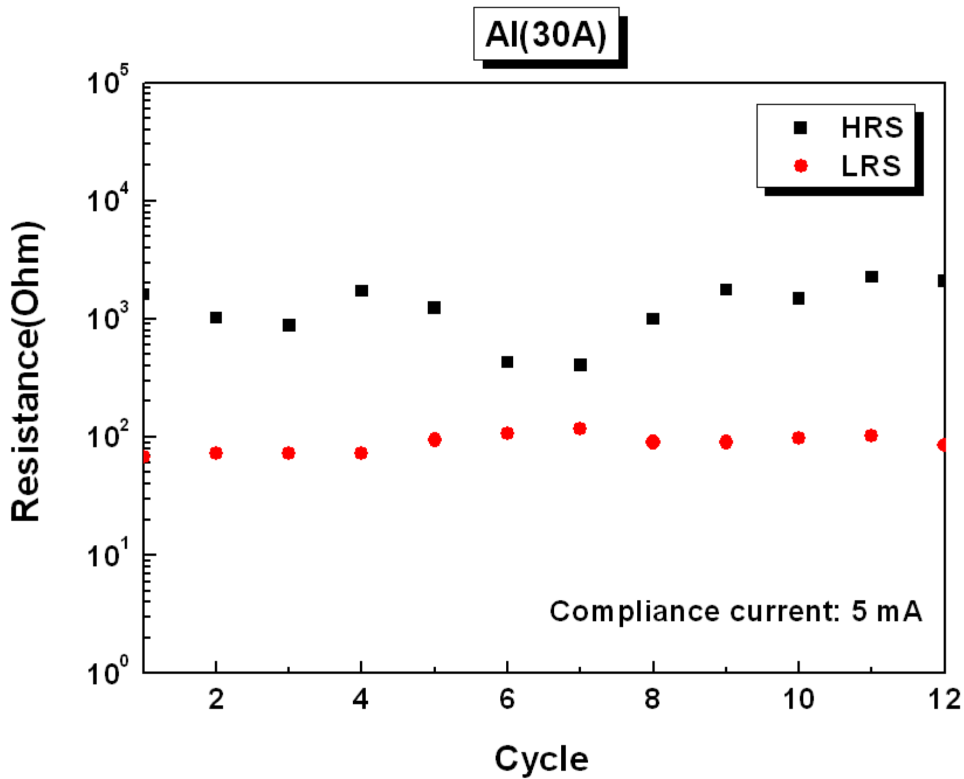

Fig. 3-53 Resistance of HRS and LRS of Al(30 Å)/HfO_x/TiN structure by 0.08 V read bias.

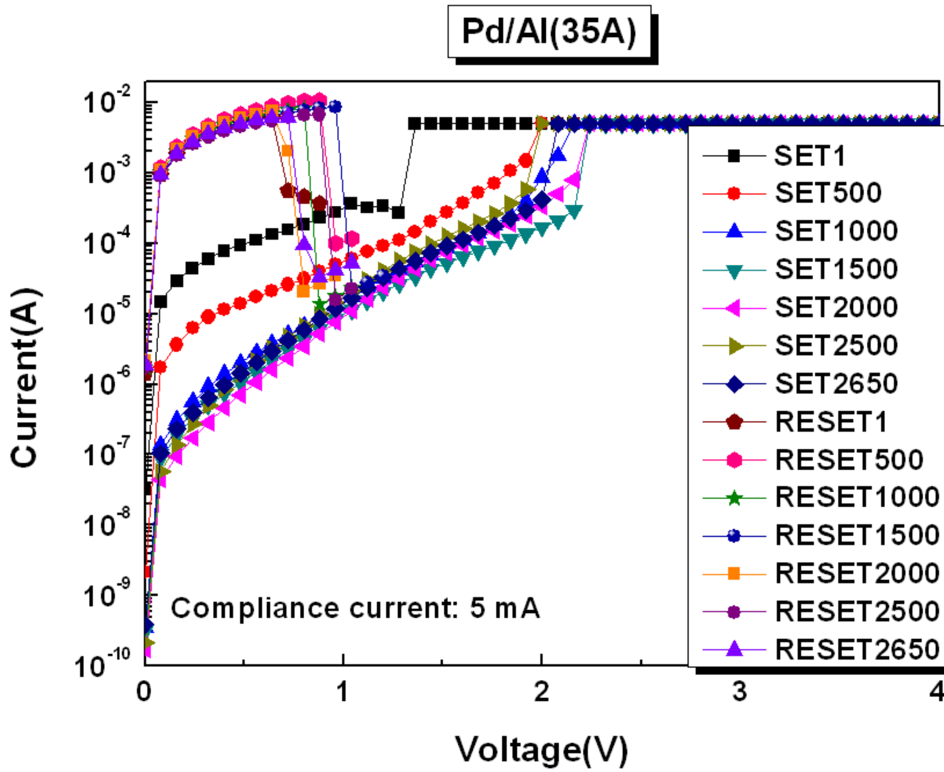

Fig. 3-54 The typical I-V curve of Pd/Al(35 Å)/HfO_x/TiN structure (1~2650 cycles).

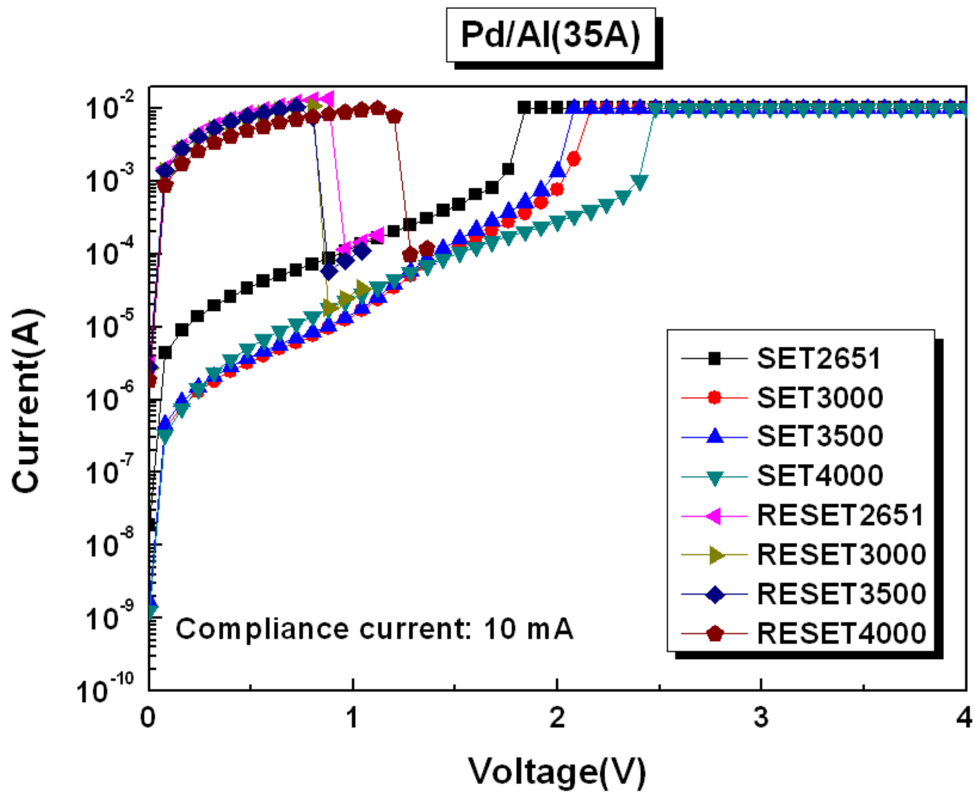

Fig. 3-55 The typical I-V curve of Pd/Al(35 Å)/HfO_x/TiN structure (2651~4000 cycles).

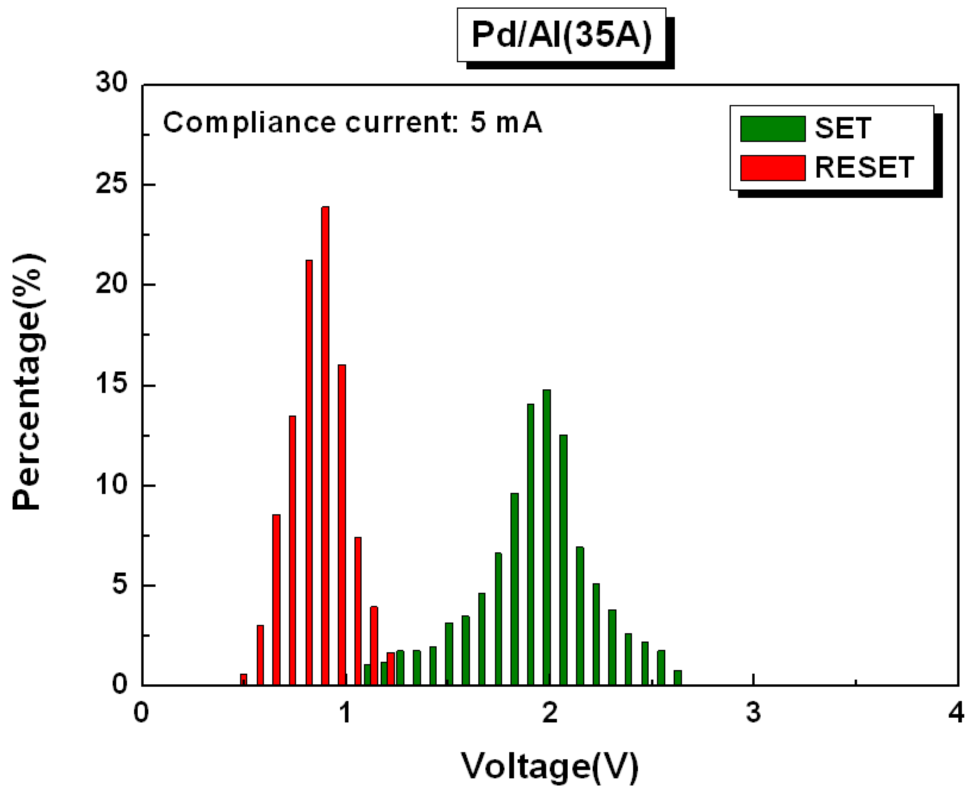

Fig. 3-56 Distribution of V_{SET} and V_{RESET} of Pd/Al(35 Å)/HfO_x/TiN structure (1~2650 cycles).

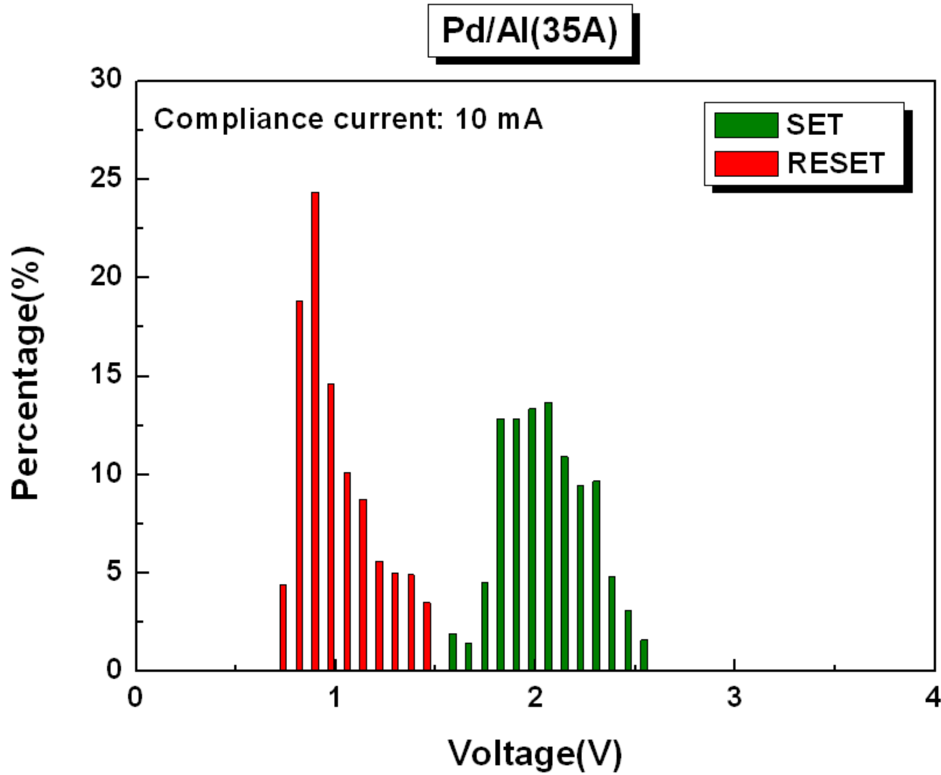

Fig. 3-57 Distribution of V_{SET} and V_{RESET} of Pd/Al(35 Å)/HfO_x/TiN structure (2651~4000 cycles).

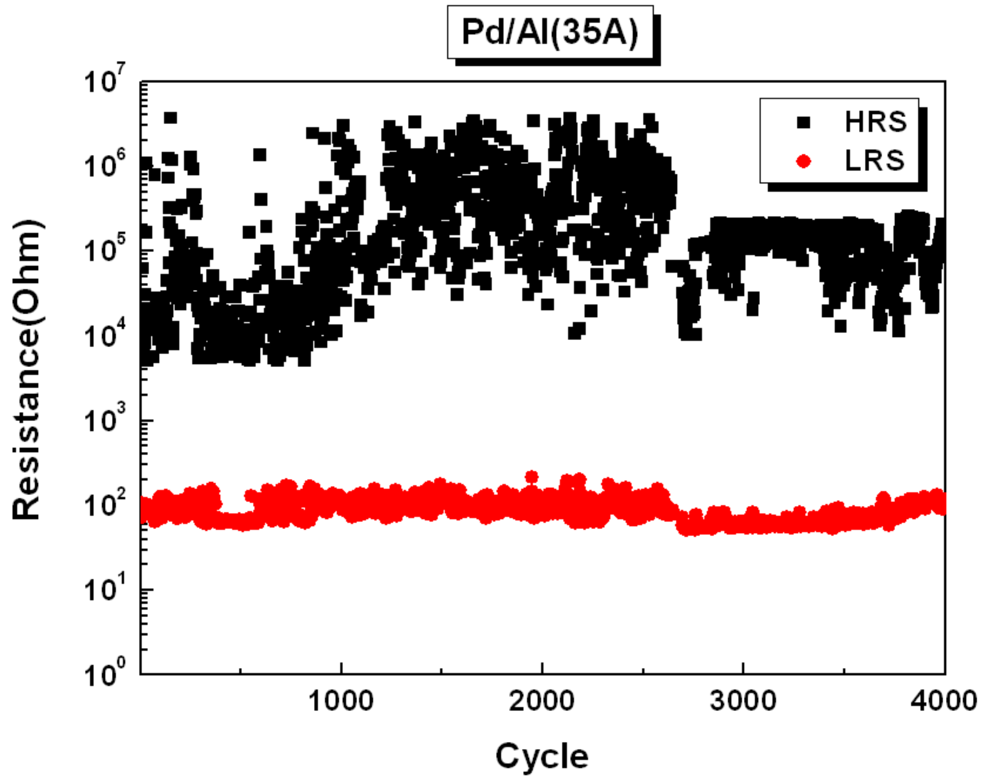

Fig. 3-58 Resistance of HRS and LRS of Pd/Al(35 Å)/HfO_x/TiN structure by 0.08 V read bias.

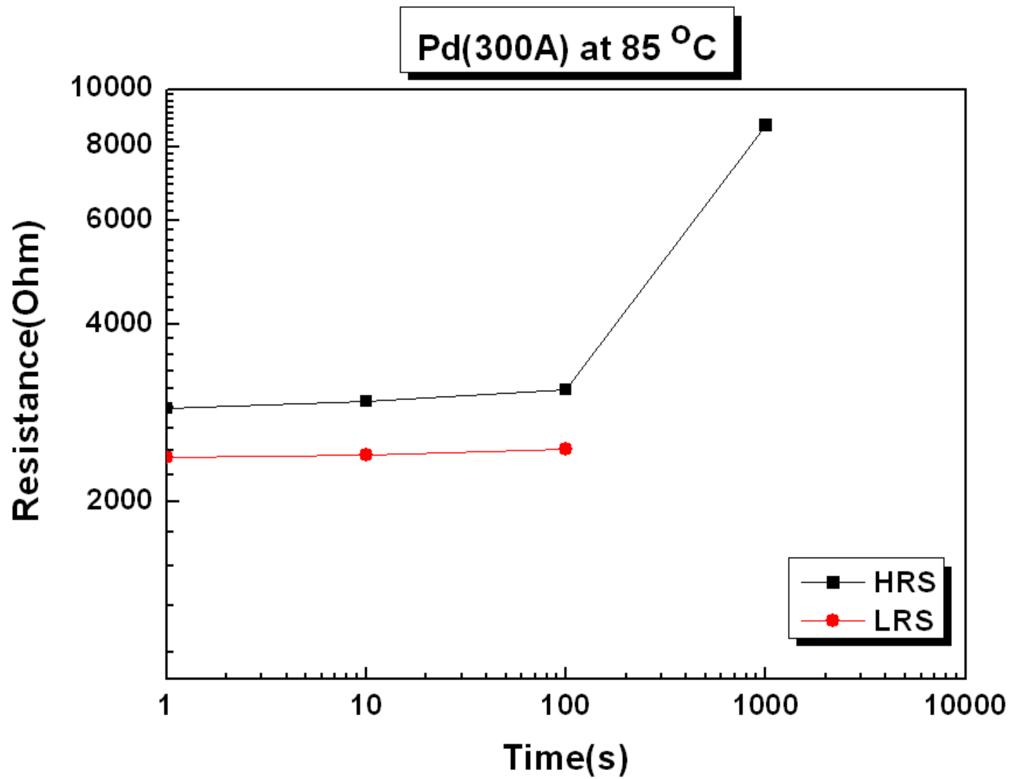

Fig. 3-59 Retention time of Pd/HfO_x/TiN structure at 85 ℃ by 0.08 V read bias.

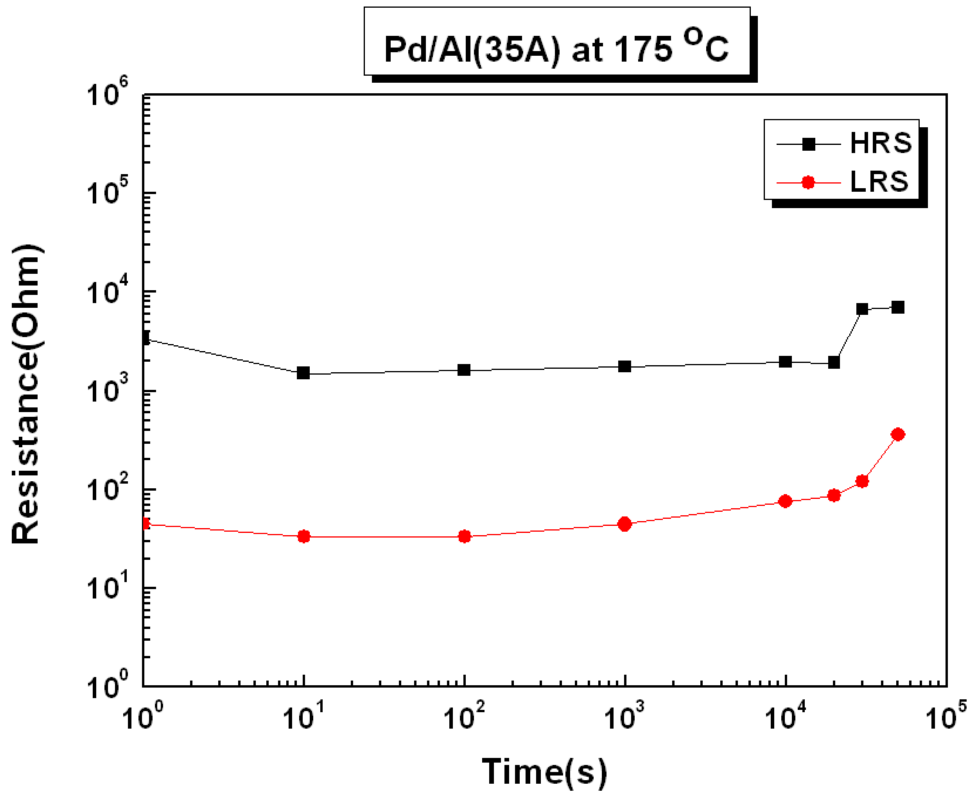

Fig. 3-60 Retention time of Pd/Al(35 Å)/HfO_x/TiN structure at 175 ℃ by 0.08 V read bias.

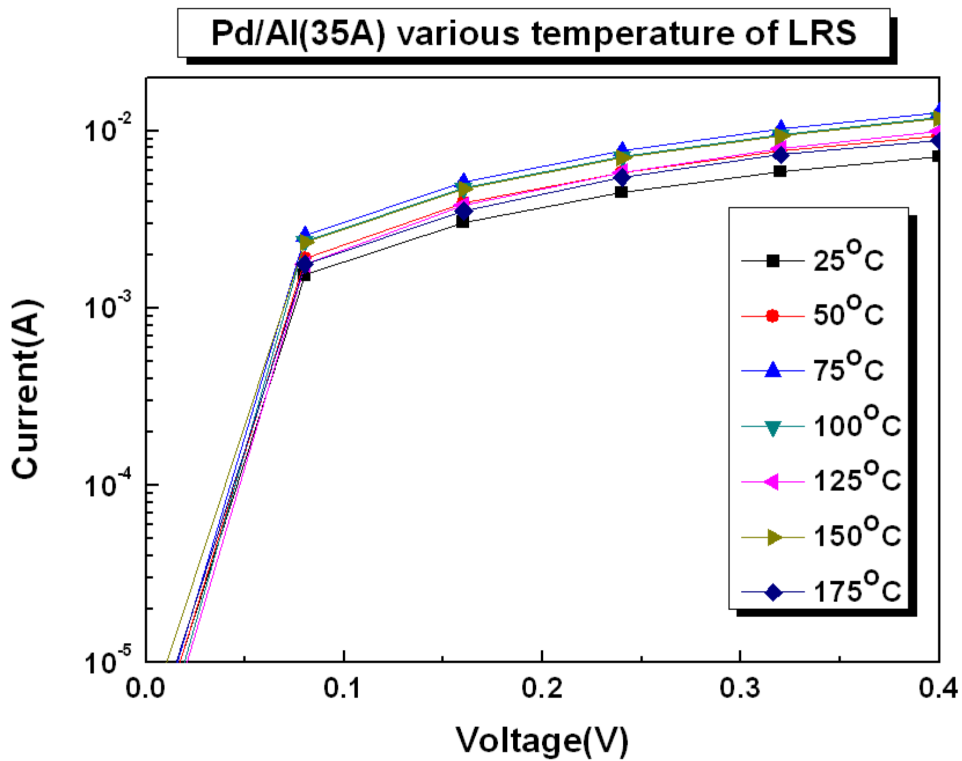

Fig. 3-61 Temperature dependence of LRS at low to median bias.

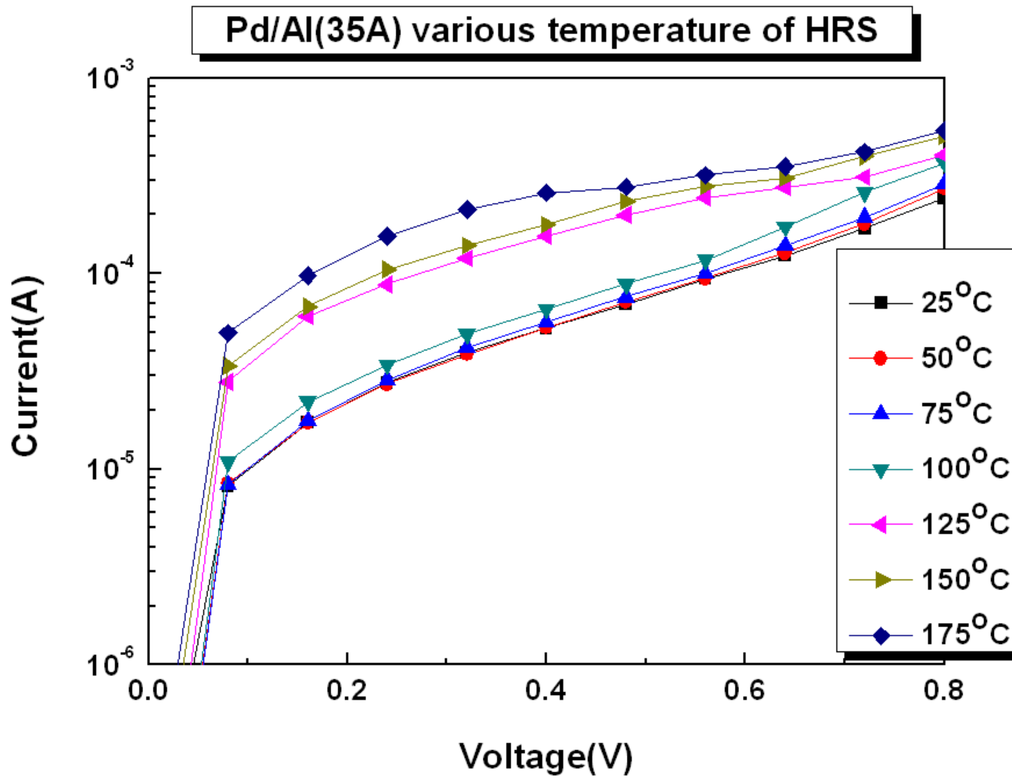

Fig. 3-62 Temperature dependence of HRS at low to median bias.

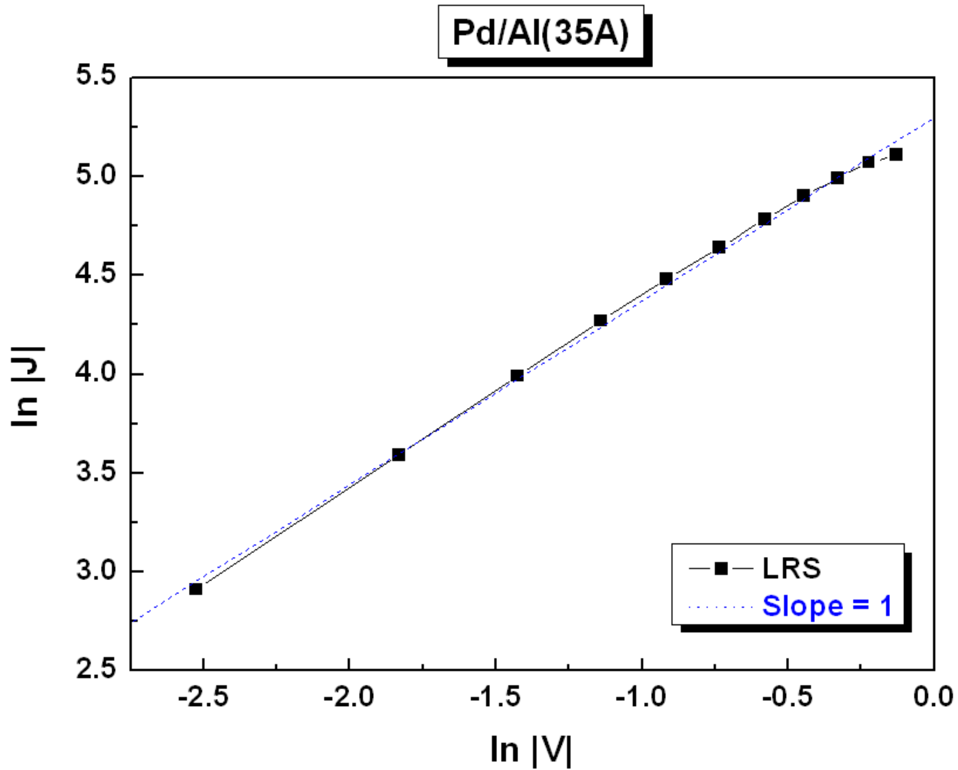

Fig. 3-63 I-V curve fitting of LRS.

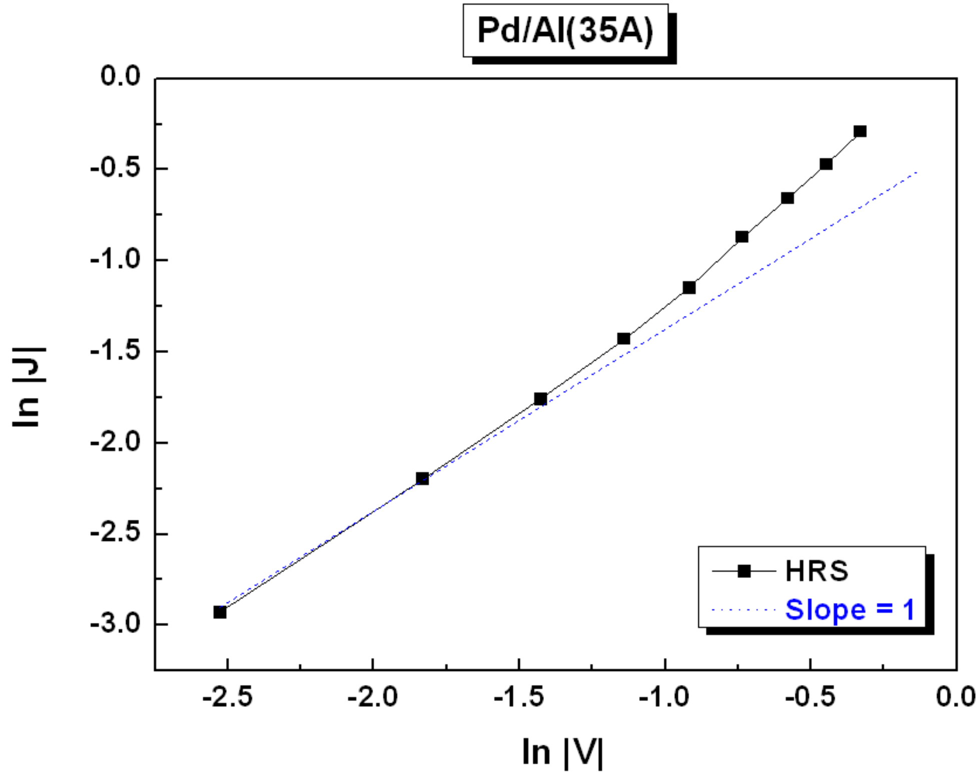

Fig. 3-64 I-V curve fitting of HRS at small bias region.

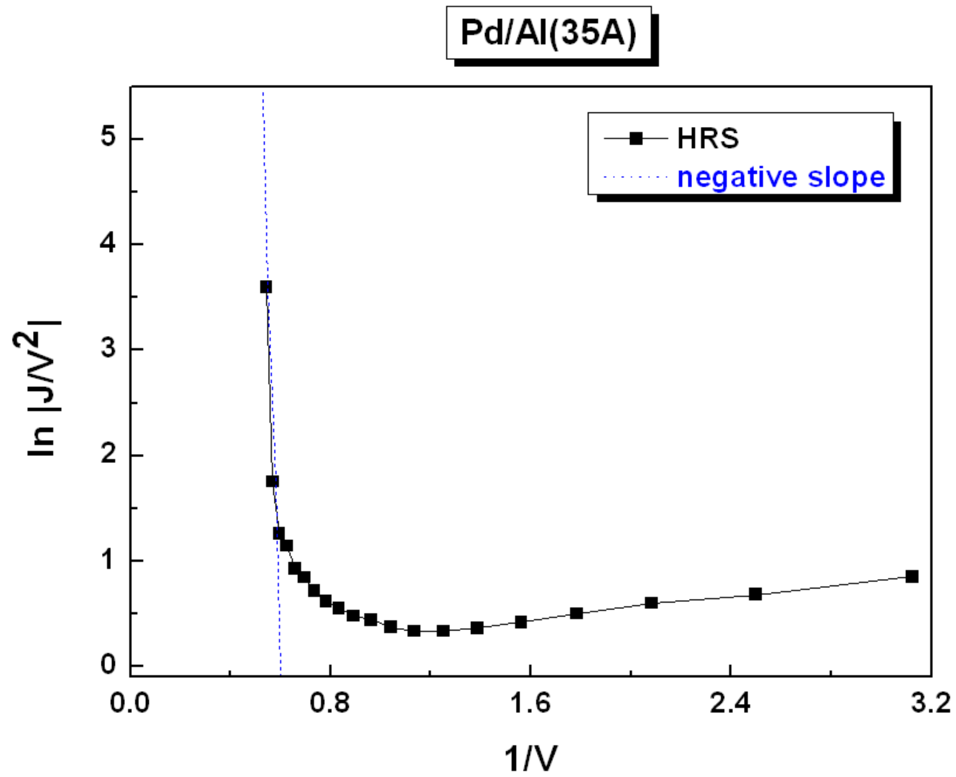

Fig. 3-65 I-V curve fitting of HRS at large bias region.

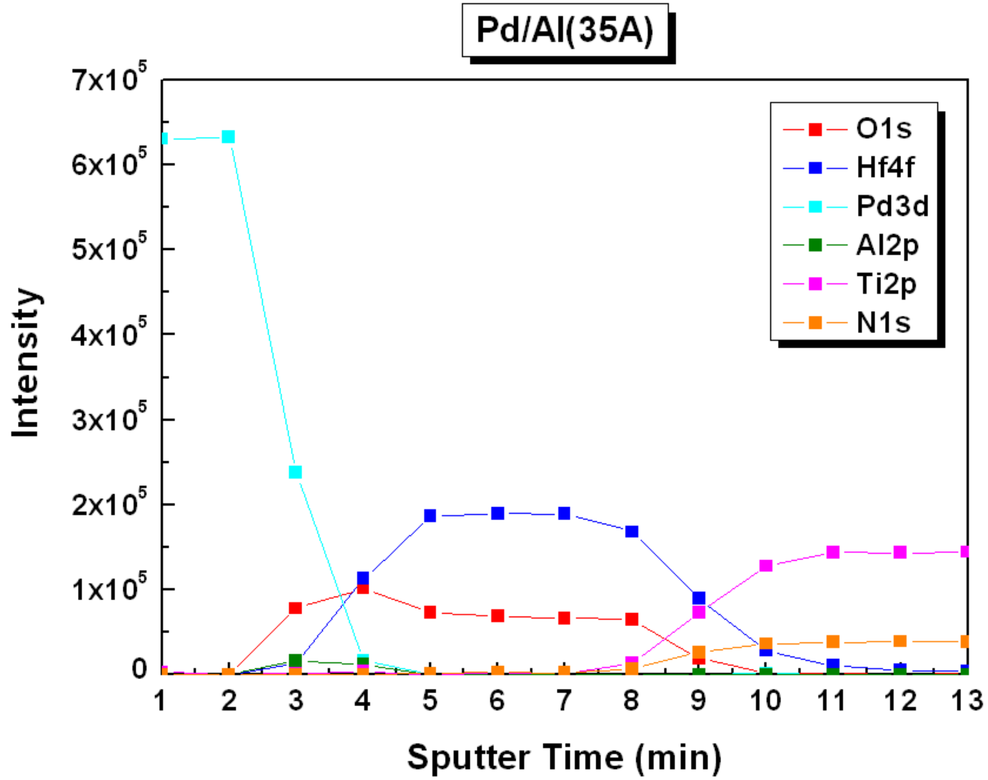

Fig. 3-66 XPS intensity of Pd/Al/HfO_x/TiN structure.

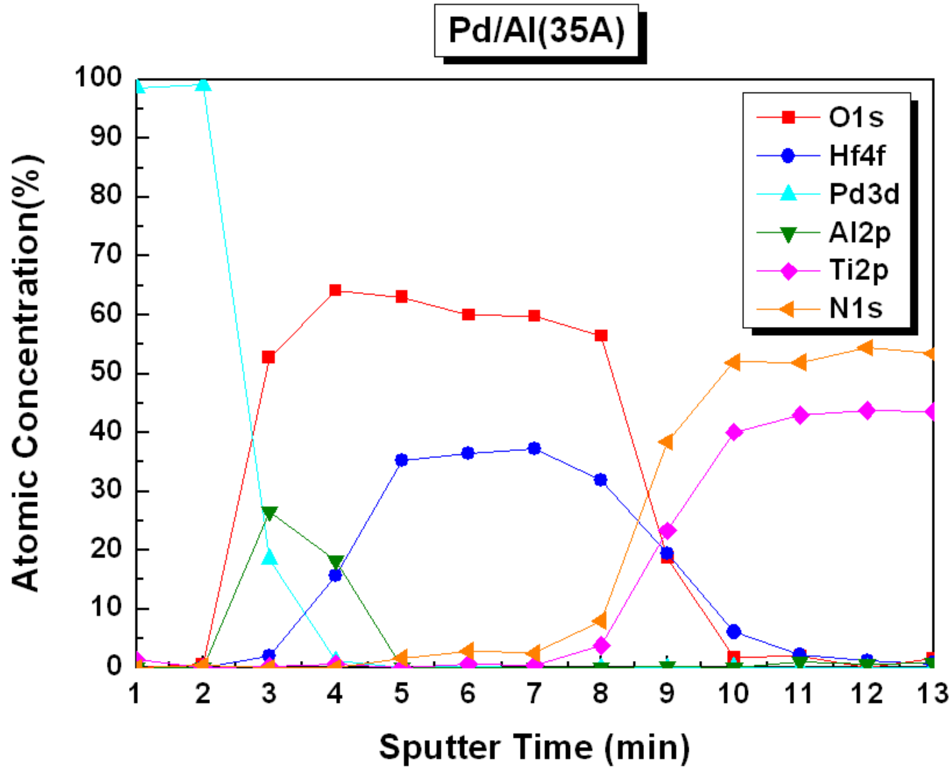

Fig. 3-67 XPS atomic concentration of Pd/Al/HfO_x/TiN structure.

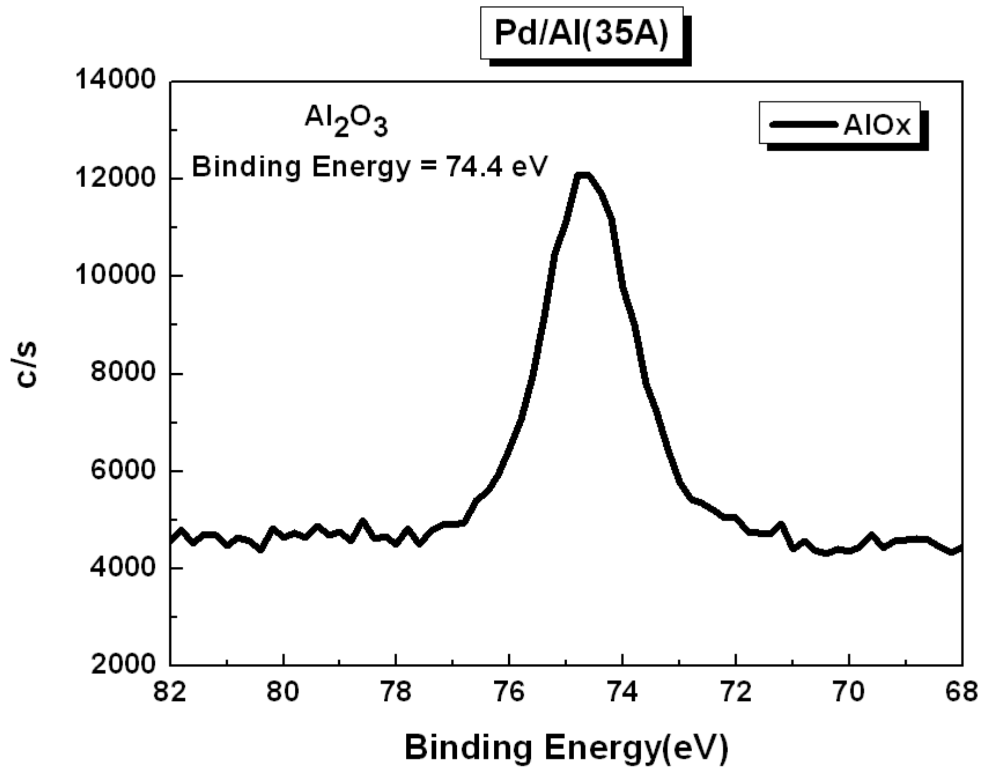

Fig. 3-68 XPS binding energy of Al/HfO_x interface.

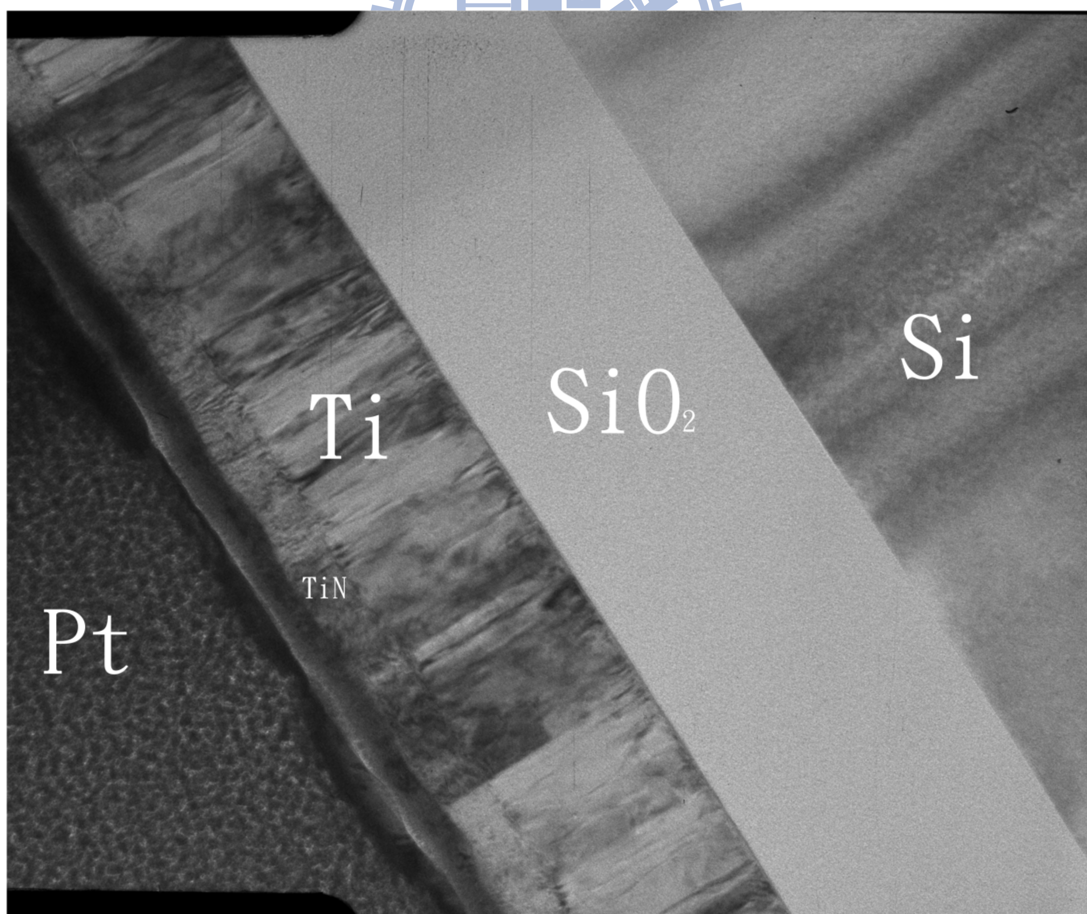

Fig. 3-69 TEM micrograth of Pd/Al/HfO_x/TiN/Ti/SiO2/Si structure.

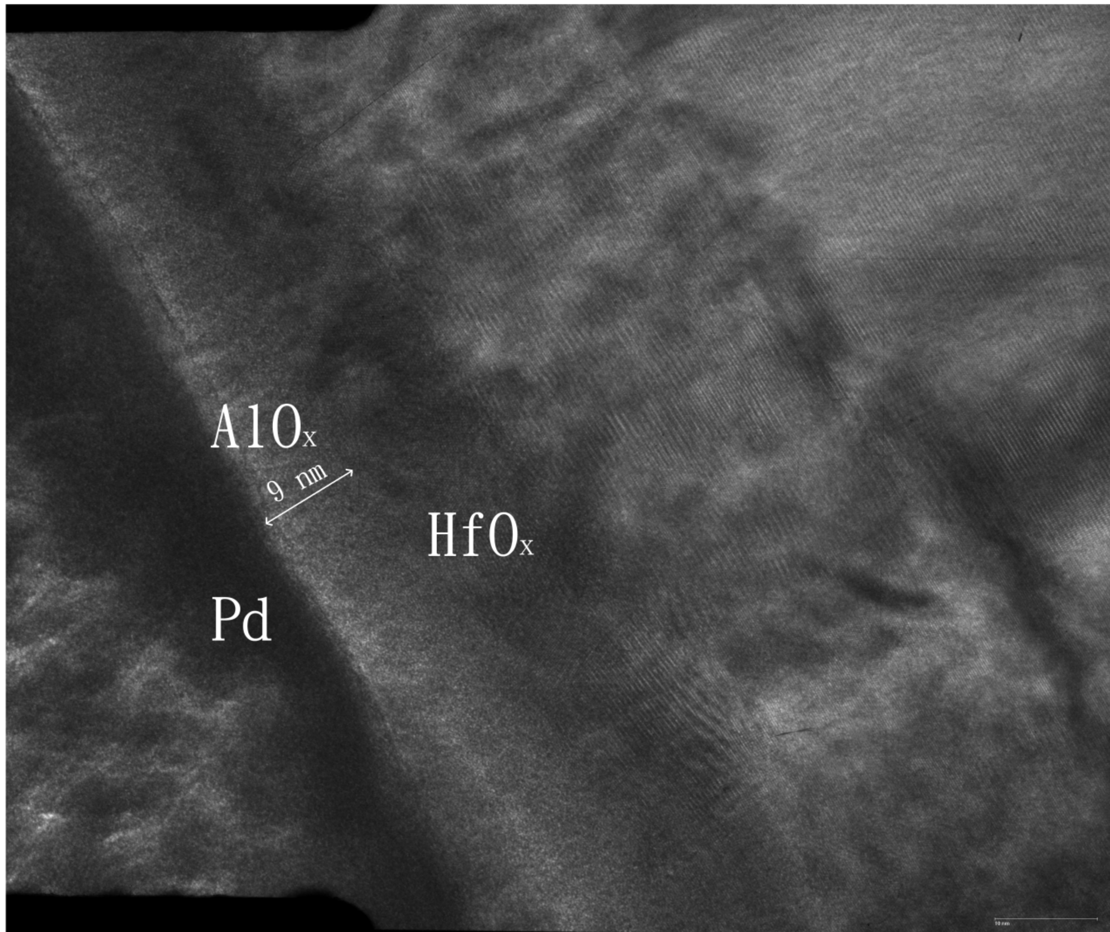

Fig. 3-70 High resolution TEM image of Al/HfOx interface.

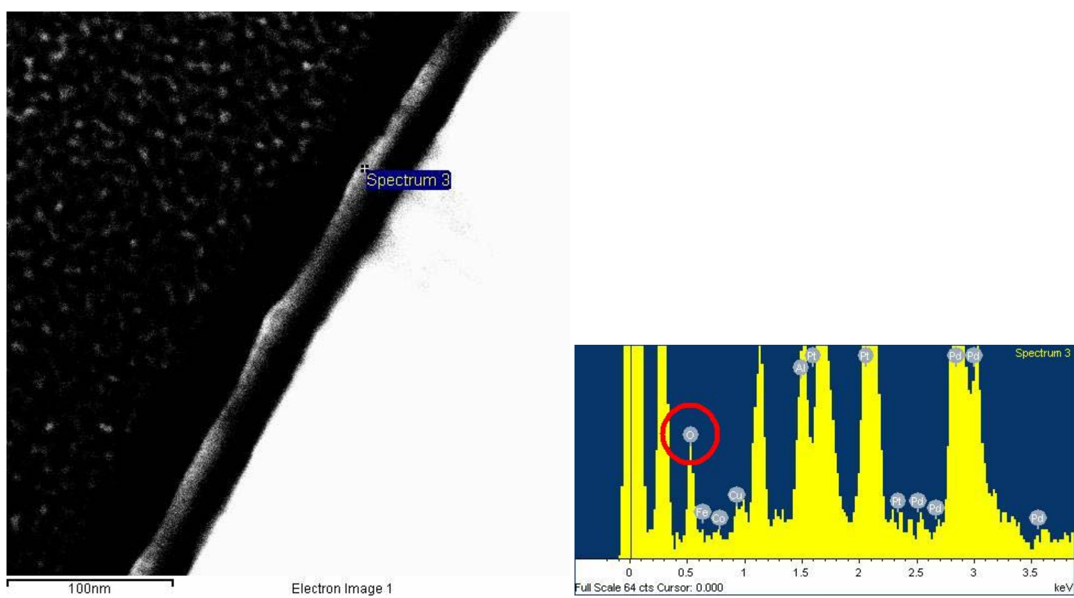

Fig. 3-71 EDS analysis of the Al layer.

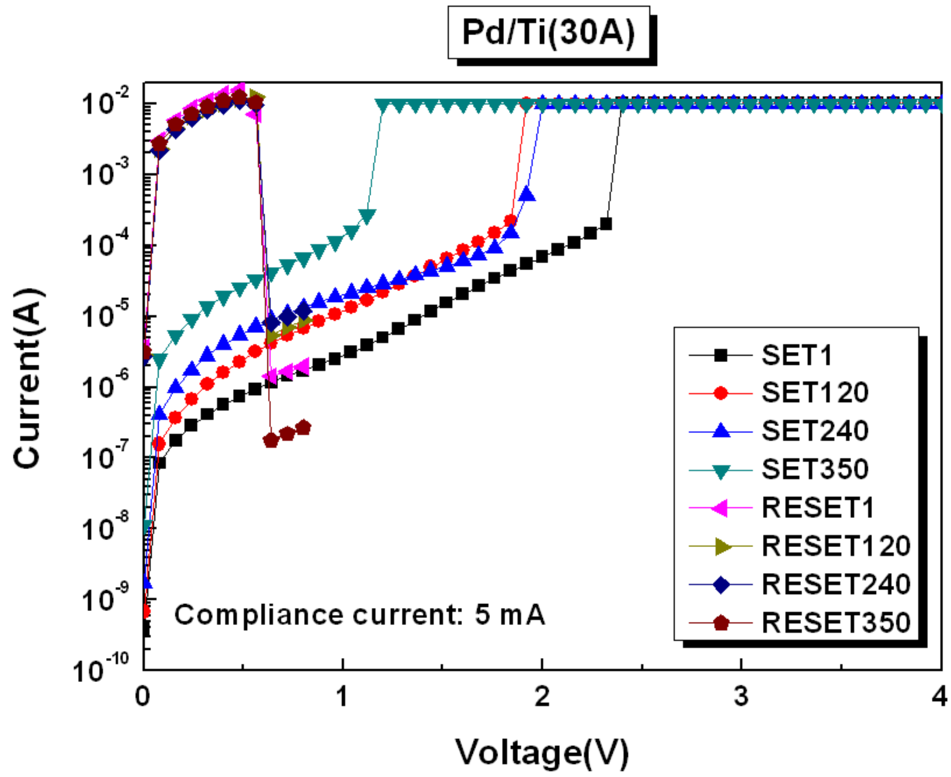

Fig. 3-72 The typical I-V curve of Pd/Ti(30 Å)/HfO_x/TiN structure.

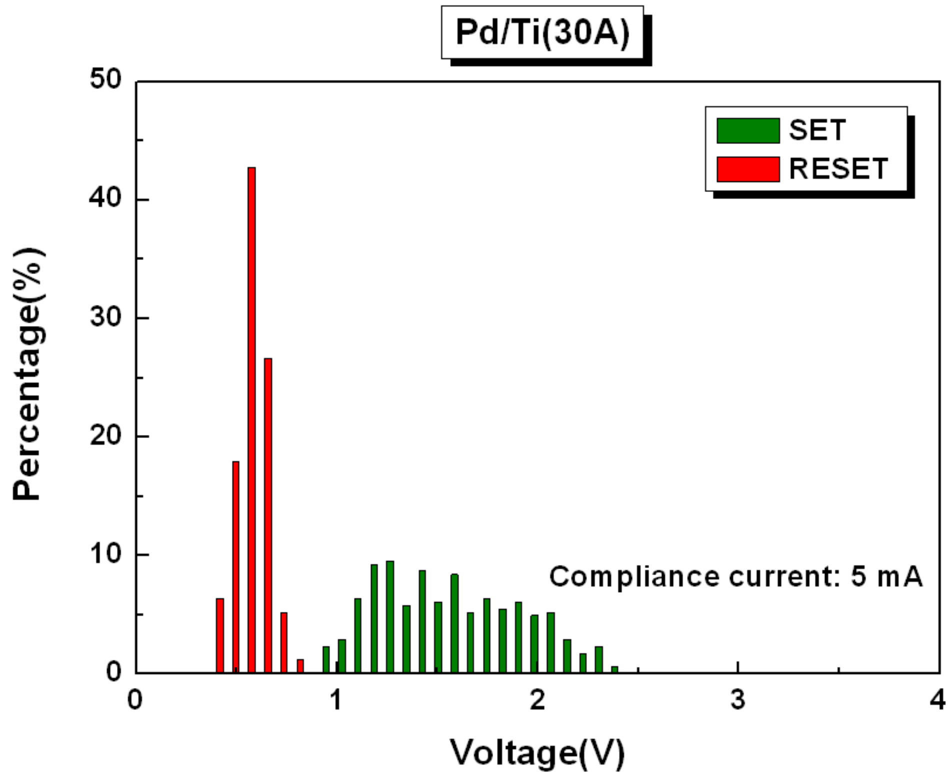

Fig. 3-73 Distribution of V_{SET} and V_{RESET} of Pd/Ti(30 Å)/HfO_x/TiN structure.

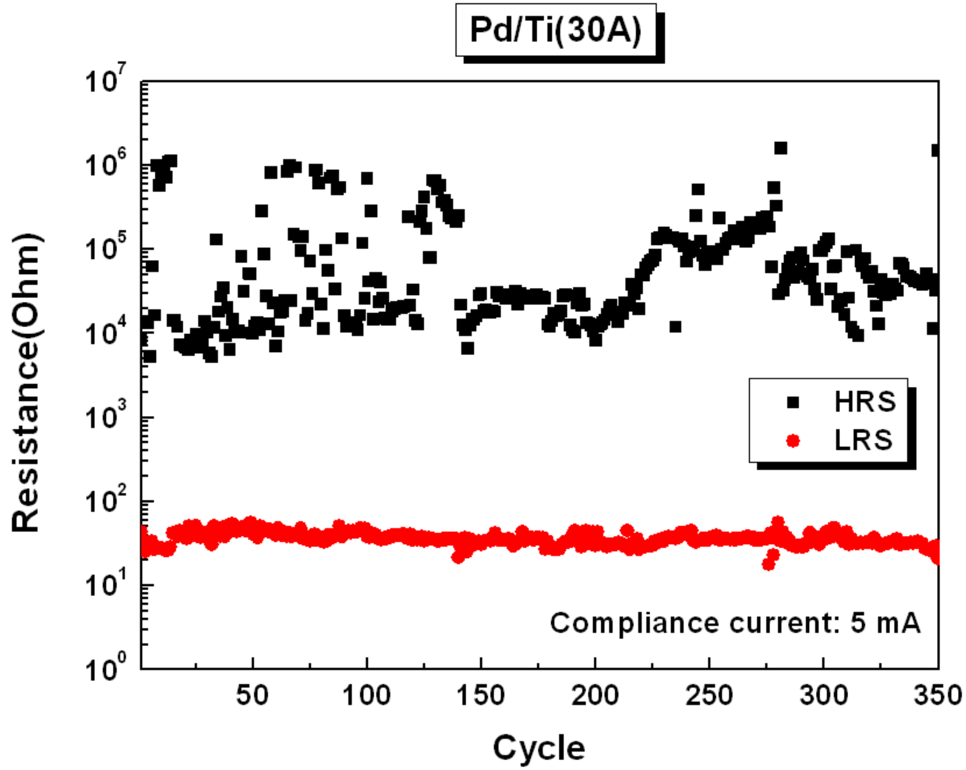

Fig. 3-74 Resistance of HRS and LRS of Pd/Ti(30 Å)/HfOx/TiN structure by 0.08 V read bias.

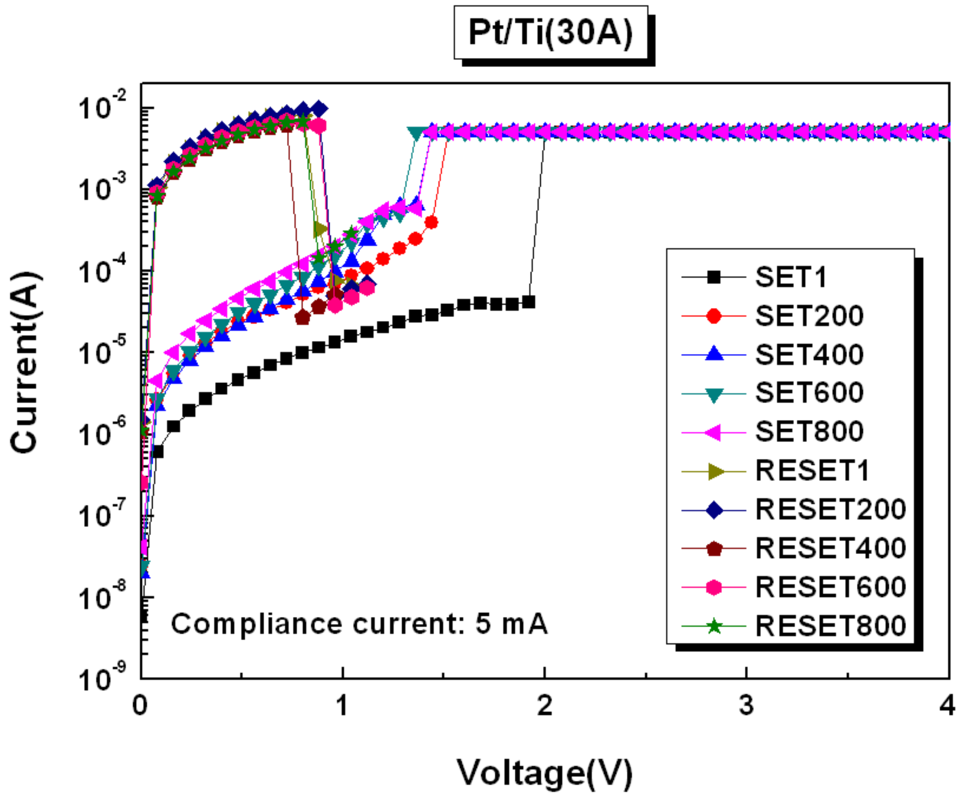

Fig. 3-75 The typical I-V curve of Pt/Ti(30 Å)/HfOx/TiN structure.

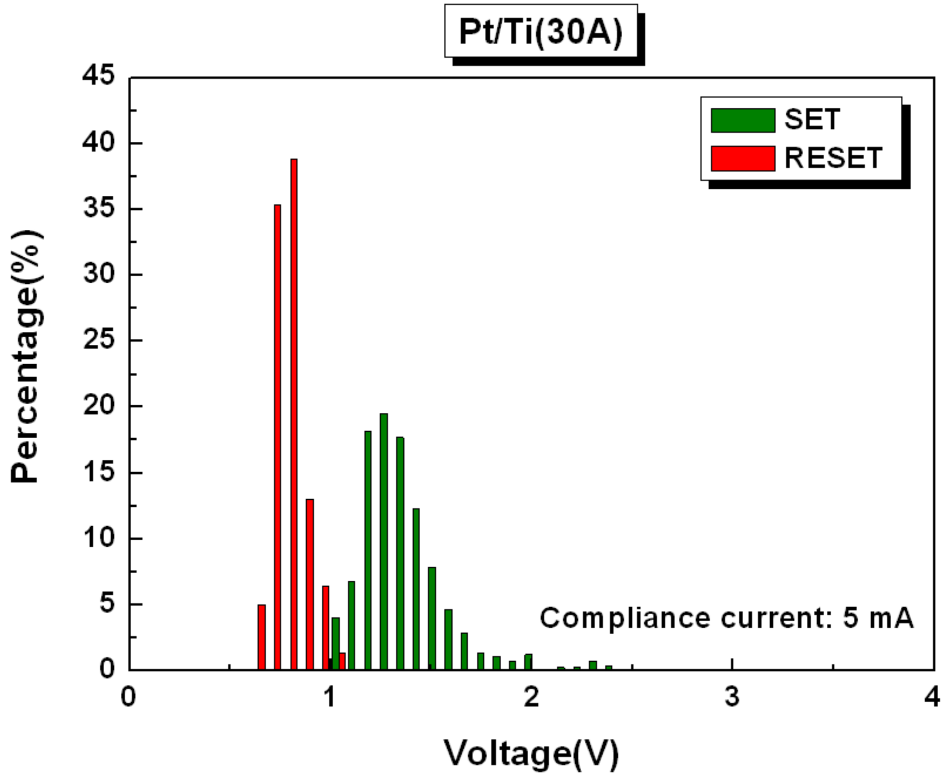

Fig. 3-76 Distribution of V_{SET} and V_{RESET} of Pt/Ti(30 Å)/HfO_x/TiN structure.

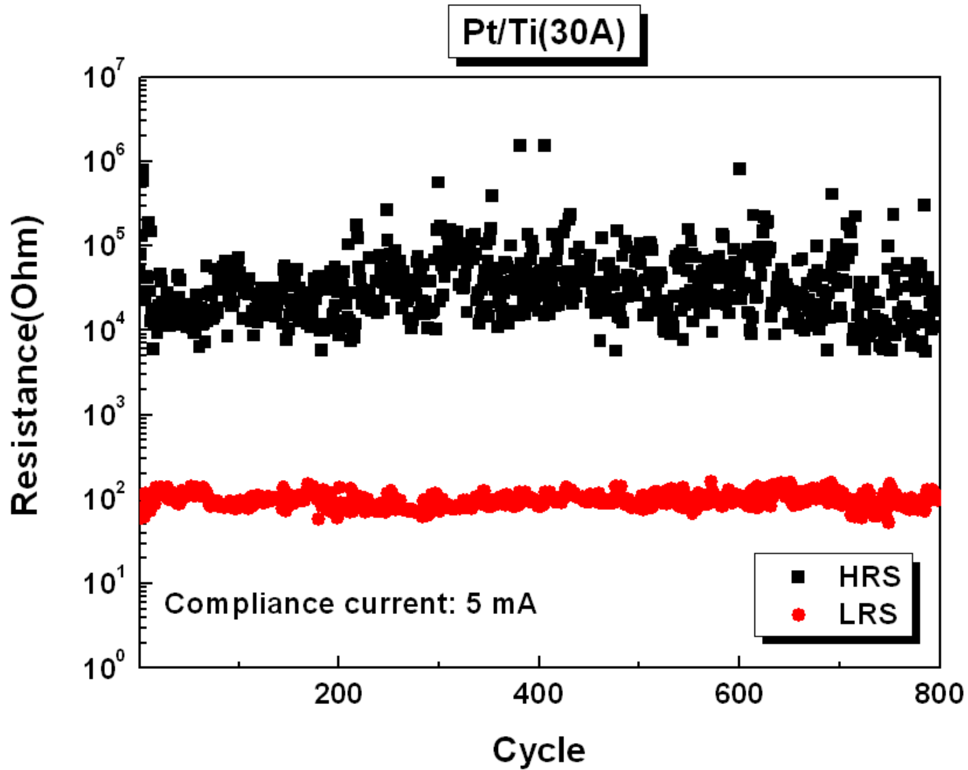

Fig. 3-77 Resistance of HRS and LRS of Pt/Ti(30 Å)/HfO_x/TiN structure by 0.08 V read bias.

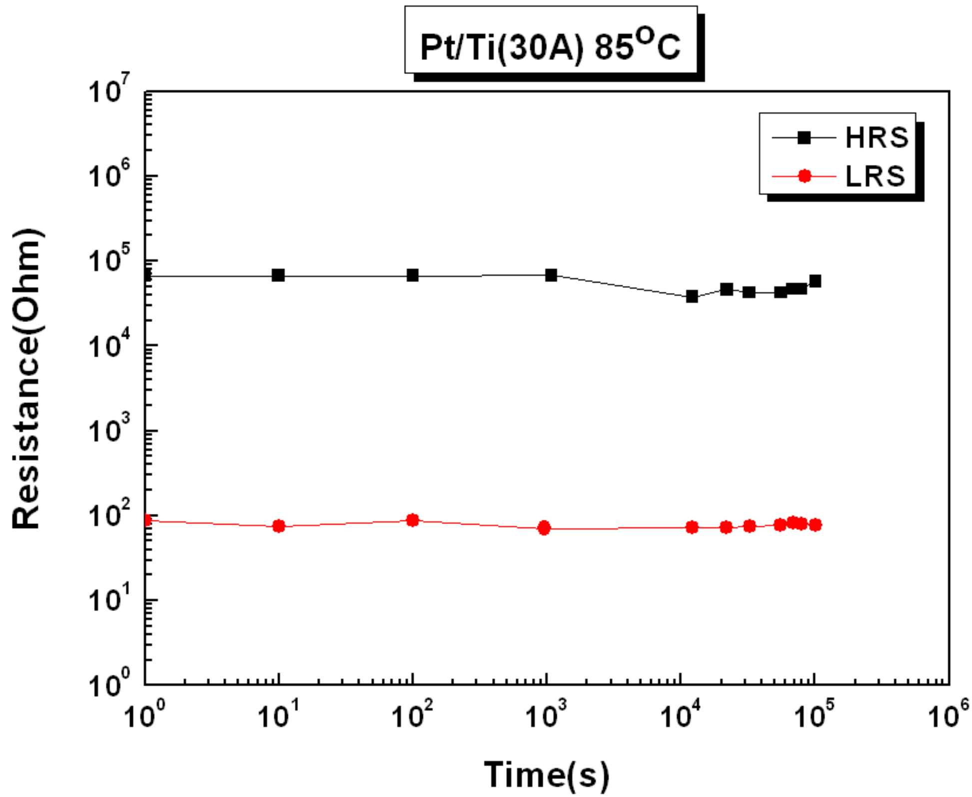

Fig. 3-78 Retention time of Pt/Ti(30 Å)/HfO_x/TiN structure at 85 ℃ by 0.08 V read bias.

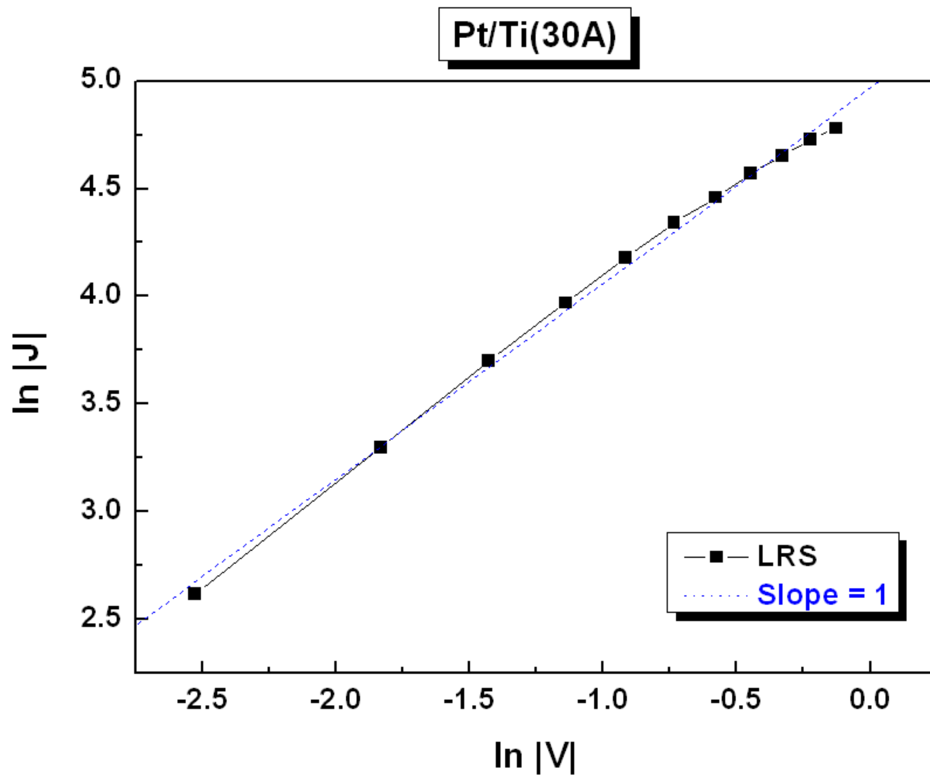

Fig. 3-79 I-V curve fitting of LRS of Pt/Ti(30 Å)/HfO_x/TiN structure.

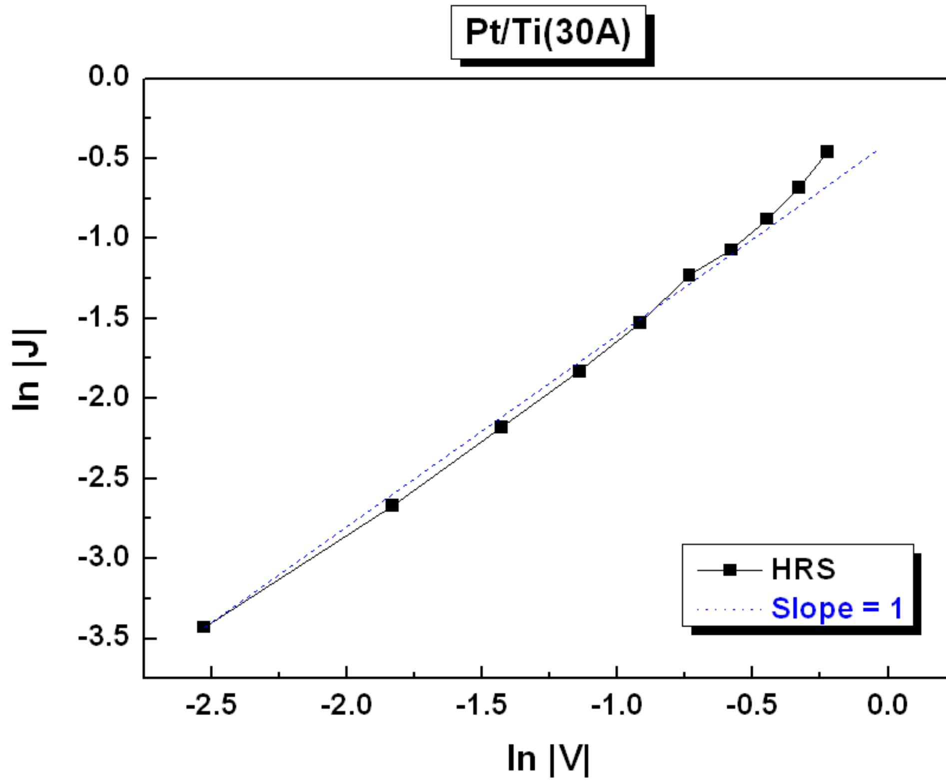

Fig. 3-80 I-V curve fitting of HRS of Pt/Ti(30 Å)/HfO_x/TiN structure at small bias region.

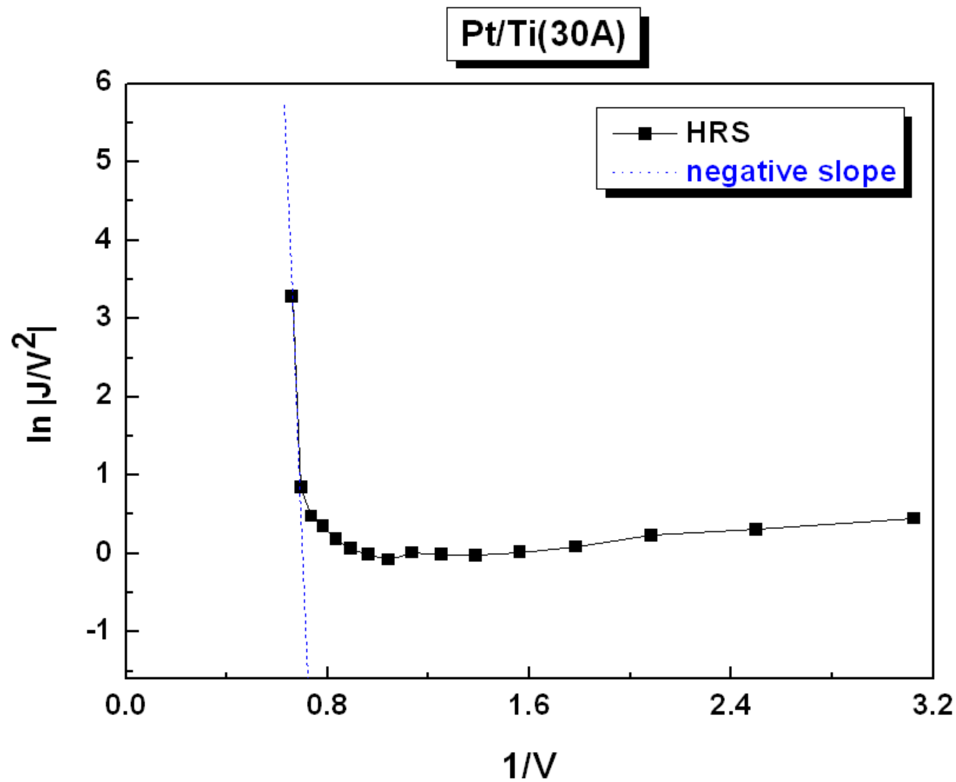

Fig. 3-81 I-V curve fitting of HRS of Pt/Ti(30 Å)/HfO_x/TiN structure at large bias region.

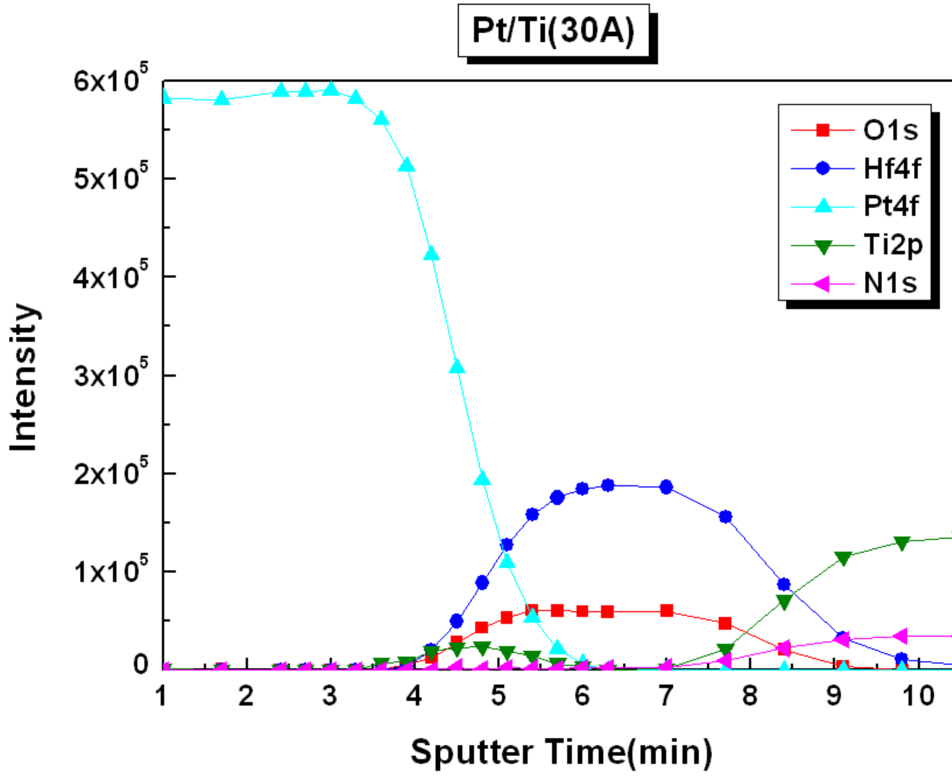

Fig. 3-82 XPS intensity of Pt/Ti/HfOx/TiN structure.

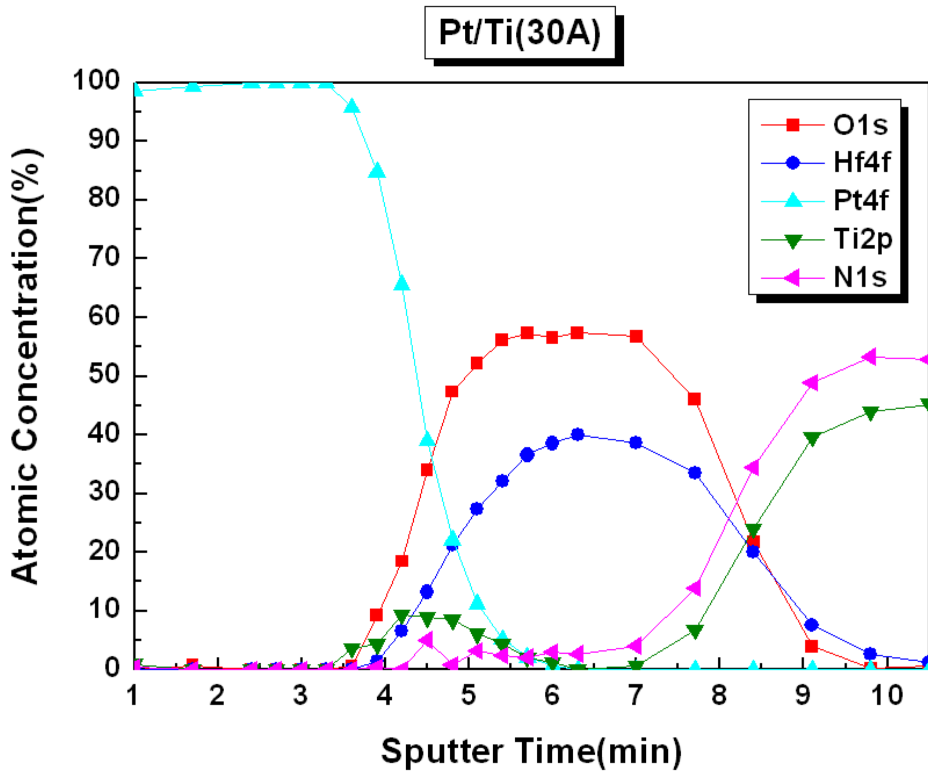

Fig. 3-83 XPS atomic concentration of Pt/Ti/HfOx/TiN structure.

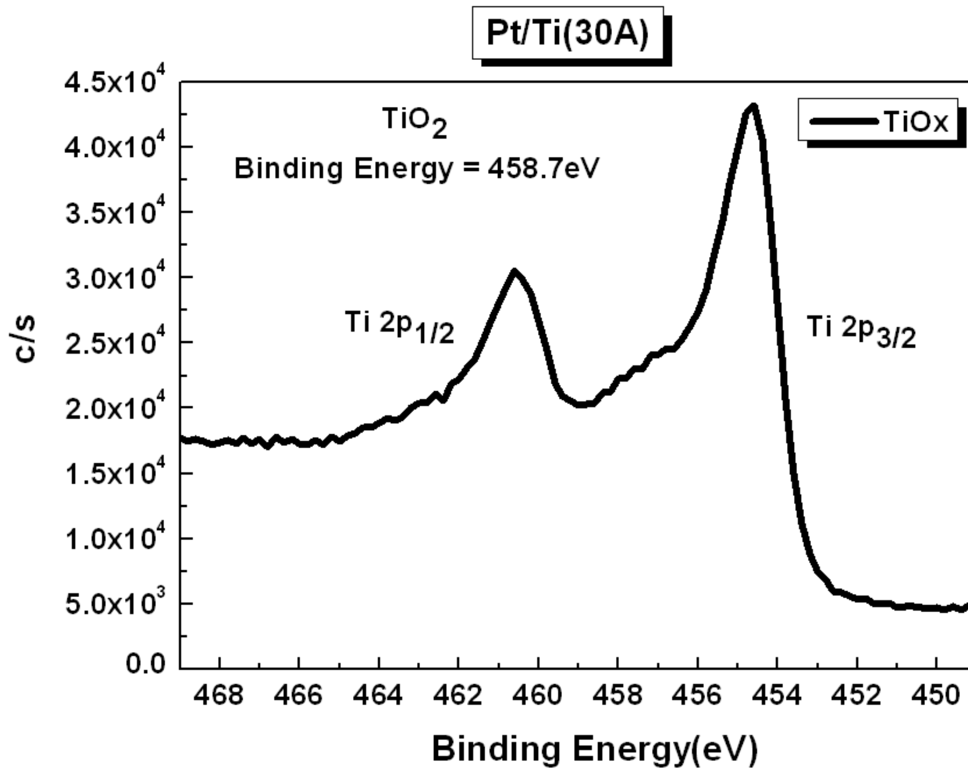

Fig. 3-84 XPS binding energy of Ti/HfOx interface.

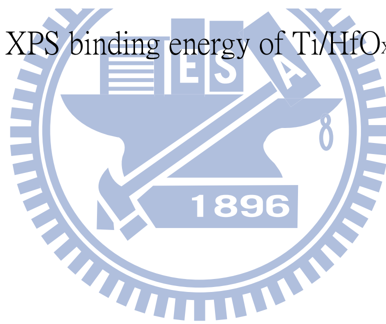

Chapter 4 Conclusion

In summary, we discuss to influence resistive switching characteristics of resistive memory for different compliance current. The different metals were used as the electrode based on the HfO_x/TiN structure, and the resistive switching characteristics of those devices were investigated in this thesis.

Afterward, we discuss the electrode dependence with various metals work function and free energy of oxidation of various metals. For the same compliance current, lower free energy of oxidation of metals were observed no resistive switching characteristics, and higher free energy of oxidation of metals is bad for endurance test. Because lower free energy of oxidation of metals were easier formed metal oxide at interface, which resulted the filaments were not ruptured and no resistive switching, and higher free energy of oxidation of metals on resistive switching is easier losing oxygen ions. Therefore, the electrode dependence on resistive switching does not result with result from work function, but result with free energy of formation of oxidation of metals. The metal oxide created at the interface between HfO_x and the metal electrode affects the resistive switching characteristics.

The final part in this thesis, we demonstrate good resistive switching characteristics of inert metal/reactive metal/HfO_x/TiN structure, the top electrode such as Pd/Al, Pd/Ti, Pd/TiO, Pt/Ti ,and etc, and thickness of the reactive metal is related with free energy of formation of oxidation of the metal and free energy of formation of oxidation of Hf. In our device, which can be operated switching at 175 ℃, and the endurance is over 4000 switching cycles by sweeping dc voltage. Afterward, the data retention time of HRS and LRS is over 5×10^4 seconds at 175 ℃ under static air, which is over 10^5 seconds at 85 ℃.

Chapter 5 Future Work

In this thesis, we know that the appropriate O_2, N_2 and temperature on interface can improve the electrical properties. Therefore, the plasma treatment and heat treatment on interface is the needful. Unipolar measurement is necessary, which can avoid V_{SET} and V_{RESET} overlap each other. Pulse I-V measurement can decrease measurement time to avoid the sample is broken at long measurement time. We know that Hf has lower free energy of oxidation. Therefore, some higher free energy material oxide is used, such as NiO, Ta_2O_5. The free energy of formation of oxidation of metals is important for selecting the metal electrode. Therefore, the alloy as top electrode is considered, such as $Pt_{1-X}Al_X$, $Pd_{1-X}Ti_X$. We are hopeful that future research will focus on these views to further make the RRAM in commercial applications come true, leading to better uniformity and reliability of manufacture.

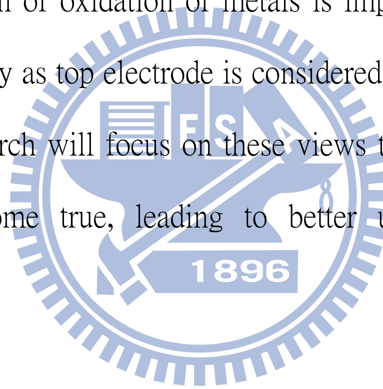
1896

References

[1] K. Kim, J. H. Choi, and H. S. Jeong, "The future prospect of nonvolatile memory," in Proc. VLSI-TSA-Tech 2005, pp. 88-94.

[2] Daniele Ielmini, "Reliability issues and modeling of Flash and post-Flash memory (Invited Paper)," Microelectronic Engineering 86, 2009, pp. 1870-1875.

[3] Changseok Kang, Jungdal Choi, Jaesung Sim, Changhyun Lee, Yoocheol Shin, Jintaek Park, Jongsun Sel, Sanghun Jeon, Youngwoo Park, and Kinam Kim, "Effects of Lateral Charge Spreading on the Reliability of TANOS (TaN/AlO/SiN/Oxide/Si) NAND Flash Memory," IEEE, 45th Annual International Reliability Physics Symposium, Phoenix, 2007, pp. 167-170.

[4] Hang-Ting Lue, Szu-Yu Wang, Erh-Kun Lai, Kuang-Yeu Hsieh, Rich Liu, and Chih Yuan Lu, "A BE-SONOS (Bandgap Engineered SONOS) NAND for Post-Floating Gate Era Flash Memory," IEEE, 2007, pp. 1-2.

[5] T. Nakamura, Y. Fujimori, N. Izumi, and A. Kamisawa, "Fabrication technology of ferroelectric memories," Japanese Journal of Applied Physics, Vol. 37, No. 3B, 1998, pp.1325-1327.

[6] R. Moazzami, "Ferroelectric thin film technology for semiconductor memory," Semicond. Sci. Technol., Vol. 10, 1995, pp. 375-390.

[7] T. Hayashi, Y. Igarashi, D. Inomata, T. Ichimori, T. Mitsuhashi, K. Ashikaga, T. Ito, M. Yoshimaru, M. Nagata, S. Mitarai, H. Godaiin, T. Nagahama, C. Isobe, H. Moriya, M. Shoji, Y. Ito, H. Kuroda, and M. Sasaki, "A novel stack capacitor cell for high density FeRAM compatible with CMOS logic," in IEDM Tech. Dig., 2002, pp. 543-546.

[8] J. M. Slaughter, R. W. Dave, M. Durlam, G. Kerszykowski, K. Smith, K. Nagel, B. Feil, J. Calder, M. DeHerrera, B. Garni, and S. Tehrani, "High speed toggle MRAM with MgO-based tunnel junctions," in IEDM Tech. Dig., 2005, pp. 873-876.

[9] R. Leuschner, U. K. Klostermann, H. Park, F. Dahmani, R. Dittrich, C. Grigis, K. Hernan, S. Mege, C. Park, M. C. Clech, G. Y. Lee, S. Bournat, L. Altimime, and G. Mueller, "Thermal select MRAM with a 2-bit cell capability for beyond 65nm technology node," in IEDM Tech. Dig.,2006, pp. 1-4.

[10] C. C. Hung, Y. S. Chen, D. Y. Wang, Y. J. Lee, W. C. Chen, Y. H. Wang, C. T. Yen, S. Y. Yang, K. H. Shen, C. P. Chang, C. S. Lin, K. L. Su, H. C. Cheng, Y. J. Wang, D. L. Tang, M. J. Tsai, and M. J. Kao, "Adjacent-reference and self-reference sensing scheme with novel orthogonal wiggle MRAM cell," in IEDM Tech. Dig., 2006, pp. 1-4.

[11] R. Neale, D. Nelson, Gordon Moore, "Nonvolatile and reprogrammable, the read-mostly memory is here," Electronics, 1970, pp. 56-60.

[12] S. Lai and T. Lowrey, "OUM-a 180 nm nonvolatile memory cell element technology for stand alone and embedded applications," in IEDM Tech. Dig., 2001, pp. 803-806.

[13] S. Lai, "Current status of the phase change memory and its future," in IEDM Tech. Dig., 2003, pp. 255-258.

[14] A. Redaelli, A. Pirovano, F. Pellizzer, A. L. Lacaita, D. Ielmini, and R. Bez, "Electronic switching effect and phase change transition in chalcogenide materials," IEEE Electron Device Lett., Vol. 25, No. 10, 2004, pp. 684-686.

[15] D. S. Suh, K. H. P. Kim, J. S. Noh, W. C. Shin, Y. S. Kang, C. Kim, Y. Khang, and I. K. Yoo, "Critical quenching speed determining phase of $Ge_2Sb_2Te_5$ in Phase-Change Memory," in IEDM Tech. Dig., 2006, pp. 1-4.

[16] Roberto Bez, Agostino Pirovano, "Non-volatile memory technologies: emerging concepts and new materials," ELSEVIER, Materials Science in Semiconductor Processing, 2004, pp. 349-355.

[17] W. W. Zhuang, W. Pan, B. D. Ulrich, J. J. Lee, L. Stecker, A. Burmaster, D. R. Evans, S. T. Hsu, M. Tajiri, A. Shimaoka, K. Inoue, T. Naka, N. Awaya, K. Sakiyama, Y. Wang, S. Q. Liu, N. J. Wu, and A. Ignatiev, "Novell Colossal Magnetoresistive Thin Film Nonvolatile Resistance Random Access Memory (RRAM)," IEDM, 2002, pp. 193-196.

[18] Rainer Waser, and Masakazu Aono, "Nanoionics-based resistive switching memories," review articles, nature materials, Vol. 6, 2007 Nature Publighing Group, pp. 833-840.

[19] I. H. Inoue, S. Yasuda, H. Akinaga, and H. Takagi, "Nonpolar resistance switching of metal/binary-transition-metal oxides/metal sandwich," Phys. Rev. B, Vol. 77, 2008, p. 035105.

[20] I. G. Baek, M. S. Lee, S. Seo, M. J. Lee, D. H. Seo, D.-S. Suh, J. C. Park, S. O. Park, H. S. Kim, I. K. Yoo, U-In Chung and I. T. Moon, "Highly Scalable Non-volatile Resistive Memory using Simple Binary Oxide Driven by Asymmetric Unipolar Voltage Pulses," IEDM, 2004, pp. 23.6.1-23.6.4.

[21] B. J. Choi, D. S. Jeong, S. K. Kim, C. Rohde, S. Choi, J. H. Oh, H. J. Kim, C. S. Hwang, K. Szot, R. Waser, B. Reichenberg, and S. Tiedke, "Resistive switching mechanism of TiO_2 thin films grown by atomic-layer deposition," Journal of Applied Physics, Vol. 98, 2005, p. 033715

[22] A. Chen, S. Haddad, Y. C. Wu, Z. Lan, T. N. Fang, and S. Kaza, "Switching characteristics of Cu_2O metal-insulator-metal resistive memory," Applied Physics Letters, Vol. 91, 2007, p. 123517.

[23] Krzysztof szot, Wolfgang speier, Gustav bihlmayer, and Rainer waser, "Switching the electrical resistance of individual dislocations in single-crystalline $SrTiO_3$," nature material, Vol. 5, 2006, pp. 312-320.

[24] D. C. Kim, S. Seo, S. E. Ahn, D.-S. Suh, M. J. Lee, B.-H. Park, I. K. Yoo, I. G. Baek,a H.-J. Kim, E. K. Yim, J. E. Lee, S. O. Park, H. S. Kim, U-In Chung, J. T. Moon, and B. I. Ryu, "Electrical observations of filamentary conductions for the resistive memory switching in NiO films," Applied Physics Letters, Vol. 88, , 2006, p. 202102.

[25] Shangqing Liu, Naijuan Wu, Alex Ignatiev, and Jianren Li, "Electric-pulse-induced capacitance change effect in perovskite oxide thin films," Journal of Applied Physics, Vol. 100, 2006, p. 056101.

[26] Xin Chen, NaiJuan Wu, John Strozier, and Alex Ignatiev, "Spatially extended nature

of resistive switching in perovskite oxide thin films," Applied Physics Letters, Vol. 89, 2006, p. 063507.

[27] Dongsoo Lee, Dong-jun Seong, Hye jung Choi, Inhwa Jo, R. Dong ,W. Xiang, ,Seokjoon Oh, Myeongbum Pyun, Sun-ok Seo, Seongho Heo, Minseok Jo, Dae-Kyu Hwang, H. K Park, M. Chang, M. Hasan, and Hyunsang Hwang, "Excellent uniformity and reproducible resistance switching characteristics of doped binary metal oxides for non-volatile resistance memory applications," IEDM, 2006, pp. 1-4.

[28] Doo Seok Jeong, Herbert Schroeder, and Rainer Waser, "Impedance spectroscopy of TiO2 thin films showing resistive switching," Applied Physics Letters, Vol. 89, 2006, p. 082909.

[29] Kohei FUJIWARA, Takumi NEMOTO, Marcelo J. ROZENBERG, Yoshinobu NAKAMURA, and Hidenori TAKAGI, "Resistance Switching and Formation of a Conductive Bridge in Metal/Binary Oxide/Metal Structure for Memory Devices," Japanese Journal of Applied Physics, Vol. 47, No. 8, 2008, pp. 6266-6271.

[30] Akihito Sawa, "Resistive switching in transition metal oxides," review articles, materialstoday, Vol. 11, No. 6, 2008, pp. 28-36.

[31] Kyung Min Kim, Byung Joon Choi, Bon Wook Koo, Seol Choi, Doo Seok Jeong, and Cheol Seong Hwang, "Resistive Switching in Pt/Al_2O_3/TiO_2/Ru Stacked Structures," Electrochemical and Solid-State Letters, 2006, pp. G343-G346.

[32] Kyung Min Kim, Byung Joon Choi, and Cheol Seong Hwang, "Localized switching mechanism in resistive switching of atomic-layer-deposited TiO_2 thin films," Applied Physics Letters 90, 2007, p. 242906.

[33] Heng-Yuan Lee, Pang-Shiu Chen, Ching-Chiun Wang, Siddheswar Maikap, Pei-Jer Tzeng, Cha-Hsin Lin, Lurng-Shehng Lee, and Ming-Jinn Tsai, "Low-Power Switching of Nonvolatile Resistive Memory Using Hafnium Oxide," Japanese Journal of Applied Physics, Vol. 46, No. 4B, 2007, pp. 2175-2179.

[34] H. Y. Lee, P. S. Chen, T. Y. Wu, Y. S. Chen, C. C. Wang, P. J. Tzeng, C. H. Lin, F. Chen, C. H. Lien, and M. J. Tsai, "Lower Power and High Speed Bipolar Switching with A Thin Reactive Ti Buffer Layer in Robust HfO_2 Based RRAM," Electron

Devices Meeting, IEDM 2008, pp. 1-4.

[35] Heng-Yuan Lee, Pang-Shiu Chen, Tai-Yuan Wu, Ching-Chiun Wang, Pei-Jer Tzeng, Cha-Hsin Lin, Frederick Chen, Chen-Hsin Lien, and Ming-Jinn Tsai, "HfO_2 Bipolar Resistive Memory Device with Robust Endurance using AlCu as Electrode," VLSI Technology, Systems and Applications, 2008, pp. 146-147.

[36] Heng-Yuan Lee, Pang-Shiu Chen, Tai-Yuan Wu, Ching-Chiun Wang, Pei-Jer Tzeng, Cha-Hsin Lin, Frederick Chen, Ming-Jinn Tsai, and Chen-Hsin Lien, "Electrical evidence of unstable anodic interface in Ru/HfO_x/TiN unipolar resistive memory," Applied Physics Letters 92, 2008, p. 142911.

[37] W. J. Zhu, Tso-Ping Ma, Fellow, IEEE, Takashi Tamagawa, Member, IEEE, J. Kim, and Y. Di, "Current Transport in Metal/Hafnium Oxide/Silicon Structure," IEEE Electron device letters, Vol. 23, No. 2, 2002.

[38] Kaupo Kukli, Mikko Ritala, Timo Sajavaara, Juhani Keinonen, and Maekku Leskela, "Comparison of hafnium oxide films grown by atomic layer deposition from iodide and chloride precursors," Thin Solid Films 416, 2002, pp. 72-79.

[39] Seunghyup Lee, Wan-Gee Kim, Shi-Woo Rhee, and Kijung Yong, "Resistance Switching Behaviors of Hafnium Oxide Films Grown by MOCVD for Nonvolatile Memory Applications," ECS, Vol. 155, 2008, pp. H92-H96.

[40] Kentaro Kinoshita, Tetsuro Tamura, Masaki Aoki, Yoshihiro Sugiyama and Hitoshi Tanaka, "Lowering the Switching Current of Resistance Random Access Memory Using a Hetero Junction Structure Consisting of Transition Metal Oxides," Japanese Journal of Applied Physics, Vol. 45, No. 37, 2006, pp. L991-L994.

[41] M. Yin, P. Zhou, H. B. Lv, J. Xu, Y. L. Song, X. F. Fu, T. A. Tang, B. A. Chen, and Y. Y. Lin, "Improvement of Resistive Switching in Cu_xO Using New RESET Mode," IEEE, Vol. 29, No. 7, 2008.

[42] Bing Sun, Lifeng Liu, Nuo Xu, Bin Gao, Yi Wang, Dedong Han, Xiaoyan Liu, Ruqi Han, and Jinfeng Kang, "The Effect of Current Compliance on the Resistive Switching Behaviors in TiN/ZrO_2/Pt Memory Device," Japanese Journal of Applied Physics, Vol. 48, 2009, p. 04C061.

[43] Yoshihiro Sato, Koji Tsunoda, Kentaro Kinoshita, Hideyuki Noshiro, Masaki Aoki, and Yoshihiro Sugiyama, “Sub-100-μA Reset Current of Nickel Oxide Resistive Memory Through Control of Filamentary Conductance by Current Limit of MOSFET,” IEEE, Vol. 55, No. 5, 2008.

[44] Seung-Eon Ahn, Myoung-Jae Lee, Youngsoo Park, Bo Soo Kang, Chang Bum Lee, Ki Hwan Kim, Sunae Seo, Dong-Seok Suh, Dong-Chirl Kim, Jihyun Hur, Wenxu Xianyu, Genrikh Stefanovich, Huaxiang Yin, In-Kyeong Yoo, Jung-Hyun Lee, Jong-Bong Park, In-Gyu Baek, and Bae Ho Park, “Write Current Reduction in Transition Metal Oxide Based Resistance-Change Memory,” Advanced Materials, 2008, Vol. 20, pp. 924-928.

[45] Chih-Yang Lin, Chen-Yu Wu, Chung-Yi Wu, Tzyh-Cheang Lee, Fu-Liang Yang, Chenming Hu, Fellow, IEEE, and Tseung-Yuen Tseng, Fellow, IEEE, “Effect of Top Electrode Material on Resistive Switching Properties of ZrO_2 Film Memory Devices,” IEEE, Vol. 28, No. 5, 2007, pp. 366-368.

[46] Chih-Yang Lin, Chung-Yi Wu, Chen-Yu Wu, Tseung-Yuen Tsenga, and Chenming Hu, “Modified resistive switching behavior of ZrO_2 memory films based on the interface layer formed by using Ti top electrode,” Journal of Applied Physics, Vol. 102, 2007, p. 094101.

[47] C. B. Lee, B. S. Kang, A. Benayad, M. J. Lee, S.-E. Ahn, K. H. Kim, G. Stefanovich, Y. Park, and I. K. Yoo, “Effects of metal electrodes on the resistive memory switching property of NiO thin films,” Applied Physics Letters 93, 2008, p. 042115.

[48] S. Seo, M. J. Lee, D. C. Kim, S. E. Ahn, B.-H Park, Y. S. Kim, I. K. Yoo, I. S. Byun, I. R. Hwang, S. H. Kim, J.-S. Kim, J. S. Choi, J. H. Lee, S. H. Jeon, S. H. Hong, and B. H. Park, “Electrode dependence of resistance switching in polycrystalline NiO films,” Applied Physics Letters 87, 2005, p. 263507.

[49] Young Ho Do, June Sik Kwak, Jin Pyo Hong, Kyooho Jung, and Hyunsik Im, “Al electrode dependent transition to bipolar resistive switching characteristics in pure TiO_2 films,” Journal of Applied Physics, Vol. 104, 2008, p. 114512.

[50] Hangbing Lv, Ming Wang, Haijun Wan, Yali Song, Wenjing Luo, Peng Zhou, Tingao Tang, Yinyin Lin, R. Huang, S. Song, J. G. Wu, H. M. Wu, and M. H. Chi, “Endurance enhancement of Cu-oxide based resistive switching memory with Al

top electrode," Applied Physics Letters 94, 2009, p. 213502.

[51] A. Sawa, T. Fujii, M. Kawasaki, and Y. Tokura, "Interface transport properties and resistance switching in perovskite-oxide heterojunctions," in Proc. SPIE, 2005, p. 59322C.

[52] S. Seo, M. J. Lee, D. C. Kim, S. E. Ahn, B. H. Park, Y. S. Kim, I. K. Yoo, I. S. Byun, I. R. Hwang, S. H. Kim, J. S. Kim, J. S. Choi, J. H. Lee, S. H. Jeon, S. H. Hong, and B. H. Park, "Electrode dependence of resistance switching in polycrystalline NiO films," Applied Physics Letters, Vol. 87, 2005, p. 263507.

[53] Musarrat Hasan, Rui Dong, H. J. Choi, D. S. Lee, D.-J. Seong, M. B. Pyun, and Hyunsang Hwang, "Uniform resistive switching with a thin reactive metal interface layer in metal-$La_{0.7}Ca_{0.3}MnO_3$-metal heterostructures," Applied Physics Letters, Vol. 92, 2008, p. 202102.

[54] Musarrat Hasan, Rui Dong, H. J. Choi, D. S. Lee, D.-J. Seong, M. B. Pyun, and Hyunsang Hwang, "Effect of ruthenium oxide electrode on the resistive switching of Nb-doped strontium titanate," Applied Physics Letters, Vol. 93, 2008, p. 052908.

[55] Song-Lin Li, D. S. Shang, J. Li, J. L. Gang, and D. N. Zheng, "Resistive switching properties in oxygen-deficient $Pr_{0.7}Ca_{0.3}MnO_3$ junctions with active Al top electrodes," Journal of Applied Physics, Vol. 105, 2009, p. 033710.

[56] Hiroyasu Kawano, Keiji Shono, Takeshi Yokota, and Manabu Gomi, "Enhancement of Switching Capability on Bipolar Resistance Switching Device with Ta/$Pr_{0.7}Ca_{0.3}MnO_3$/Pt Structure," Applied Physics Express, Vol. 1, 2008, p. 101901.

[57] Keiji Shono, Hiroyasu Kawano, Takeshi Yokota, and Manabu Gomi, "Origin of Negative Differential Resistance Observed on Bipolar Resistance Switching Device with Ti/$Pr_{0.7}Ca_{0.3}MnO_3$/Pt Structure," Applied Physics Express, Vol. 1, 2008, p. 055002.

[58] Kyung Min Kim, Byung Joon Choi, Yong Cheol Shin, Seol Choi, and Cheol Seong Hwang, "Anode-interface localized filamentary mechanism in resistive switching of TiO_2 thin films," Applied Physics Letters, Vol. 91, 2007, p. 012907.

[59] S. Seo, M. J. Lee, D. H. Seo, E. J. Jeoung, D.-S. Suh, Y. S. Joung, I. K. Yoo, I. R.

Hwang, S. H. Kim, I. S. Byun, J.-S. Kim, J. S. Choi, and B. H. Park, "Reproducible resistance switching in polycrystalline NiO films," Applied Physics Letters, Vol. 85, No. 23, 2004, pp. 5655-5657.

[60] A. Sawa, T. Fujii, M. Kawasaki, and Y. Tokura, "Interface resistance switching at a few nanometer thick perovskite manganite active layers," Applied Physics Letters, Vol. 88, 2006, p. 232112.

[61] Gyeong-Su Park, Xiang-Shu Li, Dong-Chirl Kim, Ran-Ju Jung, Myoung-Jae Lee, and Sunae Seo, "Observation of electric-field induced Ni filament channels in polycrystalline NiOx film," Applied Physics Letters, Vol. 91, 2007, p. 222103.

[62] Lee-Eun Yu, Sungho Kim, Min-Ki Ryu, Sung-Yool Choi, and Yang-Kyu Choi, "Structure Effects on Resistive Switching of Al/TiO_x/Al Devices for RRAM Applications," IEEE, Vol. 29, No. 4, 2008, pp. 331-333.

[63] A. Baikalov, Y. Q. Wang, B. Shen, B. Lorenz, S. Tsui, Y. Y. Sun, Y. Y. Xue, and C. W. Chu, "Field-driven hysteretic and reversible resistive switch at the Ag-$Pr_{0.7}Ca_{0.3}MnO_3$ interface," Applied Physics Letters, Vol. 83, No. 5, 2003, pp. 957-959.

[64] A. Sawa, T. Fujii, M. Kawasaki, and Y. Tokura, "Hysteretic current–voltage characteristics and resistance switching at a rectifying Ti/$Pr_{0.7}Ca_{0.3}MnO_3$ interface," Applied Physics Letters, Vol. 85, No. 18, 2004, pp. 4073-4075.

[65] S. Tsui, A. Baikalov, J. Cmaidalka, Y. Y. Sun, Y. Q. Wang, Y. Y. Xue, C. W. Chu, L. Chen and A. J. Jacobson, "Field-induced resistive switching in metal-oxide interfaces," Applied Physics Letters, Vol. 85, No. 2, 2004, pp. 317-319.

[66] T. Fujii, M. Kawasaki, A. Sawa, H. Akoh, Y. Kawazoe, and Y. Tokura, "Hysteretic current–voltage characteristics and resistance switching at an epitaxial oxide Schottky junction $SrRuO_3$ /$SrTi_{0.99}Nb_{0.01}O_3$," Applied Physics Letters, Vol. 86, 2005, p. 012107.

[67] A. Sawa, T. Fujii, M. Kawasaki, and Y. Tokura, "Highly rectifying $Pr_{0.7}Ca_{0.3}MnO_3$ /$SrTi_{0.9998}Nb_{0.0002}O_3$ p-n junction," Applied Physics Letters, Vol. 86, 2005, p. 112508.

[68] Hyunjun Sim, Hyejung Choi, Dongsoo Lee, Man Chang, Dooho Choi, Yunik Son,

Eun-Hong Lee, Wonjoo Kim, Yoondong Park, In-Kyeong Yoo and Hyunsang Hwang, "Excellent Resistance Switching Characteristics of Pt/$SrTiO_3$ Schottky Junction for Multi-bit Nonvolatile Memory Application," IEEE, 2005.

[69] M. J. Sanchez, M. J. Rozenberg, and I. H. Inoue, "A mechanism for unipolar resistance switching in oxide nonvolatile memory devices," Applied Physics Letters, Vol. 91, 2007, p. 252101.

[70] S. B. Lee, S. C. Chae, S. H. Chang, J. S. Lee, S. Seo, B. Kahng, and T. W. Noh, "Scaling behaviors of reset voltages and currents in unipolar resistance switching," Applied Physics Letters, Vol. 93, 2008, p. 212105.

[71] An Chen, Member, IEEE, Sameer Haddad, Member, IEEE, and Yi-Ching Wu, "A Temperature-Accelerated Method to Evaluate Data Retention of Resistive Switching Nonvolatile Memory," IEEE, Vol. 29, No. 1, 2008, pp. 38-40.

[72] Jang-Sik Lee, Chang-Seok Kang, Yoo-Cheol Shin, Chang-Hyun Lee, Ki-Tae Park, Jong-Sun Sel, Viena Kim, Byeong-In Choe, Jae-Sung Sim, Jungdal Choi and Kinam Kim, "Data Retention Characteristics of Nitride-Based Charge Trap Memory Devices with High-k Dielectrics and High-Work-Function Metal Gates for Multi-Gigabit Flash Memory," Japanese Journal of Applied Physics, Vol. 45, No. 4B, 2006, pp. 3213-3216.

[73] Jang-Sik LEE, and Seung-Li Joo, "Enhanced Fatigue and Data Retention Characteristics of Pb(Zr,Ti)O_3 Thin Films by the Selectively Nucleated Lateral Crystallization Method," Japanese Journal of Applied Physics, Vol. 40, No. 1, 2001, pp. 229-233.

[74] H. B. Lv, M. Yin, X. F. Fu, Y. L. Song, L. Tang, P. Zhou, C. H. Zhao, T. A. Tang, B. A. Chen, and Y. Y. Lin, "Resistive Memory Switching of Cu_xO Films for a Nonvolatile Memory Application," IEEE, Vol. 29, No. 4, 2008, pp. 309-311.

[75] Agostino Pirovano, Andrea Redaelli, Fabio Pellizzer, Federica Ottogalli, Marina Tosi, Daniele Ielmini, Andrea L. Lacaita, Senior Member, IEEE, and Roberto Bez, "Reliability Study of Phase-Change Nonvolatile Memories," IEEE, Vol. 4, No. 3, 2004, pp. 422-427.

[76] R. Dong, Q. Wang, L. D. Chen, D. S. Shang, T. L. Chen, X. M. Li, and W. Q. Zhang,

"Retention behavior of the electric-pulse-induced reversible resistance change effect in Ag-$La_{0.7}Ca_{0.3}MnO_3$-Pt sandwiches," Applied Physics Letters, Vol. 86, 2005, p. 172107.

[77] R. Soni, C. Schindler, M. Weides, A. Rüdiger, C. Kügeler, R. Waser, "A Novel Dual-Layered Electrolytic Resistance Memory with Enhanced Retention," IEEE, 2008, pp. 764-766.

[78] Kyooho Jung, Hongwoo Seo, Yongmin Kim, Hyunsik Im, JinPyo Hong, Jae-Wan Park and Jeon-Kook Lee, "Temperature dependence of high- and low-resistance bistable states in polycrystalline NiO films," Applied Physics Letters, Vol. 90, 2007, p. 052104.

[79] Chih-Tsung Tsai, Ting-Chang Chang, Po-Tsun Liu, Yi-Li Cheng, and Fon-Shan Huang, "Low temperature improvement on silicon oxide grown by electron-gun evaporation for resistance memory applications," Applied Physics Letters, Vol. 93, 2008, p. 052903.

[80] S. H. Chang, J. S. Lee, S. C. Chae, S. B. Lee, C. Liu, B. Kahng, D.-W. Kim, and T.W. Noh, "Occurrence of Both Unipolar Memory and Threshold Resistance Switching in a NiO Film," PRL, Vol. 102, 2009, p. 026801.

[81] Chikako Yoshida, Kohji Tsunoda, Hideyuki Noshiro, and Yoshihiro Sugiyama, "High speed resistive switching in Pt/TiO_2/TiN film for nonvolatile memory application," Applied Physics Letters, Vol. 91, 2007, p. 223510.

[82] Chih-Yang Lin, Dai-Ying Lee, Sheng-Yi Wang, Chun-Chieh Lin, and Tseung-Yuen Tseng, "Effect of thermal treatment on resistive switching characteristics in Pt/Ti/Al_2O_3/Pt devices," Surface & Coatings Technology, Vol. 203, 2008, pp. 628-631.

[83] M. J. Lee, Y. Park, S. E. Ahn, B. S. Kang, C. B. Lee, K. H. Kim, W. X. Xianyu, I. K. Yoo, J. H. Lee, S. J. Chung, Y. H. Kim, C. S. Lee, K. N. Choi and K. S. Chung, "Comparative structural and electrical analysis of NiO and Ti doped NiO as materials for resistance random access memory," Journal of Applied Physics, Vol. 103, 2008, p. 013706.

[84] Ugo Russo, Student Member, IEEE, Daniele Ielmini, Member, IEEE, Carlo Cagli,

and Andrea L. Lacaita, Senior Member, IEEE, "Self-Accelerated Thermal Dissolution Model for Reset Programming in Unipolar Resistive-Switching Memory (RRAM) Devices," IEEE, Vol. 56, No. 2, 2009, pp. 193-199.

[85] Zhen Xu, Michel Houssa, Stefan De Gendt and Marc Heyns, "Polarity effect on the temperature dependence of leakage current through HfO_2/SiO_2 gate dielectric stacks," Applied Physics Letters, Vol. 80, No. 11, 2002, pp. 1975-1977.

[86] Hyoungsub Kim, Ann Marshall, Paul C. McIntyre, and Krishna C. Saraswat, "Crystallization kinetics and microstructure-dependent leakage current behavior of ultrathin HfO_2 dielectrics: In situ annealing studies," Applied Physics Letters, Vol. 84, No. 12, 2004, pp. 2064-2066.

[87] Chih-Yang Lin, Sheng-Yi Wang, Dai-Ying Lee, and Tseung-Yuen Tseng, "Electrical Properties and Fatigue Behaviors of ZrO_2 Resistive Switching Thin Films," Journal of The Electrochemical Society, Vol. 155, No. 8, 2008, pp. H615-H619.

[88] Ming-Tsong Wang, Shao-You Deng, Tsung-Hong Wang, Bonds Yi-Yi Cheng, and Joseph Ya-min Lee, "The Ohmic Conduction Mechanism in High-Dielectric-Constant ZrO_2 Thin Films," Journal of The Electrochemical Society, Vol. 152, No. 7, 2005, pp. G542-G544.

[89] Yi-Sheng Lai, Chia-Hsun Tu, Dim-Lee Kwong, and J. S. Chen, "Charge-Transport Characteristics in Bistable Resistive Poly (N-Vinylcarbazole) Films," IEEE, Vol. 27, No. 6, 2006, pp. 451-453.

[90] Chun-Chieh Lin, Chih-Yang Lin, Meng-Han Lin, Chen-Hsi Lin, Member, IEEE, and Tseung-Yuen Tseng, Fellow, IEEE, "Voltage-Polarity-Independent and High-Speed Resistive Switching Properties of V-Doped $SrZrO_3$ Thin Films," IEEE, Vol. 54, No. 12, 2007, pp. 3146-3151.

[91] Wen-Yuan Chang, Yen-Chao Lai, Tai-Bor Wu, Sea-Fue Wang, Frederick Chen, and Ming-Jinn Tsai, "Unipolar resistive switching characteristics of ZnO thin films for nonvolatile memory applications," Applied Physics Letters, Vol. 92, 2008, p. 022110.

[92] T. Busani and R. A. B. Devine, "Nonvolatile memory and antifuse behavior in

Pt/a-TiO_2/Ag structures," J. Vac. Sci. Technol., Vol. 26, No. 5, 2008, pp.1817-1820.

[93] L. Goux, J. G. Lisoni, T. Gille, K. Attenborough, and D. J. Wouters, "Low-Voltage Resistive Switching within an Oxygen-Rich Cu/SbTe Interface for Application in Nonvolatile Memory," Electrochemical and Solid-State Letters, Vol. 11, No. 9, 2008, pp. H245-H247.

[94] S. M. Sze, Physics of Semiconductor Devices, 2nd ed. New York: John Wiley & Sons, 1981, pp. 402-407.